

Norwegian University  
of Life Sciences

**Master's Thesis 2021 60 ECTS**

Faculty of Chemistry, Biotechnology and Food Science

# **The impact of impaired biosynthesis of menaquinone on biofilm and macrocolony formation in *Staphylococcus aureus***

Henriette Sætre Olsen

Biotechnology



## **Acknowledgement**

This master thesis was completed as a part of the Master program in Biotechnology at the University of Life Sciences (NMBU). It was conducted in the Molecular Microbiology research group at the Faculty of Chemistry, Biotechnology and Food Science (KBM) in the period from August 2020 to May 2021.

First and foremost, I would like to thank my supervisor, Dr. Morten Kjos, for guiding me through this project, both in the lab and especially during the writing process. Your support has been a great help. I would also like to thank my co-supervisor Dr. Volha Shapaval for all the help and guidance she provided regarding FTIR-spectroscopy analysis.

My sincere gratitude must be expressed to Dr. Danae Morales Angeles for following me every step in the lab. I am very thankful for all the advice you have given me and for answering all my stupid questions.

Finally, a big thank you to everyone at the Molecular Microbiology research group for creating such a great work environment. And a thank you to my fellow master students Marie, Anna and Maria for entertainment and moral support.

Henriette Sætre Olsen

Ås, June 2020

## Abstract

*Staphylococcus aureus* (*S. aureus*) is known to cause biofilm-associated infections in humans. Biofilms are surface associated microbial communities and is characterized as three-dimensional structures with cells embedded in a self-produced extracellular matrix. Due to the protective nature of biofilms, these infections are difficult to eradicate and often become chronic. Biofilms are often resistant or less susceptible to host immune agents or antibiotics, therefore it is of great interest to find alternative treatment methods. In order to find potential treatments, it is important to study the biofilm formation of these bacteria to better understand the underlying regulations and effects that determine how the final biofilm structure and composition is determined. Among other things, respirational processes have been shown to influence the biofilm formation. Specifically, molecules involved in electron transport are therefore critical for biofilm formation and potential targets for anti-biofilm compounds. In this work, we have therefore studied several depletion, deletion and complementation mutants of *S. aureus* genes involved in synthesis of menaquinone, and important electron carrier during respiration in *S. aureus*, in order to explore how this affects the biofilm structure and composition.

Initially, we show that biofilm macrocolonies of *S. aureus* strains harbouring deletions of genes involved in menaquinone synthesis display altered morphological characteristics when grown in aerobic environments. Deletion of *ubiE*, encoding the last enzyme in the menaquinone biosynthesis pathway, resulted in biofilm macrocolonies with lack of structures (e.g. wrinkling) which was observed for the wild-type grown under the same conditions, as well as reduced biofilm formation on abiotic surfaces. Upon complementation of the *ubiE* mutant, the wrinkling phenotype was restored. CRISPR interference depletion strains targeting other genes in the menaquinone synthesis did also reveal phenotypic changes in macrocolonies for *menA*. Interestingly, lack of structuring of the biofilm was also observed for the cell when grown anaerobically, demonstrating that loss of structures most probably was a result of altered metabolism in the mutants. Further analysis of the extracellular matrix (ECM) of the biofilms using FTIR spectroscopy and direct quantification of ECM extracts showed large differences in the chemical composition of the macrocolony ECMs (including differences in quantity and compositions of proteins, eDNA and possibly polysaccharides, both between knockout mutants and wild-type, and between strain grown aerobically and anaerobically). Together, this can tell us that genes that participates in the synthesis of menaquinone have an impact on the final chemical composition of *S. aureus* biofilms.

## Sammendrag

*Staphylococcus aureus* (*S. aureus*) er kjent for å forårsake biofilmassosierte infeksjoner hos mennesker. Biofilmer er overflateassosierte mikrobielle samfunn og er karakterisert som tredimensjonale strukturer med celler innkapslet i en egenproduser ekstracellulær matriks. På grunn av biofilmens beskyttende natur er disse infeksjonene vanskelige å bekjempe og blir ofte kroniske. Biofilm er ofte resistent eller mindre mottakelig for vertens immunsystem eller antibiotika, og det er derfor av stor interesse å finne alternative behandlingsmetoder. For å finne mulige behandlinger er det avgjørende å vite hvordan biofilmdannelsen skjer hos disse bakteriene, og forstå de underliggende regulatoriske effektene som bestemmer hvordan den endelige biofilmstrukturen og sammensetningen er. Blant annet har respiratoriske prosesser vist seg å ha en effekt på biofilmdannelsen. Molekyler involvert i elektrontransporten er derfor kritiske for dannelsen av biofilm og mulige mål for anti-biofilmforbindelser. I dette arbeidet har vi derfor studert flere delesjons-, depleksjons- og komplementerings-mutanter av *S. aureus* gener involvert i syntesen av menaquinone, en viktig elektronbærer under respirasjonen i *S. aureus*, for å utforske hvordan dette påvirker biofilm strukturen og sammensetningen.

Innledningsvis viser vi at biofilm makrokolonier av *S. aureus* stammer som bærer delesjoner av gener involvert i menaquinone syntesen viser endrede morfologiske egenskaper når de dyrkes i aerobe omgivelser. Fjerning av *ubiE*, som koder for det siste enzymet i biosynteseveien til menaquinone, resulterte i biofilmmakrokolonier med manglende strukturer (eks. rynker) som ble observert for villtypen dyrket under samme forhold, samt redusert biofilmdannelse på abiotiske overflater. Ved komplementering av *ubiE*-mutanten ble den strukturelle fenotypen gjenopprettet. CRISPR interferens depleksjonsstammer av andre gener i menaquinone syntesen viste også fenotypiske endringer hos makrokolonier for genet *menA*. Interessant nok, ble det også observert mangel på biofilm strukturering for celler som vokste anaerobt, noe som demonstrerer at tap av strukturer sannsynligvis var et resultat av endret metabolisme i mutantene. Videre analyse av den ekstracellulære matriksen (ECM) til biofilmene ved bruk av FTIR-spektroskopi og direkte kvantifisering av ECM-ekstrakter viste store forskjeller i den kjemiske sammensetningen av ECM fra makrokolonier (inkludert forskjeller i mengde og sammensetning av proteiner, eDNA og antakelig polysakkarider, både mellom delesjonsmutanter og villtype og mellom stammer dyrket aerobt og anaerobt. Samlet kan dette fortelle oss at gener som deltar i syntesen av menaquinone har innvirkning på den endelige kjemiske sammensetningen av *S. aureus* biofilmer.

# Index

1 Introduction .....	1
1.1 <i>Staphylococcus aureus</i> .....	1
1.1.1 Antibiotic resistance in <i>S. aureus</i> .....	1
1.1.2 Pathogenesis and virulence factors of <i>S. aureus</i> .....	2
1.2 Biofilm .....	3
1.2.1 Structure and composition of biofilms .....	3
1.2.2 Attributes of biofilms .....	4
1.2.3 Formation of biofilms in <i>S. aureus</i> .....	5
1.3 Menaquinone and metabolism in <i>S. aureus</i> .....	8
1.3.1 Respiration and fermentation in <i>S. aureus</i> .....	8
1.3.2 Menaquinone and the menaquinone biosynthetic pathway .....	9
1.3.3 The two-component regulatory systems, SaeRS and SrrAB, responds to changes in the respiratory metabolism in <i>S. aureus</i> . .....	11
1.4 Tools and techniques used to study biofilm in this work .....	12
1.4.1 Macrocolonies .....	12
1.4.2 Crystal violet assay.....	13
1.4.3 Fourier-transform infrared spectroscopy .....	13
1.4.4 Congo Red assay for biofilms .....	15
1.5 Main objectives of this study.....	16
2 Materials.....	17
2.1 Strains.....	17
2.2 Primers .....	18
2.3 Antibiotics .....	18
2.4 Chemicals .....	19
2.5 Kits .....	20
2.6 Equipment .....	20
2.7 Recipes for growth mediums, buffers and solutions .....	20
3 Methods.....	22
3.1 Growth and storage of <i>S. aureus</i> and <i>E. coli</i> .....	22
3.2 Isolation of chromosomal DNA .....	22
3.3 Plasmid isolation .....	23
3.4 Polymerase Chain reaction .....	23
3.4.1 Amplification of inserts for plasmid cloning.....	24
3.4.2 PCR for screening of potential transformants .....	25
3.5 Gel electrophoresis .....	26
3.5.1 Agarose gel electrophoresis.....	26

3.5.2	Extraction of DNA from agarose gels or PCR product .....	27
3.6	Plasmid construction .....	28
3.6.1	Construction of complementation plasmids and strains .....	29
3.6.2	Construction of CRISPR interference strains .....	30
3.7	Transformation of <i>E. coli</i> and <i>S. aureus</i> strains .....	32
3.7.1	Preparation of chemically competent <i>E. coli</i> .....	32
3.7.2	<i>E. coli</i> transformation .....	32
3.7.3	Preparation of electrocompetent <i>S. aureus</i> .....	33
3.7.4	<i>S. aureus</i> transformation.....	33
3.8	Sanger sequencing.....	34
3.9	Determining operon structures by RT-PCR .....	34
3.10	Growth analysis.....	35
3.11	Small colony assay with knockout strains of <i>aroC</i> and <i>ubiE</i> .....	36
3.12	Congo red susceptibility test .....	36
3.13	Biofilm assays .....	37
3.13.1	Crystal violet quantification .....	37
3.13.2	Macrocolony assay .....	37
3.13.3	Quantification of the extracellular matrix in macrocolonies .....	38
3.13.4	FTIR-spectroscopy to analyse composition of macrocolonies.....	39
3.13.5	Robustness of macrocolonies .....	40
4	Results .....	41
4.1	<i>ubiE</i> and <i>aroC</i> are important for macrocolony structuring .....	41
4.2	Growth analysis and complementation of <i>ubiE</i> and <i>aroC</i> deletion mutants .....	42
4.3	Macrocolony structuring are restored upon genetic complementation, but not by chemical complementation .....	45
4.4	<i>S. aureus</i> does not form structured macrocolonies under anaerobic conditions.....	47
4.5	Knockdown of other <i>men</i> -genes in the menaquinone biosynthesis pathway results in altered macrocolony formation .....	49
4.6	The chemical composition of the extracellular matrix (ECM).....	52
4.6.1	FTIR spectroscopy analyses reveal differences in the chemical composition of macrocolonies between aerobic and anaerobic macrocolonies .....	52
4.6.2	FTIR-spectroscopy analyses show variation in chemical composition of macrocolonies between wild-type and menaquinone biosynthesis mutants.....	56
4.6.3	Direct quantification of proteins, extracellular DNA and polysaccharides in ECM .....	59
4.6.4	Robustness of macrocolonies .....	61
4.7	Crystal violet assay reveal that the deletion of <i>ubiE</i> , but not <i>aroC</i> , lead to reduced biofilm formation on the solid liquid interface .....	62
4.8	<i>S. aureus</i> form small colony variants when either <i>ubiE</i> or <i>aroC</i> is deleted .....	64
4.9	Deletion of <i>ubiE</i> results in increased resistance to Congo Red.....	65

5 Discussion .....	67
5.1 Deletion of <i>ubiE</i> results in reduced growth and altered biofilm formation .....	67
5.2 Complementation of the <i>ubiE</i> :: <i>spc</i> deletion .....	68
5.3 The altered macrocolony biofilm formation is a result of altered metabolism in the <i>ubiE</i> deletion strain .....	69
5.4 Physical biochemical properties of the macrocolonies. Why are structured macrocolonies only formed in the cells growing with a respiratory metabolism? .....	70
5.5 The two-components systems SaeRS and SrrAB may be important for regulation of ECM products in wild-type and $\Delta ubiE$ .....	72
5.6 Interpretation of the Congo Red experiment. Interesting results but unexpected .....	73
5.7 <i>ubiE</i> and menaquinone as a drug-target .....	73
5.8 Advantages and limitations of FTIR spectroscopy for analysis of staphylococcal macrocolony biofilms.....	74
6 Concluding remarks and future perspectives .....	76
References .....	77
Appendix .....	84

# 1 Introduction

## 1.1 *Staphylococcus aureus*

*Staphylococcus aureus* (*S. aureus*) is a well-known Gram-positive bacterium which commonly colonizes healthy humans but can also be a frequent cause of both community and hospital acquired infections (Lowy, 1998; Tong, Davis, Eichenberger, Holland, & Fowler, 2015). This bacterium was first described in the 1880s, and is characterized as yellow coloured, spherical cocci which grows in clusters (Lowy, 1998). Due to the ability of the bacterium to adapt to different environments, it can colonize various tissues in the human body including skin and mucous membranes (most often in the nasal area) (Lindsay, 2014; Lowy, 1998; Zecconi & Scali, 2013). It is estimated that approximately 30% of the healthy human population are colonized (Tong et al., 2015), and that persistent colonization can increase the risk of developing infections caused by this opportunistic pathogen (Lowy, 1998). Ever since its discovery, *S. aureus* has become a very important pathogen, partly because of an increasing occurrence of antibiotic resistant strains. Its ability to adapt to various different environments, and its large arsenal of virulence factors are also a reason for the increasing relevance of *S. aureus* in human medicine (Zecconi & Scali, 2013).

### 1.1.1 Antibiotic resistance in *S. aureus*

*S. aureus* is fundamentally susceptible to antibiotics, but the bacteria has proven to be extremely adept at developing resistance short time after new antimicrobial treatments are introduced (Deurenberg & Stobberingh, 2008; Livermore, 2000). This is a huge concern given that antibiotics is the primary treatment against bacterial infections (Koch et al., 2014). The mortality rate of infections caused by *S. aureus* was approximately 80% in the early 1940s but decreased substantially upon the development of penicillin. However short time after the introduction of this  $\beta$ -lactam antibiotic, the first penicillin resistant strains were reported (Deurenberg & Stobberingh, 2008). The bacteria had started to express  $\beta$ -lactamase which inactivated the penicillin antimicrobial molecules and subsequently inhibited it from attacking the bacterial penicillin-binding proteins (PBPs) (Kranjec et al., 2021; Lowy, 2003).

Soon after the introduction of penicillin, other natural antibiotics were developed, including chloramphenicol, erythromycin, streptomycin and tetracycline (Livermore, 2000). Unfortunately, resistant *S. aureus* emerged quickly. In addition, widespread use of a  $\beta$ -lactamase-resistant methicillin antibiotic resulted in the development of several strains that are resistant to a wide range of  $\beta$ -lactam antibiotics known as methicillin resistant *S. aureus*

(MRSA) (Koch et al., 2014). MRSA strains emerge through the acquisition of a *mecA* gene, which encodes for a penicillin-binding protein (PBP2b) with reduced affinity to  $\beta$ -lactams and results in resistance to most antibiotics of this class (Kranjec et al., 2021). Increased use of vancomycin due to the fact that this was the last remaining antibiotic to which MRSA strains were reliably susceptible, led to the emergence of vancomycin-intermediates (VISA) and vancomycin-resistant (VRSA) strains that were tolerant and resistant to vancomycin, respectively (Chambers & DeLeo, 2009).

The rising numbers of multi-resistant bacteria is an increasing problem because it leads to decreasing numbers of effective antibiotics (Koch et al., 2014). The emergence of resistant strains is partly due to increased use of antibiotics, which apply a selective pressure on bacteria. This selective pressure not only result in selective advantage of resistant isolates, but also facilitates to the acquisition of resistance genes through either horizontal gene transfer or through chromosomal mutations (Chambers & DeLeo, 2009).

*S. aureus* also has the ability to cause infections in forms of biofilms. This mode of life has been shown to also further increase the resistance to antibiotics and make treatment of infection even more problematic, as explained in **Section 1.2.2**.

### **1.1.2 Pathogenesis and virulence factors of *S. aureus***

*S. aureus* harbours countless virulence related genes which make it possible for the bacteria to infect and proliferate at various sites within a host. Infection caused by this highly virulent bacterium is initiated when the bacteria gains access to host tissues beyond the mucosal surface or skin (Liu, 2009). A breach in the tissue could be a consequence of a surgical wound or accidental tissue damage (Clements & Foster, 1999). The outcome of the infection is highly depending on the combination of virulence factors, the site of infection and the host immune response (Zecconi & Scali, 2013). *S. aureus* is known, but not limited, to cause infections such as bacteraemia, endocarditis, sepsis, toxic shock syndrome, skin and soft tissue infections (SSTIs), osteomyelitis and pulmonary infections (Lowy, 1998; Tong et al., 2015).

During infection, the bacteria meet the immune reaction of the host. It is essential for its survival that the staphylococci harbours protective mechanisms which allows it to escape or counteract the immunological agents (Pollitt, Szkuta, Burns, & Foster, 2018). *S. aureus* has a large arsenal of efficient strategies to evade host defences in order to colonize and invade human and animal tissues. These mechanisms include modifications of structural components and

secretion of a large array of immune-modulating proteins which can counteract the immune defence or create a microenvironment that enables better survival (Zecconi & Scali, 2013). In addition, *S. aureus* can survive within cells. Only a few of the factors that contribute to the bacterial pathogenesis are mentioned here, and *S. aureus* can express many other mechanisms. The production of virulence factors is carefully controlled in response to cell density, energy availability and environmental signals. The best known regulator of *S. aureus* colonization and virulence is the Agr quorum sensing two-component system, which is known to regulate the expression of secreted proteins and surface proteins depending on the population density (Novick, 2003).

A key virulence mechanism of clinical significance is the biofilm formation ability of *S. aureus*. Biofilms allow *S. aureus* to persist on plastics and resist host defences as well as antibiotics (Liu, 2009). *S. aureus* is particularly adept at infecting medical devices within the human host. This includes infections of for example prosthetic heart valves, catheters and contact lenses (Donlan & Costerton, 2002). Indwelling medical devices are particularly exposed to biofilm formation due to their surface material, which facilitate bacterial adhesion (Kranjec et al., 2021).

## **1.2 Biofilm**

The biofilm mode of life allows bacteria to live as sessile bacteria in a community embedded in a self-produced extracellular matrix. The matrix of the biofilm facilitates attachment to a surface or cell-to-cell attachment (Donlan & Costerton, 2002; Fitzpatrick, Humphreys, & O'Gara, 2005; Kranjec et al., 2021).

### **1.2.1 Structure and composition of biofilms**

For a long time, the ability to form biofilm was considered an attribute only carried by a few species, but our knowledge today leads us to believe that this is a much more universal aspect among microorganisms (Wermser & Lopez, 2018). The formation of biofilm gives microorganisms a lifestyle that is entirely different from the planktonic state. In a biofilm, cells live in communities embedded in a self-produced extracellular matrix (ECM) made of extracellular polymer substances (EPS) (Chiba, Sugimoto, Sato, Hori, & Mizunoe, 2015). The ECM is mainly composed of EPSs like proteins, nucleotides (ex. extracellular DNA, eDNA) and polysaccharides, but can also contain lipids and other biopolymers. These substances

provide the biofilm with mechanical stability, mediate adhesion to abiotic or biotic surfaces and constructs a three-dimensional polymer network that interconnects and immobilizes microorganisms. In most biofilm, the matrix account for up to 90% of the total dry mass, whereas the microorganisms account for less than 10% (Flemming & Wingender, 2010). In addition, the dry mass only makes a small proportion of the total biomass, whereas water can account for up to 90% of the total mass. (Chiba et al., 2015; Flemming & Wingender, 2010). Dead cells have been observed in some biofilms. This suggest that content from lysed cell can be part of the extracellular matrix (Steven S. Branda, Vik, Friedman, & Kolter, 2005).

Properties of biofilms is greatly affected by both species or strain identity and dramatic differences in the biofilm architecture can result from small changes in the environmental conditions. Both concentration, cohesion, charge, sorption capacity, specificity, the nature of the individual components of EPS, and the three-dimensional architecture of the matrix are factors or characteristics that may have an impact on the final biofilm structure. Differences in the biofilm structure appear to reflect differences in the composition of the extracellular matrix. Biofilms can therefore seem smooth and flat, rough, fluffy or filamentous, and the degree of porosity can vary (Steven S. Branda et al., 2005; Flemming & Wingender, 2010)

### **1.2.2 Attributes of biofilms**

The extracellular matrix has diverse functions which helps the biofilm to maintain a structural integrity and let it adapt to surrounding environments. An example of the attributes of the matrix, is that it acts like a physical barrier that separate the cells embedded in the three-dimensional architecture from the surrounding environments (Wermser & Lopez, 2018). The barrier may give the matrix protective properties, that can reduce penetration of antimicrobial agents. Antimicrobial molecules must be able to diffuse through the biofilm matrix in order to inactivate encased cells. However, the diffusional barrier formed by the matrix can either decrease the transport rate of the antimicrobial agent to the inside of the biofilm or influence the reaction of the antimicrobial material with the matrix material (Donlan & Costerton, 2002). As a result of the reduced transport of antimicrobials, cells can be exposed to subinhibitory concentrations which may lead to activation of antimicrobial resistance mechanisms and also act as a reservoir for the accumulation of enzymes with the ability to inactivate antibiotics (Kranjec et al., 2021).

Due to the protective properties of the matrix against antimicrobial agents, biofilms formed by pathogens, like *S. aureus*, can develop a higher resistance to a wide variety of

antimicrobial agents in contrast to their planktonic counterparts (Chiba et al., 2015; Wermser & Lopez, 2018). Infections in forms of biofilms can therefore be more problematic to eradicate once they are established on infected tissues or medical devices. This will often result in a more intractable and chronic infection (Chiba et al., 2015). The ECM can also protect the biofilm cells from other external threats like the host immune system, in addition to give protection against desiccation, oxidizing or charged biocides, metallic cations, ultraviolet radiation, and some protozoan grazers (DeFrancesco et al., 2017; Flemming & Wingender, 2010).

Another attribute of the biofilm is its heterogeneous nature, which can be explained at several levels. One is that a biofilm can be composed of phenotypically distinct subpopulation due to the variable extracellular conditions that cells are exposed to (López, Vlamakis, & Kolter, 2010). The gene expression of bacteria embedded in a biofilm can both vary based on the cells position in the biofilm and over time. Through the course of the biofilm growth, local chemical differences of nutrient, signalling compounds and bacterial waste concentrations might occur due to the metabolic activities of the cells and diffusional processes. The physiological response of the bacteria will therefore lead to distinct metabolic and phenotypic attributes throughout the biofilm (Stewart & Franklin, 2008). *S. aureus* for instance has been shown to form biofilms containing cells in four different states. Cells located close to the surface of the biofilms, where oxygen is available, performed aerobic respiration. At the membrane interface in the bottom of the biofilm, bacteria were growing fermentatively due to lack of oxygen. In addition, a layer in the biofilm contained dormant cells which were metabolically inactive. Furthermore, the biofilm population also constitute dead cells (Rani et al., 2007). Because many antimicrobial agents target the metabolic pathways of the infective bacteria, they require the bacteria to be actively growing. Dormant cells are therefore more tolerant to certain antimicrobials because they are characterized by a low metabolic activity and a slow growth phenotype (Kranjec et al., 2021).

### **1.2.3 Formation of biofilms in *S. aureus***

*S. aureus* is known as a prolific biofilm former (Kranjec et al., 2021). The formation of *S. aureus* biofilms starts with the attachment of planktonic cells to abiotic or biotic surfaces (Moormeier & Bayles, 2017). For the adherence to biotic surface areas, the bacteria require the use of cell wall-anchored (CWA) proteins, including those of the family of microbial surface components that recognize adhesive matrix molecules (MSCRAMMs) (Cucarella et al., 2001; Moormeier & Bayles, 2017). These molecules establish non-covalent interactions with host tissue or host

proteins that coat the surface of medical devices (Le, Dastgheyb, Ho, & Otto, 2014). Several of the MSCRAMMs, *S. aureus* utilize for surface attachment, share a common LPXTG motif that anchors it to the cell wall, but have different binding capacities to host cell proteins (e.g. fibronectin, collagen and fibrinogen) (Foster & Höök, 1998). Teichoic acids have also been shown to play an important role in bacterial attachment of abiotic surfaces. Teichoic acids are polymers of glycerol phosphate or ribitol phosphate that are attached to the cell membrane (lipoteichoic acids) or cell wall (wall teichoic acids). The net negative charge of these components mediates adhesion to surfaces, and is important in the initial steps of biofilm formation (Gross, Cramton, Götz, & Peschel, 2001). Finally, release of eDNA due to the activity of cell wall degrading peptidoglycan hydrolases (including the major hydrolase Atl) can also display an important role in the adherence to surfaces (Kranjec et al., 2021).

Traditionally, the attachment stage is thought to be followed by a maturation and eventually a dispersion/detachment step. However, it has been proposed that two additional steps, multiplication and exodus, are included after the initial attachment and before the maturation (see **Figure 1.1**) (Moormeier & Bayles, 2017; Schilcher & Horswill, 2020). During the multiplication step, adherent cells begin to divide and accumulate. Because daughter cells are vulnerable to detachment, *S. aureus* are known to produce a variety of factors to help stabilize cell-to-cell interactions (Moormeier & Bayles, 2017). Shortly after the division and accumulation of cells have started, the additional stage, exodus, lead to secretion of nucleases that will digest eDNA and result in detachment and migration of a subpopulation of biofilm-associated cells (Kranjec et al., 2021).

During the maturation stage of the biofilm formation cycle, large levels of extracellular polymer substances are formed. These structures allow for cells to accumulate in multiple layers and form the three-dimensional structure (Kranjec et al., 2021). The structures that are formed during this stage (e.g. channels and mushroom-shaped structures) provide increased surface area for nutrient exchange and waste removal for deeper layers of the biofilm (Le et al., 2014; Moormeier & Bayles, 2017). The staphylococcal intercellular adhesin (PIA), which is produced by the *icaABCD* operon, has been shown to be very important for the intercellular adhesion step and is required for biofilm formation in many cases (Steven S. Branda et al., 2005; Kranjec et al., 2021).

*Staphylococcus aureus* can also form biofilm in a *ica*- or polysaccharide-independent manner (Foster, Geoghegan, Ganesh, & Höök, 2014). This pathway often rely on protein-mediated intercellular adhesion instead (Kranjec et al., 2021). *S. aureus* has been known to

harbour biofilm-associated proteins (Bap), surface protein G (SaG) and fibronectin-binding protein A (FnBPA). These proteins are found anchored to the cell wall of *S. aureus* and serve to hold cells together within the biofilm, probably through interaction with other proteins on the surface of neighbouring cells (López et al., 2010).

During the last stage of biofilm formation cycle, EPS components is degraded in order to allow bacteria to detach from the biofilm (Kranjec et al., 2021). Dispersal is known to be mediated by various components including nucleases, proteases or phenol-soluble modulins (PSMs) with surfactant properties. Nucleases (e.g. Nuc1 and Nuc2 for *S. aureus*) may be especially important during biofilm detachment when eDNA is one of the main components, meanwhile protein biofilms are susceptible to protease-mediated biofilm dispersal (Kranjec et al., 2021; Schilcher & Horswill, 2020). The PSM most likely participates in the dispersal of biofilm by disrupting noncovalent interactions between matrix components (Schilcher & Horswill, 2020). It is believed that Agr-mediated quorum sensing regulate the dispersal of *S. aureus* biofilms. The Agr system reacts to increased cell density and the accumulation of signal molecules called autoinducers (Moormeier & Bayles, 2017).

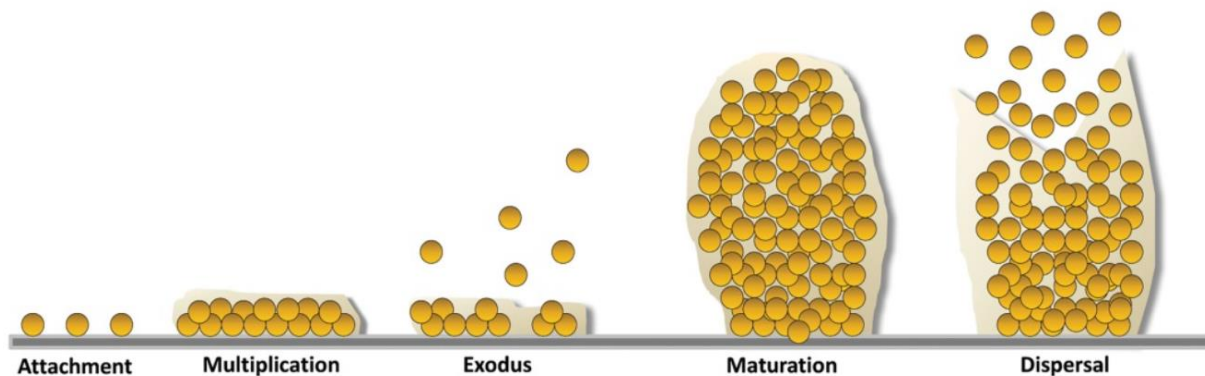


**Figure 1.1** Illustration of the five stages of biofilm formation of *S. aureus*. *S. aureus* biofilms starts with the attachment of planktonic cells to abiotic or biotic surfaces, followed by a multiplication stage where adherent cells begin to divide and accumulate while producing factors which facilitate cell-to-cell adhesion. During exodus, a subset of cells detaches and migrate from the biofilm. Large levels of extracellular matrix components are produced in the maturation stage to allow cells to accumulate in multiple layers and form three-dimensional biofilm structures. In the last stage, EPSs are degraded by nucleases, proteases and/or phenol-soluble modulins to allow dispersal of biofilm-associated cells. Figure is from Moormeier and Bayles (2017).

## 1.3 Menaquinone and metabolism in *S. aureus*

### 1.3.1 Respiration and fermentation in *S. aureus*

*S. aureus* has a remarkable ability to adapt to challenges presented by diverse environments, which allows the bacteria to colonize and invade various niches within the host (Fuchs, Pané-Farré, Kohler, Hecker, & Engelmann, 2007; Hammer et al., 2013). Because oxygen levels vary among different sites, oxygen could have been a limiting factor for bacterial survival and proliferation during an infection. However, *S. aureus* overcomes this challenge by being able to respire aerobically when oxygen levels are high, but also being capable of performing anaerobic respiration or fermentation when oxygen levels are deprived (Fuchs et al., 2007).

Respiration is a fundamental process of living organisms which involves generation of energy in forms of ATP by oxidative phosphorylation (Richardson, 2000; Simon, van Spanning, & Richardson, 2008). ATP production during respiration occurs through oxidation of dinucleotides such as NADH and FADH<sub>2</sub>, which donates electrons to the electron transport chain in the cell-membrane (Proctor, 2019). Reduced forms of dinucleotides are obtained from catabolic reactions in the glycolysis or the TCA cycle (Simon et al., 2008). Here, electrons are extracted from organic carbon (e.g. glucose or simple sugars) through several reactions and passed on to NAD<sup>+</sup> and FAD<sup>+</sup> which is reduced to NADH and FADH<sub>2</sub> (Proctor, 2019). The dinucleotides are then used by the first protein complex of the electron transport chain, where the electrons are passed on to quinones and then onto cytochromes as terminal oxidases (Proctor, 2019; Simon et al., 2008). The free energy that is released during this electron transfer process is used to generate a proton motive force across the membrane (Simon et al., 2008). This proton motive force or proton gradient is then used to drive the synthesis of ATP (Simon et al., 2008).

In aerobically respiring bacteria, oxygen is required in order to produce a proton gradient along the electron transport chain. The electrons are at last transferred to a terminal electron acceptor, oxygen, which is turned in to water (Hammer et al., 2013). Some bacteria, including *S. aureus*, have the opportunity to utilize alternative terminal electron acceptors when oxygen is not available, e.g., at a site of infection where oxygen levels gradually decrease. *S. aureus* have developed the ability to use nitrate and other similar nitrogen-containing compound as terminal electron acceptors (Balasubramanian, Harper, Shopsis, & Torres, 2017; Fuchs et al., 2007). When the bacteria both lack oxygen and an alternative terminal electron acceptor, fermentation is the only option (Hammer et al., 2013). During fermentation, the product of glycolysis, pyruvate, is not further oxidized to acetyl-CoA and TCA-cycle intermediates, but

instead reduced to lactate or other organic acids. The purpose of this is to generate  $\text{NAD}^+$  to be used for continued glycolysis. During fermentation, ATP is thus only formed by substrate-level phosphorylation during glycolysis and even though the cell does not produce as much ATP as aerobic and anaerobic respiration; the bacteria still generate enough energy to support growth and proliferation. It should be noted that the bacteria grow relatively slow. The reason is that ATP is required for many metabolic processes in the bacteria, including the synthesis of cell wall components which is needed for bacterial growth and multiplication (Proctor, 2019).

### **1.3.2 Menaquinone and the menaquinone biosynthetic pathway**

In order to drive aerobic and anaerobic respiratory electron transport a diverse range of inorganic and organic substrates can be used to donate and accept electrons (Proctor, 2019). Electrons cannot exist in aqueous solutions and their transfer from  $\text{NADH}$  or  $\text{FADH}_2$  to oxygen requires a set of carrier proteins embedded in the cell membrane (McNamara & Proctor, 2000). Quinones, which are small, freely diffusible, lipophilic, membrane-entrapped organic molecules, function as a link between electron donating enzymes and the electron accepting enzymes (Proctor, 2019). Quinones are required to donate electrons to haem molecules located within cytochromes in the electron transport chain. Many bacteria can synthesize more than one type of quinone, however *S. aureus* has been shown to utilize only a quinone called menaquinone (Wakeman et al., 2012). In *S. aureus*, menaquinone is the first electron acceptor in the electron transport chain and is responsible for accepting electrons directly from  $\text{FADH}_2$  or from a  $\text{NADH}$  oxidase complex and send them to other carrier proteins in the cell membrane. The funnelling of electron pairs from  $\text{NADH}$  and  $\text{FADH}_2$  through multi-subunit carrier proteins embedded in the cell membrane leads to the transport of protons from within the cells to the outside of the cells. The energy from this gradient is harnessed to form ATP, which is generated by the addition of an inorganic phosphate to ADP. This reaction is catalysed by a  $\text{F}_0\text{F}_1$ -ATPase (McNamara & Proctor, 2000). Because menaquinone is the first electron acceptor in the chain of molecules that receives electrons from  $\text{FADH}_2$  or a  $\text{NADH}$  oxidase complex, it is needed for the bacteria to be able to respire (Bentley & Meganathan, 1983; McNamara & Proctor, 2000). Without the shuttling of protons, the gradient would collapse and ATP synthesis would cease (Boersch, Rudrawar, Grant, & Zunk, 2018).

Menaquinone (MK), also known as vitamin  $\text{K}_2$  has a 2-methyl-1,4-napthoquinone structure with an isoprenoid side chain attached to the 3-position (**Figure 1.2**) (Panthee, Paudel, Hamamoto, Uhlemann, & Sekimizu, 2020a). The isoprenoid chain is composed of repeating

isoprene (5-carbon) units and can vary in length depending on the number of repetitions of this unit. Different forms of MK are generally referred to as MK-n, where n stands for the number of 5-carbon units in the structure (Kurosu & Begari, 2010). Which MK variant a bacterium contains is species-specific and can also vary within the same organism (Götz & Mayer, 2013; Kurosu & Begari, 2010). MKs with side chains between 7 and 9 are found in *S. aureus*, with MK-8 being the most predominant (Panthee, Paudel, Hamamoto, Uhlemann, & Sekimizu, 2020b).

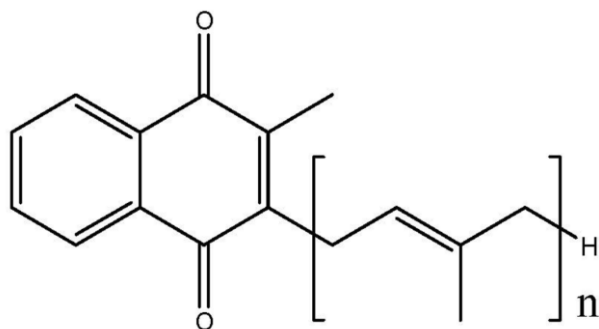


**Figure 1.2** Chemical structure of menaquinone (MK-n). MK has a 2-methyl-1,4-naphtoquinone structure with an isoprenoid side chain of varying length attached to the 3-position. The n refers to the number of repeating 5-carbon units that makes the isoprenoid side chain. The figure is taken from Szterk, Bus, Zmysłowski, and Ofiara (2018)

MK in *S. aureus* is synthesised through several reaction steps catalysed by various enzymes as seen in **Figure 1.3**. The first precursor of the synthetic pathway of MK is chorismate, which is derived from the Shikimate pathway, a pathway which links metabolism of carbohydrates to biosynthesis of aromatic compounds (Herrmann & Weaver, 1999). The gene *aroC* together with *aroB* and *aroK* is required for the synthesis of chorismate. Through six enzyme-catalysed stages (encoded by *menFDHCEB*), chorismate is converted to form the quinone skeleton 1,4-dihydroxy-2-naphtaloate-CoA (DHNA-CoA). A yet unknown men enzyme hydrolyses this skeleton creating DHNA. Further, 1,4-dihydroxy-2-naphtoate octaprenyl transferase encoded by *menA*, decarboxylates and prenylates the DHNA with products from the isoprenoid biosynthetic pathway to form dimethylmenaquinone (DMK) (Dawson, Fyfe, Gillet, & Hunter, 2011; Kurosu & Begari, 2010; Wakeman et al., 2012). In the isoprenoid biosynthesis, isoprenoids are synthesised from a five-carbon starter unit isopentenyl pyrophosphate (IPP) (Balibar, Shen, & Tao, 2009). NWMN\_1381 and *hepT* codes for the enzyme responsible for the production of the isoprenyl lipid chain. In the last step of the MK pathway, *ubiE* is predicted to encode an S-adenosylmethionine:2-DMK methyltransferase

responsible for catalysing the step in which a methyl group is attached to DMK (Wakeman et al., 2012).

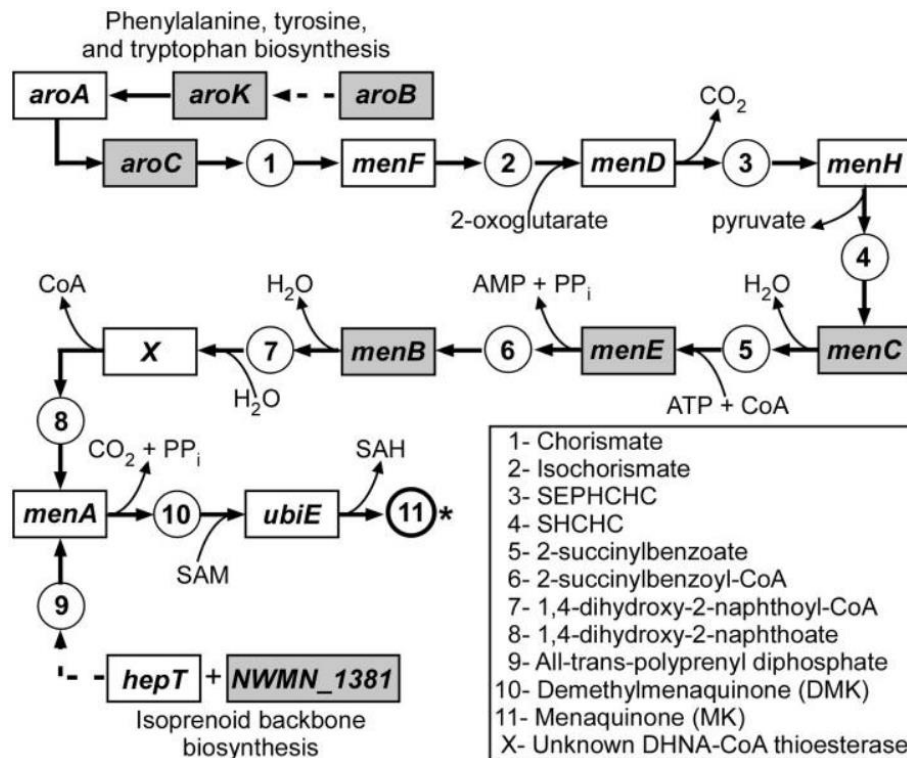


**Figure 1.3** A schematic overview of the menaquinone biosynthetic pathway in *S. aureus*. The figure illustrates the different genes that are included in the biosynthesis and in which reactions they participate in. Figure from Wakeman et al. (2012).

### 1.3.3 The two-component regulatory systems, SaeRS and SrrAB, responds to changes in the respiratory metabolism in *S. aureus*.

The ability of a bacteria to survive, grow and persist at a specific site is partly due to its ability to sense and respond to changes in different environmental conditions. Two-component systems (TCSs) are examples of regulatory pathways that gives the bacteria its adaptive character. These regulatory systems can recognise and interpret signals and lead to activation or repression of gene transcription (Ann M. Stock, Victoria L. Robinson, & Goudreau, 2000; Stephenson & Hoch, 2002). Several *S. aureus* TCSs are involved in the regulation of transcriptional activation or repression of virulence associated genes, including SaeRS and SrrAB which is believed to govern fermentative biofilm formation (Mashruwala, Gries, Scherr, Kielian, & Boyd, 2017a; Tiwari et al., 2020). SrrAB-dependent biofilms are formed upon the accumulation of reduced menaquinone as a result of decreased or impaired respiration. It has been suggested that this is partially because the SrrAB system increase the expression of a

peptidoglycan hydrolase (Atl), and decreased expression of wall teichoic acids (WTA) which leads to increased programmed cell lysis. Programmed cell lysis further leads to the release of cellular polymers that are utilized to form biofilms (Mashruwala et al., 2017a; Mashruwala, Guchte, & Boyd, 2017b). The SaeRS TCS also have an impact on the biofilm formation rate of *S. aureus* when cellular respiration is impaired. In contrast to SrrAB, the SaeRS system is stimulated by yet unidentified signal molecule(s). However, it is known that SaeRS and SrrAB influence biofilm formation independently of one another. The activation of SaeRS leads to increased expression of Atl and FnBPA, and thus lead to increased cell lysis and biofilm formation (Mashruwala et al., 2017a).

## **1.4 Tools and techniques used to study biofilm in this work**

### **1.4.1 Macrocolonies**

Several different models have been applied in order to study bacterial biofilms. Among them is the use of bacterial colonies grown on the surface of agar solidified media, commonly called macrocolonies (Steven S. Branda et al., 2005). The morphological characteristics of macrocolonies can vary greatly from very structured colonies with wrinkles, elongated folds and ridges and/or concentric ring patterns to less structured colonies with a smooth and flat phenotype. It has been confirmed that the ability of bacteria to form highly structured macrocolonies are correlated to the ability of a cell to produce an extracellular matrix (Steven S. Branda et al., 2005; Serra, Klauck, & Hengge, 2015). Because the final composition of the extracellular matrix of biofilms are affected by environmental regulations and sometimes mutational variations, macrocolonies is a highly suitable technique to study biofilm formation (Mashruwala et al., 2017b; Serra & Hengge, 2014).

The macrocolony model have been used to study biofilm formation in a variety of bacteria, including *Escherichia coli* (*E. coli*), *Bacillus subtilis* and *Vibrio fischeri* (S. S. Branda, González-Pastor, Ben-Yehuda, Losick, & Kolter, 2001; Serra et al., 2015; Yip, Geszvain, DeLoney-Marino, & Visick, 2006). Macrocolonies have also been developed as an alternative model to study biofilms in *S. aureus*. In this model, *S. aureus* are grown on agar plates supplemented with magnesium to form macrocolonies with distinct phenotypic traits (Wermser & Lopez, 2018). Chronic biofilm-associated infections of *S. aureus* have occurred in magnesium rich-niches, and it has been implied that high  $Mg^{2+}$  concentrations induce biofilm formation (Koch et al., 2014). This is believed to occur because  $Mg^{2+}$  binds teichoic acids of *Staphylococci* and lead to a rigid cell-wall. This inflexibility triggers the stress-induced  $\sigma^B$ -

factor that will eventually result in downregulation of *agr* and activate expression of biofilm related genes, and therefore result in formation of structured macrocolonies (García-Betancur et al., 2017; Koch et al., 2014).

#### **1.4.2 Crystal violet assay**

In 1985, Christensen et al. described a microtiter plate assay combined with crystal violet (CV) staining which could be used to quantify total biofilm mass of coagulase negative staphylococci (Christensen et al., 1985). Since its first discovery, the method has been modified and used to investigate biofilm formation in many different organisms and strains and is widely used for measuring biofilms in bacteria (Li, Yan, & Xu, 2003; Pitts, Hamilton, Zilver, & Stewart, 2003). Use of microtiter plates to study bacterial biofilms, can provide information about how the bacteria behaves when grown on inert surfaces typically found in natural aquatic environments or on medical devices such as catheters (Serra & Hengge, 2014). A standard CV protocol consists of growing bacteria in the bottom of a microtiter plate until biofilm has formed. Through several washing steps with saline and the staining of the biofilm with the use of CV, the total biofilm mass can be measured directly spectrophotometrically. The basic dye, crystal violet, binds to negatively charged extracellular molecules, including cell surface molecules (capsule) and polysaccharides in the matrices of mature biofilms (Steven S. Branda et al., 2005; Christensen et al., 1985; Stepanović, Vuković, Dakić, Savić, & Švabić-Vlahović, 2000) . Crystal violet has been used to distinguish adherent parental strains from adhesion-altered mutants and to rank strains by their adhesive properties. The dye does not distinguish viable cells from dead cells, and therefore the CV assay can be used to monitor the amount of biofilm but not functional biofilm (Pitts et al., 2003; Xu et al., 2016).

#### **1.4.3 Fourier-transform infrared spectroscopy**

Fourier-transform infrared (FTIR) spectroscopy is a spectroscopy method where the infrared (IR) absorption or emission spectrum of a solid, liquid or gas is measured. In this work, FTIR, is used to investigate differences in composition between macrocolony biofilms. This biophysical technique is based on obtaining information about the chemical profile of a given sample exposed to light in the IR region of the electromagnetic spectra, which extends from the visible region to the microwave region (Naumann, 2000). When light of the IR region irradiates a sample, vibrating molecular bonds within that sample can absorb energy at certain vibration frequencies. A detector collects the transmitting light IR beam and produces a raw signal. The

values that are observed for certain bands can be used to identify complex vibrational and rotational movements which may correlate to single bonds or functional groups of a molecule within the sample (Schmitt & Flemming, 1998). Because of this, FTIR can be used to detect phenotypic chemical consequences of genetic changes in microorganisms (Naumann, Helm, & Labischinski, 1991).

In contrast to other IR spectroscopy methods, which use graters and/or prisms, the FTIR spectrometer uses a so-called interferometer. Among other things, this contains a beam splitter and a moving mirror which makes it possible to create a signal that contains spectral information of all wavelengths. The interferogram, which is obtained by the raw signal, can be mathematically Fourier transformed in order to sort out the individual frequencies and get the final representation of an IR spectrum (Naumann, 2000; Schmitt & Flemming, 1998).

By measuring the light intensity before and after passage through the sample, an IR spectrum can be obtained. This kind of spectrum shows the quantity of the transmittance or the absorbance as a function of wavenumbers. Wavenumbers is the number of waves per centimetre ( $\text{cm}^{-1}$ ), usually the values range from  $10\,000\text{ cm}^{-1}$  to  $10\text{ cm}^{-1}$  throughout the IR region of the electromagnetic spectrum. This is directly proportional with the absorbed energy. Characteristic bands with information about functional groups of peptides and protein structures, polysaccharides, phospholipids and of nucleic acids can normally be observed in the spectrum in the region between  $4000$  and  $500\text{ cm}^{-1}$  (Naumann, 2000; Schmitt & Flemming, 1998). The region between  $3000$ - $2800\text{ cm}^{-1}$  provides information on the lipid skeleton, length and unsaturation of lipid carbon chains. Wavenumbers related to total lipid content, and information about ester bond ( $\text{C}=\text{O}$ ) is obtained in the region between  $1800$ - $1700\text{ cm}^{-1}$ . Information about protein, Amide I, II and III is provided by wavenumbers between  $1700$ - $1500\text{ cm}^{-1}$  (Dzurendova et al., 2020).

It can be difficult to extract relevant information from measured data by only inspecting the IR spectra itself (Rajalahti & Kvalheim, 2011). This is partly because each sample is described with thousands or hundreds of variables and the fact that often only small spectral variations separate different bacterial strains in the IR spectrum. Various mathematical and statistical tools have therefore been developed in order to further analyse the spectral information (Rajalahti & Kvalheim, 2011; Schmitt & Flemming, 1998). A principal component assay (PCA) is an example of a mathematical algorithm which is used to visualize the data from an FTIR-analysis (Ringnér, 2008). This technique is based on transformation of the original number of variables into a lower number of new variables or axes called principal components

(PC). The principal components that are derived from the data set are uncorrelated to each other and are designed to maximize the explained variance. Each object in the original data gets a score value on each PC, and can be presented in score plots, with the principal components as axes. By investigating the score values in a graphical score plot, the PCA can help reveal patterns like clusters, trends and outliers, in the data (Destefanis, Barge, Brugiapaglia, & Tassone, 2000; Rajalahti & Kvalheim, 2011). Each variable also gets a loading value on each PC which can be presented in a loading plot. This plot visualizes wavenumbers that represent bonds or functional groups that explain differences observed in the score plot. Therefore, a loading plot can be used in order to interpret patterns that are observed in the score plot (Rajalahti & Kvalheim, 2011).

As mentioned above, FTIR spectroscopy can be used for identification and characterization of microorganisms. The use of the FTIR approach was initially developed for analysing bacterial samples, but it was further applied for characterization of other microorganisms such as fungi, yeast, amoeba, and mammalian cells (Naumann et al., 1991). Several studies has also been conducted using FTIR-spectroscopy methods in order to characterize or identify microbial biofilms (Allen et al., 2004; Davies, Chakrabarty, & Geesey, 1993; Karadenizli, Kolayli, & Ergen, 2007). The extracellular matrix components of a biofilm contribute greatly to its structure and properties, therefore in the study of biofilm, identifying and determining the concentrations of such components will contribute with relevant information on the biofilm formation. The analysis of biofilm by FTIR spectroscopy gives information about the chemical composition of the matrix and the proportions of different EPS, as well as information about the cells embedded in the matrix (Di Martino, 2018; Lu, Al-Qadiri, Lin, & Rasco, 2011).

#### **1.4.4 Congo Red assay for biofilms**

Congo Red is an azo dye that has been used to distinguish biofilm-forming properties of staphylococci (Suzuki et al., 2012). In the study performed by Suzuki et al. (2012) it was observed that WTA protect *S. aureus* from anionic azo dyes, and that Congo Red can be used to detect altered levels of WTA on the bacteria due to an increased bactericidal effect against *S.aureus* mutants lacking WTA. As mentioned before, the cell wall of *S. aureus* is known to include two types of teichoic acids. The LTA glycopolymer is connected to the cytoplasmic membrane, while WTA is a glycopolymer anchored to the peptidoglycan layer (Xia, Kohler, & Peschel, 2010). Together they produce an interwoven polyanionic matrix through the

peptidoglycan (Suzuki et al., 2012). The teichoic acids have mainly three functions as components of the cell wall. They contribute to protection against harmful molecules and environmental stresses, they facilitate receptor and surface binding, and lastly they control enzyme activity and cation concentration in the cell envelope (Xia et al., 2010). The findings from the study by Suzuki et al. (2012) showed that Congo red is useful as a WTA determinant in different mutants strain of *S. aureus* and is also utilized in the current work.

### **1.5 Main objectives of this study**

Biofilm-associated infections caused by *S. aureus* are challenging to eradicate with the treatments methods and antibiotics which are available today. The ECM of the biofilm protects the cells in the biofilm from external threats like antimicrobial agents and the host immune system. Because biofilm formation is a highly regulated process, it is of great interest to identify and study genes that participate in and affect the biofilm formation of this Gram-positive bacteria in order to identify new potential treatment methods. Menaquinone is an electron carrier involved in the electron transport chain of respiring *S. aureus*, and in a previous project, the gene *ubiE*, encoding the last enzyme in the menaquinone biosynthetic pathway, was shown to affect biofilm macrocolony formation in this bacterium.

The main objectives of this study have therefore been to explore and understand how and why genetic alterations in the menaquinone synthesis pathway results in altered biofilm formation of *S. aureus*.

The specific objectives were to:

- Characterize and perform complementation studies of the *S. aureus* Newman *ubiE* deletion strain.
- Analyse how metabolism affect biofilm formation by studying the morphological characteristics of *S. aureus* biofilm macrocolonies for knockdown and knockout mutants targeting genes involved in menaquinone biosynthesis (*ubiE*, *aroC*, *menA*, *menF* and *menE*).
- Determine the chemical composition of the extracellular matrix of *S. aureus* biofilm macrocolonies and understand how changes in the menaquinone pathway affect the extracellular matrix. This part of the project involved setting up and optimizing FTIR spectroscopy methods and quantification of components from ECM extracts.

## 2 Materials

### 2.1 Strains

**Table 2.1** *S. aureus* and *E. coli* strains used in this work, with a brief description of their relevant genotype and characteristics.

Strain	Genotype and characteristics	Reference
<b><i>S. aureus</i></b>		
Newman	wild-type	(Duthie & Lorenz, 1952)
MH226	Newman pLOW-dCas9_extra_lacO, Ery <sup>R</sup>	Lab collection
HO18	Newman $\Delta ubiE$ , pLOW- <i>ubiE</i> , Ery <sup>R</sup> , Spec <sup>R</sup>	This work
HO19	Newman $\Delta ubiE$ , pLOW- <i>ubiE_hepT</i> , Ery <sup>R</sup> , Spec <sup>R</sup>	This work
HO21	Newman $\Delta ubiE$ , pLOW-lacA-m(sf)gfp, Ery <sup>R</sup> , Spec <sup>R</sup>	This work
HO28	MH226 pVL2336-sgRNA:: <i>menA</i> , Ery <sup>R</sup> , Cam <sup>R</sup>	This work
HO29	MH226 pVL2336-sgRNA:: <i>menF</i> , Ery <sup>R</sup> , Cam <sup>R</sup>	This work
HO30	MH226 pVL2336-sgRNA:: <i>gfp</i> , Ery <sup>R</sup> , Cam <sup>R</sup>	This work
MK1599	MH226 pVL2336-sgRNA:: <i>menE</i> , Ery <sup>R</sup> , Cam <sup>R</sup>	Lab collection
MK1748	Newman $\Delta aroC$ , Spec <sup>R</sup>	Lab collection
MM155	Newman $\Delta ubiE$ , Spec <sup>R</sup>	Lab collection
<b><i>E. coli</i> strains carrying plasmids</b>		
IM08B	DH10B, $\Delta dcm$ , Phelp-hsdMS, PN25-hsdS (strain expressing the <i>S. aureus</i> CC8 specific methylation genes), Amp <sup>R</sup>	(Monk, Tree, Howden, Stinear, & Foster, 2015)
HO4A	IM08B pLOW- <i>ubiE_hepT</i> , Amp <sup>R</sup>	This work
HO12	IM08B pLOW- <i>ubiE</i> , Amp <sup>R</sup>	This work
HO22	IM08B pVL2336-sgRNA:: <i>menF</i> , Amp <sup>R</sup>	This work
HO27	IM08B pVL2336-sgRNA:: <i>menA</i> , Amp <sup>R</sup>	This work
MH198	IM08B pLOW_dCas9_extra_lacO, Amp <sup>R</sup>	Lab collection
MK1518	IM08B pVL2336_mCherry, Amp <sup>R</sup>	Lab collection
MM172	IM08B pVL2336-sgRNA:: <i>gfp</i> , Amp <sup>R</sup>	Lab collection
MK1435	IM08B pLOW-SA1866_long-m(sf)gfp (hele), Amp <sup>R</sup>	Lab collection
DMA017	IM08B pLOW-2861, Amp <sup>R</sup>	Lab collection
IM33	IM08B pLOW-lacA-m(sf)gfp, Amp <sup>R</sup>	Lab collection

## 2.2 Primers

**Table 2.2** List of primers used in this work, including the 5'-3' nucleotide sequence and a short description.

Name	Sequence 5'-3'	Description	Reference
HSO001	CGCAGACGATACTTGCTGCA	R	This work
HSO002	CAGGAGAATCACATGGACCTCAA	F	This work
HSO003	GTAGAGGTAATTAAGCATGGCTGAC	F	This work
HSO004	GGCGTATCAGAATATGAATCCAT	F	This work
HSO005	CTTTATAGCCAAGGTGCATTGC	R	This work
HSO006	AAGTAGTGATTTCCGGATGTCCATC	R	This work
HSO007	TAACCATGCATCACGTGGTG	R	This work
Dma007	CCGGAGGTGTAGCATGTCTCA	F	Lab collection
Dma008	GGCTTAACTATGCGGCATCAG	R	Lab collection
Dma105	GGAGGTGACAGGAGGAAATTTAAATGGCTGA CAATAAAGCAAATAAAGAG	F	Lab collection
Dma106	ACGCGCGGCCGCTTAATCACCTTTGGTATTATC TTTTTCTTTATAGCCAAGG	R	Lab collection
Dma113	ACTCTGCGCCGCTACGTGTTTCTTGAACCCA TTTTTTTC	R	Lab collection
Dma114	GGAGGTGACAGGAGGAAATTTAAATGGAAAC AACTGTTAGCAAATTGGA	F	Lab collection
Dma115	AATGGAATTGCCGTTTGAAGAC	F	Lab collection
Dma116	ATGGCCGTTAAAGATAATCGTGTAC	F	Lab collection
MK25	AAATCTCGAAAATAATAGAGGGA	R	Lab collection
MK26	GGATAACCGTATTACCGCCT	F	Lab collection

## 2.3 Antibiotics

**Table 2.3** List of antibiotics used in this work, with information about Stock solution and suppliers.

Antibiotic	Stock solution	Product number	Supplier
Ampicillin	100 mg/ml	A-9518	Sigma-Aldrich
Chloramphenicol, C <sub>11</sub> H <sub>12</sub> Cl <sub>2</sub> N <sub>2</sub> O <sub>5</sub>	10 mg/ml	C0378	Sigma-Aldrich
Erythromycin, C <sub>37</sub> H <sub>67</sub> NO <sub>13</sub>	5 mg/ml	E6376	Sigma-Aldrich
Spectinomycin	100 mg/ml	S9007-5G	Sigma-Aldrich

## 2.4 Chemicals

**Table 2.4** List of chemicals used in this work.

Chemical	Product number	Supplier
1 kb DNA ladder		New England BioLabs
Agar powder		Merck
Agarose	15510-027	Invitrogen
Bacto™ Brain heart infusion	237200	BD Diagnostics
Bacto™ Tryptic soy broth	286220	BD Diagnostics
Bacto™ Yeast Extract		BD Diagnostics
BsmBI	R0580	NewEngland BioLabs
Congo Red	C0378	Sigma-Aldrich
Crystal violet	340244K	BDH Laboratory Supplies
DMSO	D8418-50ml	Sigma-Aldrich
dNTPs	N0447	NewEngland BioLabs
EDTA, C <sub>10</sub> H <sub>16</sub> N <sub>2</sub> Na <sub>2</sub> O <sub>8</sub> ·2H <sub>2</sub> O	20 296.360	VWR
Gel Loading Dye Purple (6X)	B7025S	New England BioLabs
Glucose, C <sub>6</sub> H <sub>12</sub> O <sub>6</sub>	10117gK	VWR
Glycerol, C <sub>3</sub> H <sub>8</sub> O <sub>3</sub>	1.04094.1000	Merck
Hydrochloric acid, HCl	30721	Riedel-De Haën
IPTG, Isopropyl-β-D-thiogalactosidase		Sigma-Aldrich
Isopropanol		VWR
Lysostaphin		Sigma-Aldrich
Lysozyme		Sigma-Aldrich
Magnesium chloride hexahydrate, MgCl <sub>2</sub> ·6H <sub>2</sub> O	63072	Fluka
NotI-HF	R3189	NewEngland BioLabs
peqGeen	PEQL37-501	Saveen Werner
Phusion® High-Fidelity DNA polymerase	M0530	NewEngland BioLabs
RedTaq® ReadyMix™	R2523	Sigma-Aldrich
RNase A		Sigma-Aldrich
SaII-HF	R3138	NewEngland BioLabs
Sodium chloride (NaCl)	1.06464.1000	Merck
Sodium dodecyl sulphate (SDS)		Merck
Sodium hydroxide, NaOH	1.06469	Merck
Sucrose, C <sub>12</sub> H <sub>22</sub> O <sub>11</sub>	102745C	BHD
T4 DNA ligase	M0202L	NewEngland BioLabs
Tryptone		BD Biosciences
Yeast extract	1.04086.0250	Merck

## 2.5 Kits

**Table 2.5** List of kits used in this work

Name	Product number	Supplier
NucleoSpin® Gel and PCR Clean-up	740609.250	Machnery-Nagel
E.Z.N.A.® Plasmid Mini kit I	D9643-02	Omega Bio-Tek

## 2.6 Equipment

**Table 2.6** Overview of equipment used in this work. Additional standard laboratory equipment was also used but is not listed in this table.

Equipment	Model	Supplier
96-well polystyrene microtiter plates	82.1581.001	Sarstedt
Electroporation system	Micropulser electroporator	BioRad
	Pulse controller	BioRad
FTIR (HTS-XT)	VERTEX 70 (High Throughput Screening eXTension)	Bruker Optics
Gel imager	GelDoc-1000	BioRad
Microplate reader	FLUOstar OPTIMA FL	BMG Labtech
	Synergy H1 Hybrid Reader	BioTek®
PCR machine	ProFlex PCR systems	Applied Biodynamics
Spectrophotometer	NanoDrop 2000	Thermo-Fischer Scientific
Stereomicroscope	AxioZoom. V16	Zeiss
ULTRA-TURRAX®	T25	IKA®

## 2.7 Recipes for growth mediums, buffers and solutions

### 1% Phosphate buffered saline (PBS)

3 g NaCl, 0,1006 g KCl, 0,890 g Na<sub>2</sub>HPO<sub>4</sub> and 0,1568 g KH<sub>2</sub>PO<sub>4</sub> were dissolved in 500 ml dH<sub>2</sub>O. pH was adjusted to pH=7,4. The solution was sterilised by autoclavation.

### 10xTEN-buffer

The 10x TEN (Tris-EDTA-NaCl) buffer contains 0.1 M Tris-HCl (pH 8.0), 0.01 M EDTA (pH 8.0) and 1 M NaCl.

### 50x TAE-buffer

50x TAE-buffer 242 g/L Tris-base, 7.4 g/L EDTA (pH 8.0) and 57 mL/L glacial acetic acid.

### **Brain Heart Infusion (BHI) medium**

Brain Heart Infusion-medium was prepared by dissolving 37 g BHI broth in 1 L dH<sub>2</sub>O and was sterilized by autoclaving. The media was stored at room temperature.

### **Lysogeny broth (LB)**

The Lysogeny broth medium was made by weighing 10 g/L of sodium chloride, 10 g/L of tryptone and 5 g/L of yeast extract. These were dissolved in distilled water to a volume of 1 L in total and sterilized by autoclaving. The media was stored at room temperature.

### **Tryptic Soy Broth (TSB)**

To make TSB media, 30 g of TSB (Tryptic soy broth) was weighted and dissolved in dH<sub>2</sub>O to a volume of 1 L. Media was sterilized by autoclaving and stored at room temperature.

### **Agar plates**

When media was used to make agar plates, 15 g/L of agar was added to the flasks of media before adding distilled water and autoclaving. The media was cooled down in 55 °C water bath until use. Antibiotics were added when necessary. This included spectinomycin (100 µg/ml), erythromycin (5 µg/ml), chloramphenicol (10 µg/ml) or ampicillin (100 µg/ml). 100 µM MgCl<sub>2</sub> was added to agar plates used for studying macrocolonies. The agar media was poured in petri dishes and let to dry, and then stored at 4 °C.

### **Staphylococcus lysis buffer**

Buffer used for lysis of *S. aureus* was prepared by dissolving NaOH in dH<sub>2</sub>O and mix with SDS to make a final solution containing 40 mM NaOH and 0,2% SDS.

## 3 Methods

### 3.1 Growth and storage of *S. aureus* and *E. coli*

Growth of bacteria on plates was done in incubators at 37 °C. For liquid cultures the bacteria were grown at 37 °C with shaking. Bacteria grown under anaerobic conditions were incubated in anaerobic jars. Oxygen was removed using anaerobe atmosphere generating bags. *E. coli* strains were grown in liquid LB media or on LB plates, with 100 µg/ml ampicillin for selection when appropriate. *S. aureus* was either grown with TSB or BHI medium on agar plates or in liquid media. When appropriate, antibiotics were added in the following concentrations: 5 µg/ml erythromycin, 100 µg/ml spectinomycin or 10 µg/ml chloramphenicol. Cultures of both *E. coli* and *S. aureus* were prepared as frozen stocks by adding glycerol to a final concentration of 25% to liquid cultures. Frozen stocks were stored at -80 °C. A complete list of bacterial strains of *S. aureus* and *E. coli* can be found in **Table 2.1**.

### 3.2 Isolation of chromosomal DNA

Chromosomal DNA from the Newman strain of *S. aureus* was isolated using Promega Quick protocol. Cells were harvested from overnight cultures by centrifugation at maximum speed (>13 000 x g) for 2 minutes. The cell-pellet was resuspended in 100 µl EDTA (50 mM), 5 µl lysozyme (100 mg/ml) and 1 µl lysostaphin (10 mg/ml) and incubated at 37 °C for 30 minutes. The sample was mixed gently with 600 µl Nucleic Lysis buffer (Promega), followed by a 5-minute incubation at 80 °C. When the sample had cooled down at room-temperature, 5 µl RNase A (10 mg/ml) was added and the sample was incubated for additionally 30 minutes at 37 °C and cooled down to room temperature. In the next step, 200 µl Protein precipitation buffer (Promega) was added and mixed by vortexing, prior to incubation for 5 minutes on ice. This was followed by a centrifugation step at maximum speed for 3 minutes. For DNA precipitation, the supernatant was added to a 2 ml tube containing 600 µl room-tempered isopropanol and mixed by inversion. The sample mix was centrifuged at maximum speed for 2 minutes, and the supernatant was discarded. To the tube containing the sample, 600 µl 70% room tempered EtOH was added, and the solution was mixed. Another centrifugation step at maximum speed for 2 minutes was performed and the supernatant was removed. The sample was air-dried for approximately 15 minutes until completely dry. At the end, the pellet was resuspended in 50 µl dH<sub>2</sub>O and incubated for 15-30 minutes at 60 °C. The DNA concentration was measured spectrophotometrically using Nanodrop 2000 (Thermo-Fisher Scientific), and the obtained

DNA was analysed by agarose gel electrophoresis. More about agarose gel electrophoresis is found in **Section 3.5**.

### **3.3 Plasmid isolation**

Plasmids used as vectors in the cloning process in this work were isolated from different bacterial strains of *E. coli* using the E.Z.N.A® Plasmid DNA mini Kit I. A complete list of strains carrying plasmids included in this work is presented in **Table 2.1**. Bacterial frozen stocks with the plasmid of interest were inoculated in 5 ml of LB media with 100 µg/ml of ampicillin and grown overnight at 37 °C with shaking. In the following day, the bacterial cultures were transferred to a centrifugation tube and centrifuged at 4000 x g for 5 minutes. The supernatant was removed, and the pellets were resuspended in 250 µl of Solution I with RNase A (100 µg/ml). To make a clear lysate, 250 µl Solution II were added to the solution and mixed by gentle rotation. In the next step, 350 µl of Solution III were added, followed by immediate rotations and inversion of the tube until a white flocculent was formed. The samples were centrifuged at maximum speed (>13000 x g) for 10 minutes, and the supernatant was transferred to a HiBind DNA Mini Column and centrifuged at maximum speed for 1 minute. The filtrate was collected in a 2 ml collection tube and discarded. Then, 500 µl HBC (High salt wash) buffer was added to the column and centrifuged at maximum speed for 1 minute. The filtrate was discarded and 650 µl DNA wash buffer was added, before the samples again were centrifuged at maximum speed for 30 seconds. The washing step was repeated a second time. The empty column was centrifuged at maximum speed for 2 minutes to make sure that it was completely dry before DNA was eluted from the column. 30 µl of Elution buffer were added to the column and samples were incubated for 1 minute at room temperature. Samples were centrifuged for 1 minute at maximum speed. The isolated DNA was stored at -20 °C.

### **3.4 Polymerase Chain reaction**

Polymerase chain reaction (PCR) is a versatile and highly efficient method used for amplification of DNA. This relatively simple *in vitro* principle was first introduced in 1985, and since then it has been widely used by researchers and clinicians to diagnose diseases, clone and sequence genes, and carry out sophisticated quantitative and genomic studies (Garibyan, 2013; Lo & Chan, 2006). Three temperature specific steps are required for a successful PCR reaction; 1. Denaturation, 2. Annealing and 3. Extension. The first step involves a thermal

denaturation of the target DNA, at 94-98 °C, which will open up the double helix structure of the DNA. Following this step is annealing of synthetic oligonucleotide primers which are specific to regions up- and downstream from the template DNA. The temperature is lowered to 40-65 °C depending on the melting temperature (T<sub>m</sub>) of the primers used in the reaction. The annealing of these primers will allow a DNA polymerase to copy the template DNA strand and make an extension of the annealed primers in the last step (Lo & Chan, 2006). This results in a synthesis of a new DNA strand which is complementary to the DNA template strand. The extension or elongation of the PCR product is performed at 72 °C, which is when most commercially available DNA polymerases shows optimal activity. In theory, with each repetition of these three steps, the number of copied DNA molecules doubles. Normally the steps are repeated in 25 to 30 cycles which makes it possible to generate large amounts of DNA from a relatively small sample (Garibyan, 2013).

PCR reactions in this work were performed using two different DNA polymerases, either Phusion® High-Fidelity (HF) or RedTaq® polymerase. Phusion® HF polymerase, which has a superior proof-reading capability and processivity, was utilized to amplify inserts to be cloned into plasmid backbones during construction of new plasmids. The Taq DNA polymerase, on the other hand, has less proofreading capacity, and was used for screening of potential transformants of *E. coli* or *S. aureus* to ensure right insert length in plasmids.

### 3.4.1 Amplification of inserts for plasmid cloning

The PCR using Phusion® HF polymerase was performed by adding chromosomal DNA from Newman in a PCR tube together with 5x Phusion HF buffer, dNTPs, dH<sub>2</sub>O, forward- and reverse primers and Phusion DNA polymerase as shown in **Table 3.1**. A list of primers used in this work are presented in **Table 2.2**.

**Table 3.1** Components and final concentrations for each reaction using Phusion® High-Fidelity (HF) DNA Polymerase PCR.

Component	Final concentration/volume
dH <sub>2</sub> O	To a final volume of 25 µl or 50 µl
5x Phusion HF buffer	1x
10 mM dNTPs	200 µM
10 µM Forward primer	0,5 µM
10 µM Reverse primer	0,5 µM
Template DNA	<250 ng
Phusion DNA polymerase	1,0 units/50 µl PCR

The conditions used during amplification for Phusion PCR are presented in **Table 3.2**. Alterations to the cycling conditions were made based on the length of the amplified product and the melting temperature ( $T_m$ ) of the primers.

**Table 3.2** Thermocycling conditions used for Phusion® High-Fidelity DNA Polymerase PCR.

Cycles	Duration	Temperature
1	30 seconds	98 °C
25-35	10 seconds 30 seconds 15-30 seconds per kb <sup>1</sup>	98 °C 45-72 °C <sup>2</sup> 72 °C
1	5 minutes	72 °C

<sup>1</sup> Duration of the elongation step depended on the length of the amplicon.

<sup>2</sup> Annealing temperature depended on the melting temperature of the primers used. Primers used in this work had normally a melting point of approximately 55 °C.

After amplification of specific DNA segments, the amplicons were visualised using agarose gel electrophoresis. Amplicons with the right lengths were cut from the gel and purified (see **Section 3.5** for more information about agarose gel electrophoresis and purification). Fragments were used in restriction digestion and ligation processes to obtain new plasmids for transformation.

### 3.4.2 PCR for screening of potential transformants

The screening using RedTaq® polymerase was performed by picking a selection of colonies from agar plates with potential transformants (see **Section 3.7** for more information about transformation) and screen the plasmid insert through amplification by PCR and visualization in agarose gel electrophoresis. *E. coli* colonies were picked directly from the agar plates and added in a pre-made PCR mix reaction as shown in **Table 3.3**. *S. aureus*, on the other hand are Gram-positive bacteria which is harder to lyse. This required an additional step before PCR. Colonies were picked from the agar plate and added in PCR tubes with 30 µl Lysis buffer (40 mM NaOH, 0,2% SDS). Tubes were incubated for 5 minutes at 98 °C. The solution was cooled on ice for approximately 5 minutes and diluted in 200 µl dH<sub>2</sub>O. Diluted samples were used as template in the PCR analysis, 4 µl of the lysate were used in PCR with a total reaction volume of 25 µl. A general overview of the cycling conditions used in this work for PCR with RedTaq® polymerase is shown in **Table 3.4**.

**Table 3.3** Composition of reactions included in Red Taq® ReadyMix™ PCR.

Component	Final concentration/Volume
Taq 2x Master mix <sup>1</sup>	1x
10 µM Forward primer	0,2 µM
10 µM Reverse primer	0,2 µM
dH <sub>2</sub> O	To a final volume of 25 µl
Template DNA	2-4 µl

<sup>1</sup>Red Taq 2x Master mix is composed of buffer, dNTPs, the Taq polymerase and an inert loading dye.

**Table 3.4** PCR program used for Red Taq® ReadyMix™ PCR

Cycles	Duration of cycle	Temperature
1	2 minutes	95 °C
25	30 seconds	95 °C
	40 seconds	50-65 °C <sup>2</sup>
	60 seconds per kb <sup>1</sup>	72 °C
1	5 minutes	72 °C

<sup>1</sup>The time used for this step varies depending on length of the amplicon for the given reaction.

<sup>2</sup>The temperature used during annealing depends on the melting temperature of the primers used, in this work most primers had a melting temperature of approximately 55 °C.

Amplicons from the PCR reactions were visualised using agarose gel electrophoresis as shown in **Section 3.5**. Promising transformants were inoculated in liquid media (TSB or BHI for *S. aureus*, or LB for *E. coli*) with appropriate antibiotics, and cultures were grown overnight. The next day, frozen stocks were made of the bacteria by diluting the cultures with 25% glycerol for storage at -80 °C.

## 3.5 Gel electrophoresis

### 3.5.1 Agarose gel electrophoresis

Agarose gel electrophoresis is a highly efficient method used for separation of DNA fragments of different sizes. The analysis is performed by loading samples containing DNA in wells of a filamentous agarose gel and apply an electric current. Because the phosphate backbone of the DNA is negatively charged, DNA fragments will migrate towards the positively charged anode. Due to polymers in the gel, DNA fragments of different sizes will migrate at different rates through the gel. The distance travelled is inversely proportional to the log of its molecular weight. This means that shorter fragments will travel further than longer fragments, because it meets less resistance from the porous gel composition (Lee, Costumbrado, Hsu, & Kim, 2012).

In this work, agarose gel electrophoresis was used to analyse gDNA and PCR fragments. 1 % agarose gel was used, unless otherwise is indicated. The agarose gel was prepared by boiling a solution of agarose in 1x TAE (40 mM Tris-Acetate, 1 mM EDTA) buffer. Dissolved agarose was supplemented with peqGreen (1  $\mu$ l/50 ml) to enable visualisation of the DNA bands in UV-light. The agarose solution was poured into a container, and combs was placed in the gel to make wells. The gel was dried at room temperature and transferred to a chamber containing 1x TAE buffer that covered the gel. DNA samples (between 1 and 60  $\mu$ l) were loaded to the wells in the gel. To make the application of the samples easier, the DNA samples were mixed with 6x loading buffer (Gel Loading Dye Purple (6X), NewEngland Biolabs) to a final concentration of 1 x for the loading buffer. The loading buffer contains a dye and glycerol which gives visual colour to the samples and makes them heavier in the buffer and allows them to sink to the bottom of the well. PCR products obtained with RedTaq® ReadyMix™ (Sigma-Aldrich) were directly added to the gel as the PCR mix contains a loading dye. To be able to roughly determine the lengths of the fragments, a 1 kb ladder with fragments of known lengths were added to one of the wells and used for comparison. Gels were run at 90 V for approximately 20 minutes until the samples had been sufficiently separated. DNA bands were visualized on a GelDoc system (BioRad).

### **3.5.2 Extraction of DNA from agarose gels or PCR product**

Nucleospin® Gel and PCR Clean-up Kit (Machnery-Nagel) was used to isolate and purify DNA fragments from PCR products or restriction digestion, or from DNA fragments separated using agarose gel electrophoresis. To isolate DNA fragments from agarose gel, DNA fragments with desired length were cut from the agarose gel and completely dissolved in buffer NTI (ca. 200  $\mu$ l buffer/100 mg gel) at 55 °C. Amplicons obtained from PCR products or fragments from restriction digestion were isolated by mixing with buffer NTI (1:2). The entire volume of the dissolved gel or fragments mixed with NTI were transferred to a Nucleospin® Gel and PCR Clean-up Column and centrifuged at 11 000 x g for 30 sec. The NTI buffer facilitates binding of DNA to the silica-membrane in the spin column. In order to wash away salts and contaminants from the samples, 700  $\mu$ l of NT3 buffer were added and the spin columns were centrifuged at 11 000 x g for 30 seconds. The washing step with NT3 buffer was repeated two times to ensure a clean sample. In the next step, the empty spin column was centrifuged at 11 000 x g for 1 minute to remove any residual ethanol from buffer NT3. The flow through were discarded and the column was placed in a clean 1,5 mL eppendorf-tube. The DNA were

eluted and collected in the Eppendorf tube by incubating the spin column with 15-40  $\mu$ l Buffer NE for 1 minute and centrifuge at 11 000 x g for 1 minute. The eluate was stored at -20 °C. To determine the purity of the sample and concentration of the DNA, the absorbance (260 nm) was measured by spectroscopy in a Nanodrop 2000 (Thermo-Fisher Scientific).

### 3.6 Plasmid construction

Restriction digestion and ligation was used in this work in order to construct expression plasmids used for complementation and for construction of sgRNA plasmids used for CRISPR interference. Digestion using specific restriction enzymes were applied to both template DNA and vector DNA in order to make compatible ends and allow them to bind. Primers used for amplification of the insert of interest were designed with overhangs that introduced specific sequences, known as recognition sites, that can be recognised and cut by enzymes. Recognition sites that were introduced to the amplicons were already existing in the plasmids.

Restriction digestion in this work were performed on amplified fragments and purified plasmids to produce sticky ends. The digested PCR fragments and plasmid backbones were then ligated using T4 DNA ligase. In the table below (**Table 3.5**) is a general overview of a standard restriction enzyme reaction used in this work. The reaction mix were prepared on ice, and the restriction digestion was performed through an incubation time at a specific temperature depending on the enzymes used.

**Table 3.5** Information about components included in a standard restriction enzyme reaction

Component	Volume/Final concentration
DNA	1-4 $\mu$ g
Buffer <sup>1</sup>	5 $\mu$ l
Restriction enzyme(s) <sup>2</sup>	1 $\mu$ l
dH <sub>2</sub> O	to a final volume of 50 $\mu$ l

<sup>1</sup> 10 x CutSmart buffer were used for NotI and SalI, 10 x NEB 3.1 buffer were used for BsmBI.

<sup>2</sup> 1  $\mu$ l of each enzyme were added to the reaction mix when a double digestion was performed.

After restriction digestion, the digested fragments were purified using a Nucleospin® Gel and PCR Clean-up Kit (Machnery-Nagel). The reaction mix containing the vectors were heat-inactivated according to guidelines given for the specific enzymes. After inactivation of the enzymes, the digested plasmids were separated through gel electrophoresis and purified from gel. Inserts were then ligated using T4 DNA ligase. A general ligation protocol using the T4 DNA ligase is presented in the table below (**Table 3.6**).

**Table 3.6** Components used in a standard T4 DNA ligase reaction

Components	Volume/Final concentration
T4 DNA Ligase buffer (10X)	2 $\mu$ l
Vector DNA <sup>1</sup>	~50 ng
Insert DNA <sup>1</sup>	~37.5 ng
dH <sub>2</sub> O	to a final volume of 20 $\mu$ l
T4 DNA Ligase	1 $\mu$ l

<sup>1</sup> The volume or amount of the inserts added with the plasmid was determined from measured concentrations and molar ratios between the plasmid and fragments (molar ratio of 1:3 was used in the case of making complementation strains). For the construction of sgRNA plasmids for CRISPR interference, 2,5  $\mu$ l of vector backbone was added together with 14,5  $\mu$ l annealing product.

After all the components were added to the ligation reaction, the samples were incubated for 10 minutes at room temperature. The ligase was then inactivated by a following incubation at 65 °C for 10 minutes. The ligated product was stored at -20 °C until further use.

### 3.6.1 Construction of complementation plasmids and strains

Two strains, HO18 ( $\Delta ubiE::spc$ ,  $P_{spac-ubiE}$ ) and HO19 ( $\Delta ubiE::spc$ ,  $P_{spac-ubiE\_hepT}$ ) (see **Table 2.1**), were constructed in order to complement the deletion mutant ( $\Delta ubiE$ ) of *S. aureus*. Both *ubiE* and a version containing, *ubiE\\_hepT* were included as inserts, because the deletion of *ubiE* would also have affected the *hepT* gene which is located downstream from *ubiE* in the same operon. Both of the plasmid constructs were made using pLOW 2861 plasmid vector as backbone. pLOW contains an IPTG inducible promoter,  $P_{spac}$ , located in front of a multiple cloning site where inserts of interest can be inserted and expressed through IPTG induction (Liew et al., 2011). A plasmid, from the lab collection was included as a control for the complementation experiment. The control strain (HO21) contained pLOW-lacA-m(sf)gfp.

In order to obtain the inserts, PCRs were performed using chromosomal DNA from the Newman strain as template to amplify fragments containing the *ubiE* and *ubiE-hepT* gene (primers dma105 with dma106 and dma105 with dma113, respectively (see **Table 2.2**). The primers included recognition site for the restriction enzymes NotI and SallI, which were introduced to the amplicon during the PCR analysis. The forward primer, dma105, with the recognition site for SallI, also contains a ribosomal binding site (RBS) in the overhang. Amplified product was run on a gel electrophoresis, and bands with correct lengths were cut from the gel and purified with NucleoSpin® Gel and PCR clean-up kit (Machery-Nagel). DNA concentrations were determined using a Nanodrop 2000 spectrophotometer (Thermo-Fisher Scientific).

DNA fragments and plasmids (pLOW 2861, see **Table 2.1**) were digested using the restriction enzymes NotI and Sall. These enzymes will cut and make sticky ends that allows the fragments to bind the ends of the plasmid. The digestions were performed by adding DNA together with the enzymes, 10X CutSmart Buffer and dH<sub>2</sub>O as shown in **Table 3.5**. The reaction mix was prepared on ice and the digestion was performed at 37 °C for 30 minutes to ensure that the fragments had been sufficiently digested.

Inactivation of enzymes were performed by an incubation at 65 °C for 20 minutes. The digested product of the plasmid was run in an agarose gel electrophoresis and were then cut out and purified with the use of the NucleoSpin® Gel and PCR clean-up kit. The digested product of the amplified fragments was purified directly using NucleoSpin® Gel and PCR clean-up kit. Concentrations were determined using a Nanodrop 2000 (Thermo-Fisher Scientific).

Ligations were performed with T4 DNA Ligase as shown in **Section 3.6**. 5 µl of the ligation mix were transformed into competent *E. coli* cells (IM08B). The next day, colonies were screened by colony PCR (**Section 3.4.2**). Plasmid was isolated (from colonies which screened correctly) and sequenced by Sanger sequencing to ensure correct sequence of the inserts. The plasmids with correct sequence and as well as a control plasmid from the lab collection, pLOW-lacA-m(sf)gfp, were transformed into competent MM155 cells ( $\Delta ubiE$ ). The results from this process were bacterial deletion strains of the *ubiE* gene that can be complemented for *ubiE* (HO18) or *ubiE\_hepT* (HO19) using IPTG as an inducer, and a control strain containing the pLOW-lacA-m(sf)gfp (HO21).

### 3.6.2 Construction of CRISPR interference strains

In order to explore the role of other genes in the menaquinone biosynthetic pathway, knockdown strains of the genes *menA* and *menF* were created. In addition, we already had a knockdown strain of the gene *menE* in stock form earlier lab work, which were also included in further assays. To knockdown gene expression of the genes mentioned above, a two-plasmid system of CRISPR interference using an IPTG titratable promotor was used. One plasmid (pLOW-dCas9) encoded a catalytically inactive Cas9 protein (dCas9) that can bind DNA without cleaving it. The second plasmid encode a sgRNA sequence which contains a 20-bp gene specific region and a dCas9 binding region. The sgRNA can make a complex together with the dCas9 and guide it to a gene-specific site. The dCas9-sgRNA complex will form and bind a gene of interest, thereby inhibiting transcriptional components and downregulating gene transcription (Stamsås et al., 2018).

New sgRNA plasmids to allow targeting of new genes were constructed using so-called Golden Gate cloning. In this process, a vector is digested with type IIS restriction enzymes which cuts the DNA sequences outside of this recognition site to generate non-palindromic overhangs. New 20 bp gene-specific sequences are introduced by oligonucleotide duplexes of 20 nt gene specific sequences flanked by 4 nt flanking sequences on both sides which are complementary to overhangs in the plasmid vector (Qi et al., 2013). The oligonucleotides were designed beforehand by Morten Kjos (NMBU) and Xue Liu (University of Lausanne, Switzerland), and is presented in **Table 3.7**. Oligonucleotides duplexes were made by annealing two oligonucleotides per gene. The annealing was performed by adding 2,5 µl of two corresponding primers to a PCR tube together with 5 µl buffer 10xTEN (0,1 M Tris-HCl, 0,01 M EDTA, 1 M NaCl). dH<sub>2</sub>O was added to a total volume of 50 µl. The tubes containing primers were incubated at 95 °C for 5 minutes in a thermal cycler (ProFlex PCR systems, Applied Biosystems) and cooled down at room temperature.

**Table 3.7** Primers used to make oligonucleotides that codes sgRNA used in CRISPRi depletion.

Gene	Orientation	Primer sequence (5'-3')
SAOUHSC_00980 ( <i>menF</i> )	R	TATAAAAAAATGATACAATATAATA
	F	AAACTATTATATTGTATCATTTTT
SAOUHSC_00982 ( <i>menA</i> )	R	TATAACGGAAGCAGTTAATGTATG
	F	AAACCATACATTAAGCTGCTCCGT

The plasmid pVL2336 was isolated from *E. coli* MK1518 (**Table 2.1**). The purified plasmid was digested with BsmBI to remove an insert and generate overhangs in pVL2336. The reaction mix was set up as shown in **Table 3.5**, and the digestion was performed through a 2-hour incubation at 55 °C. An agarose gel electrophoresis was performed to separate the backbone from the insert. The fragment corresponding to the backbone was cut from an agarose gel and purified using the NucleoSpin® Gel and PCR clean-up kit (Machnery-Nagel).

The oligonucleotides and the digested backbone of pVL2336 were then ligated with T4 DNA ligase as shown in **Section 3.6**, 2,5 µl of the vector backbone with 14,5 µl annealing product were used. The ligated mix was used to transform competent *E. coli* IM08B cells (see **Section 3.7.1** and **3.7.2**). Transformants were screened and the plasmids were sequenced. Plasmids with the correct sequencing results were transformed into competent *S. aureus* MH266 cells (Newman pLOW-dCas9\_extra\_lacO) (**Section 3.7.3** and **3.7.4**) which already carried the pLOW-dCas9.

### **3.7 Transformation of *E. coli* and *S. aureus* strains**

In order to introduce genetic information to a bacterium through transformation, a requirement is that they are in a state of competence. The definition of competence is the ability of cells to take up and utilize exogenous DNA from surrounding environment. And even though some bacteria can take up linear and sometimes circular DNA through natural competence, this only refer to a subset of bacterial species. (Swords, 2003). Several methods for induction of a competent state have therefore been developed for bacteria that originally is non-transformable, including a chemical or electrical approach.

#### **3.7.1 Preparation of chemically competent *E. coli***

In this work, the preparation of competent cells of *E. coli* was done by using a CaCl<sub>2</sub> method. This allowed introduction of foreign DNA in forms of plasmid into the cells. How calcium chloride makes it possible for cells to take up DNA is unknown, but several speculations are made. Among other it is believed that CaCl<sub>2</sub> facilitate DNA binding to the cell-surface, which enabled DNA to enter the cell through use of heat-shock (Chang, Chau, Landas, & Pang, 2017).

To make competent cells, cultures of *E. coli* IM08B cells were grown in 3 ml LB medium at 37 °C overnight. The next day, the culture was diluted 1:100 with LB media and grown to an OD<sub>600</sub> of 0,3. The cells were centrifuged for 5 minutes at 4000 x g, and the pellet was resuspended in ice-cold 100 mM CaCl<sub>2</sub> (1/2 of the starting volume) and stored on ice for 30 minutes. Cells were centrifuged as described previously. The pellet was resuspended in 100 mM CaCl<sub>2</sub> (1/10<sup>th</sup> of the starting volume). For long time storage of competent cells, the cells were resuspended in 20 % glycerol with 100 mM CaCl<sub>2</sub> and stored in -80 °C.

#### **3.7.2 *E. coli* transformation**

*E. coli* transformation was performed following standard heat-shock. Cells were thawn on ice and approximately 1 µg of plasmid or 10 µl of ligation mixture was added to 100 µl of competent cells. The cells were incubated on ice for 30 minutes and heat-shocked at 37 °C for 5 minutes or 42 °C for 30 seconds. After heat shocking, the cells were diluted with 400 µl of LB medium and incubated at 37 °C with shaking for 30-60 minutes. Following this incubation step, 100 µl of the bacterial culture were plated onto agar plates containing LB medium supplemented with 100 µg/ml ampicillin. The leftover volumes of bacteria were centrifuged at 13 000 x g for 30 seconds, and a higher concentration of bacteria were plated on same types of

plates. The plates were incubated over night at 37 °C. The next day, transformants were screened by colony PCR with specific primers (see **Table 2.2** for complete list of primers used in this work). Details of PCR used to screen for potential transformants can be found in **Section 3.4.2**.

### **3.7.3 Preparation of electrocompetent *S. aureus***

Electroporation has been used to introduce DNA into many procaryotic cell, including *S. aureus*. When applying electrical impulses to electrocompetent cells, it can cause reversible transient pores in the cell membrane where DNA pass through and be taken up by the cell (Kraemer & Iandolo, 1990).

To make electrocompetent cells of *S. aureus*, cells were inoculated in 5 ml BHI and incubated at 37 °C with shacking overnight. The media was supplemented with appropriate antibiotics, and 25 µM menaquinone-4 (MK-4) if necessary. The overnight cultures were then re-inoculated 1:100 in BHI and grown to an OD<sub>600</sub> between 0,4 and 0,6. The cells were kept on ice for approximately 10 minutes. After incubation, the cells were transferred to a 50 ml nunc-tube and harvested. Samples were centrifuged for 10 minutes at 4 °C and at 4000 x g, and the supernatant was discarded. Following this step is a series of washing steps were performed (all centrifugations was performed for 5 minutes, at 4 °C, and at 4000 x g). Cells were washed two times in 35 ml ice-cold dH<sub>2</sub>O. After that, the cells were washed in 25 ml ice cold 10 % glycerol three times. In the final step, the pellet was resuspended in 2-3 ml ice cold 10% glycerol with 0,5 M sucrose and 50-200 µl were aliquoted to 1,5 mL Eppendorf tubes and stored at -80 °C until used.

### **3.7.4 *S. aureus* transformation**

Transformation of *S. aureus* was performed using electroporation. Electrocompetent *S. aureus* (stored -80 °C) were thawed on ice and 50 µl of cells were mixed with approximately 750 – 1000 ng of plasmid DNA (1-10 µl depending on plasmid concentration) in a 1 mm electroporation cuvette. The cells were electroporated at 2.1 V, 100 Ω and 25 µF, and 950 µl TSB with 0,5 M sucrose were quickly added. After electroporation, the cells were incubated for 2 hours at 37 °C with shaking. Following the incubation, 100 µl of the cells were plated on TSA plates with appropriate selective antibiotics. Cells in the remaining culture were pelleted by centrifugation at 13 000 x g for 30 seconds, and a higher concentration of bacteria were plated on BHI or TSA

plates with appropriate antibiotics. The plates were incubated overnight at 37 °C, and transformants were screened (**Section 3.4.2**).

### **3.8 Sanger sequencing**

Plasmids from screened transformants were sequenced to ensure no mutations had occurred within the insert region of the plasmid and that the entire insert had been amplified. Samples that were sent for sequencing contained 5 µM primer and plasmid DNA at a final concentration of 80-100 ng/µl. The primer and DNA were diluted in distilled water. Sanger sequencing was performed by Eurofins.

### **3.9 Determining operon structures by RT-PCR**

Reverse transcription PCR was used in this work to verify which genes are part of the *ubiE* operon. RT-PCR combines synthesis of cDNA from RNA and PCR and is a method that can be used to study gene expression (Santos, Sakai, Machado, Schippers, & Greene, 2004).

In this work, primers were designed to amplify fragments containing several combinations of the genes NMWN\_1381 (unknown name), *ubiE*, *hepT* and *ndk*. The position of the primers are shown in **Figure 3.1**, and a complete list of primer sequences are presented in **Table 2.2**. cDNA made from mRNA of Newman in another project was used (provided by the lab). Chromosomal DNA of Newman was used as a control to ensure that the primers bind and amplify the correct regions. Phusion DNA polymerase was utilized, as described in **Section 3.4.1**. Amplicons from PCR were visualised through agarose gel electrophoresis as described in **Section 3.5.1**. Visualization on agarose gel would reveal if different genes are transcribed together and if they are in the same operon.

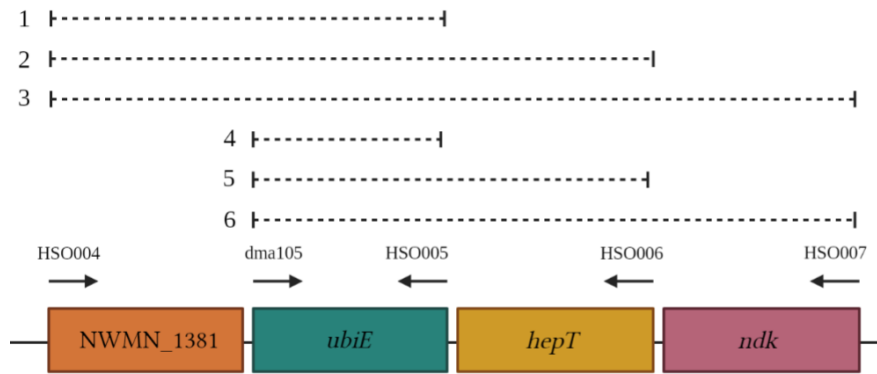


**Figure 3.1** Illustration of assumed operon structure of the *ubiE*-operon. Primers used for reverse transcription PCR and where they bind the chromosomal DNA of Newman is indicated.

### 3.10 Growth analysis

Growth assays with deletion strains, depletion strains and complementation strains of *S. aureus* were performed in microtiter plates, and growth were measured spectrophotometrically in order to compare growth rate with wild-type. In addition, the growth curves allow us to find the optimal concentration of IPTG inducer for complementation experiments and optimal concentrations of MK-4 used for complementation of the *ubiE* deletion during macrocolony growth.

Bacterial deletion and complementation strains were grown overnight at 37 °C in 5 ml BHI media supplemented with appropriate antibiotics and/or IPTG or MK-4 when necessary. Overnight cultures were diluted 1/100 with media. Cultures were grown to early exponential phase and diluted to an OD<sub>600</sub> of 0,005 in TSB with and without IPTG or MK-4. Diluted bacterial cultures were then applied to wells in a 96-well microtiter plate with a total volume of 200 µl in each well. The wells contained two-fold decreasing concentrations of IPTG of MK-4.

In order to determine the effect of gene depletions using CRISPR interference, depletion strains were grown overnight in 5 ml TSB with appropriate antibiotics at 37 °C. Overnight cultures were diluted 1/100 in TSB with antibiotics and grown until early exponential phase. Strains were diluted to OD<sub>600</sub> of 0,005 in TSB media with appropriate antibiotics, with and without 300 µM IPTG to a total volume of 300 µl in a 96-well microtiter plate.

The assays were performed with triplicates for each test condition. A blank and control without IPTG or MK-4 were also included in the assays. Growth was monitored for approximately 10-15 hours at 37 °C using a Synergy H1 Hybrid microtiter plate reader

(BioTek®) or FLUOstar OPTMA FL (BGM Labtech). OD<sub>600</sub> was measured at 10-minute intervals.

MK-4 were dissolved in 96% ethanol. Originally dimethyl sulfoxide (DMSO) was used as a solvent, but growth assays revealed that DMSO without MK-4 had an impact on the growth of mutant strains which would disrupt the results and lead to wrong assumptions. A growth curve showing how DMSO affected growth of mutant strains are presented in the appendix (Figure A2.)

### 3.11 Small colony assay with knockout strains of *aroC* and *ubiE*

*S. aureus* strains that are incapable of respiring presents small colony variants; bacteria with low metabolism that form small non-pigmented colonies (Harris & Richards, 2006; Mashruwala et al., 2017b). Our theory suggests that the deletion for *ubiE* or *aroC* affects the respirational pathway, and we therefore wanted to investigate if these deletion mutants might present the SCV phenotype. If they presented this colony morphology it was also of interest to further investigate if the supplementation of MK-4 could revert this phenotype.

The assay was performed as described by Wakeman et al. (2012). Wild-type,  $\Delta ubiE$  and  $\Delta aroC$  were grown over night at 37 °C with shaking in TSB media with appropriate antibiotics. The following day, strains were streaked onto plain TSB agar plates, or plates supplemented with 12,5 µM or 50 µM MK-4. The plates were either incubated in oxic or anoxic conditions at 37 °C. Anaerobic growth were performed in anaerobic jars. After a 48-hour incubation the plates were imaged.

### 3.12 Congo red susceptibility test

A congo red susceptibility assay was performed in order to better understand how wall-teichoic acids were affected in *Staphylococcal* mutant strains. Wall-teichoic acids has been shown to protect *S. aureus* against lysis from different dyes, including Congo red (Suzuki et al., 2012). Therefore, a change in susceptibility to this dye can highlight differences in the compositions of the cell wall in different bacterial strains regarding wall-teichoic acids.

The Congo Red susceptibility assay was performed as described by DeFrancesco et al. (2017). Cultures of wild-type,  $\Delta ubiE$  and  $\Delta aroC$  were grown at 37 °C with shaking. After a night of incubation, the cultures were diluted 10-fold ( $10^0 - 10^{-6}$ ), and 2 microliters of each dilution was

spotted to TSB agar plates. In this assay, plates composed of only TSB agar and TSB agar plates supplemented with 0,06 % or 0,1 % (w/v) Congo Red were used. Plates were incubated under anaerobic or aerobic conditions at 37 °C. The aerobic growth plates were incubated for 24 hours, while the anaerobic growth for 48 hours. After incubation, the plates were imaged.

### **3.13 Biofilm assays**

#### **3.13.1 Crystal violet quantification**

To quantify biofilm formation of different strains of *S. aureus*, crystal violet was used to stain biofilm grown in 96-well microtiter plates. The protocol used in this work was based on a protocol developed by Christensen et al. (1985). The assay was applied in order to quantify total biofilm mass of wild-type, deletion mutants ( $\Delta ubiE$  and  $\Delta aroC$ ) and of complementation strains ( $\Delta ubiE::spc$ ,  $P_{spac-ubiE\_hepT}$  and  $\Delta ubiE::spc$ ,  $P_{spac-ubiE}$ ) of the *ubiE* knockout.

*S. aureus* strains were grown overnight in 5 ml TSB with the appropriate antibiotics and/or IPTG at 37 °C with shaking. The day after, all overnight cultures were diluted 1/100 in TSB with 1 % (w/v) NaCl and 1 % (w/v) glucose and 100  $\mu$ l of the dilutions were added to 96-well plates. Antibiotics were also included here when necessary, and 50  $\mu$ M IPTG was supplemented to media with complementation strains. Each sample was added to 8 wells each. The plates were incubated 24 hours at 37 °C to let the bacteria form biofilm in the wells. The incubation was either performed at oxic conditions or anoxic conditions. After incubation, the medium containing the planktonic cells was carefully removed and the biofilm was washed with 0,9 % (w/v) NaCl (saline). After the washing step, the biofilm was air-dried for approximately 5 minutes. The biofilm was stained by adding 0,02 % crystal violet followed by a 15-minutes incubation at room temperature. Washing steps with saline were performed until no more dye was observed in the washing solution. To visualize the amount of biofilm formation, a picture was taken of the wells. The biofilms were incubated with 200  $\mu$ l 96 % (v/v) ethanol for 10 minutes. The solution with the dye was removed and added to a new 96-well plate and optical density was measured at OD<sub>600</sub> on a plate reader (Synergy H1 Hybrid Reader, BioTek®) for quantification of total biofilm biomass.

#### **3.13.2 Macrocolony assay**

Macrocolony is commonly used as a model to investigate biofilm formation on bacteria. In this work, the macrocolony assays, was performed in order to compare morphological changes in

deletion strains (*ubiE* and *aroC*), depletion strains (*menA*, *menF* and *menE*) and complementation strains of  $\Delta ubiE$  ( $\Delta ubiE::spc$ ,  $P_{spac-ubiE\_hepT}$  and  $\Delta ubiE::spc$ ,  $P_{spac-ubiE}$ ) with wild-type. Macrocolony formation was studied as described by Wermser and Lopez (2018).

Macrocolonies of wild-type, deletion strains and complementation strains were made by making overnight cultures in liquid TSB, incubated at 37 °C with shaking. The media was supplemented with antibiotics, IPTG (50  $\mu$ M) or MK-4 (12,5  $\mu$ M or 50  $\mu$ M) when necessary. The following day, 2  $\mu$ l of the cultures were spotted in triplicates onto TSB agar plates with 100  $\mu$ M MgCl<sub>2</sub>. The agar plates also contained antibiotics and/or IPTG or MK-4 when appropriate.

Macrocolonies of CRISPRi-depletion strains were formed by first making precultures of bacterial strains in 5 ml TSB with 5  $\mu$ g/ml erythromycin and 10  $\mu$ g/ml chloramphenicol. Precultures were grown over night at 37 °C with shaking. After incubation, cultures were diluted 1/1000 in fresh TSB medium with appropriate antibiotics and grown to an OD<sub>600</sub> of 0,5. Cultures at correct cell densities were spotted onto TSB + 100  $\mu$ M MgCl<sub>2</sub> supplemented with appropriate antibiotics, with or without 300  $\mu$ M IPTG.

All macrocolonies were incubated for 5 days at 37 °C in either oxic or anoxic conditions. After the incubation the formed colonies were imaged using a stereomicroscope (Axio Zoom V16 coupled to a Zeiss AxioCam 503) and/or scraped from plates and stored in -80 °C for further use.

### 3.13.3 Quantification of the extracellular matrix in macrocolonies

Quantification of eDNA, proteins and carbohydrates from the extracellular matrix (ECM) of *S. aureus* macrocolonies were performed based on protocol used by Wermser and Lopez (2018). The aim was to determine whether macrocolonies of deletion mutants ( $\Delta ubiE$  and  $\Delta aroC$ ) had different amount of these ECM components compared to wild-type. Highly concentrated NaCl solution was utilized in order to trigger the release of the ECM components. This solution will coat the surface of the cells and ECM constituents and disrupt the attractive forces and interactions leading to detachment of ECMs from the bacterial cells (Chiba et al., 2015).

Macrocolonies, scraped from agar plates, were washed with 500  $\mu$ l PBS. The biomass was mixed lightly, trying to not disturb the matrix. Biofilms were centrifuged at 13 000 x g for 30 seconds. The supernatant was discarded and 1 ml 1,5 M NaCl was added. The samples were

thoroughly mixed by vortexing and transferred to a 5 ml tube. The samples were homogenized for 30 sec x 7 times with a high-performance dispersing instrument (Ultra-Turrax® T25). After homogenizing, the samples were normalized by measuring OD<sub>600</sub> of the samples and diluting samples in 1,5 M NaCl to a specific OD<sub>600</sub> value. For the aerobic samples, the final OD<sub>600</sub> value of diluted (1/10) samples was 0,2 and for the anaerobic samples it was 0,03. Normalized samples were centrifuged at 10 000 x g for 5 minutes, and the supernatant was transferred to a new tube and used to measure the concentration of proteins and eDNA in a Nanodrop 2000 spectrophotometer (Thermo-Fisher Scientific).

The polysaccharide concentration was determined using a phenol sulphuric acid method (performed by Dr. Danae Morales Angeles) based on the method described by Wermser and Lopez (2018). The phenol-sulphuric acid method is one of the easiest and most reliable colorimetric methods for determining carbohydrate concentrations in aqueous solutions (Jain, Karibasappa, Dodamani, & Mali, 2017; Masuko et al., 2005). In short, the principle of this method is that sulphuric acid will break down any polysaccharide, oligosaccharide, and disaccharide to monosaccharides in the sample. These monomers will then react with the phenol and produce a yellow-gold colour that can be quantified spectrophotometrically. By using a carbohydrate, such as glucose, to make a standard curve, this method can be used to quantify carbohydrates from the sample (Nielsen, 2017).

In order to quantify carbohydrates, macrocolonies were washed in PBS and resuspended in 1,5 M NaCl. OD<sub>600</sub> was normalized to 1. Cells were centrifuged for 5 minutes at 10 00 x g, and supernatant was recovered. In a 96-well microtiter plate, 28,6 µl of the ECM fraction was mixed gently with 28,6 µl 5% phenol and 143 µl sulphuric acid. The solution mix were incubated for 10 minutes at room temperature. Absorption was measured at 492 nm in a plate reader (Synergy H1 Hybrid Reader, BioTek®). Glucose was used to make a calibration curve, and three technical replicates were included for each sample.

#### **3.13.4 FTIR-spectroscopy to analyse composition of macrocolonies**

FTIR spectroscopy analyses of dissolved *S. aureus* macrocolonies and ECM extracts were conducted in order to determine the composition of extracellular matrix components. This analysis was performed on wild-type,  $\Delta ubiE$  and  $\Delta aroC$  macrocolonies grown in both aerobic and anaerobic conditions. Two biological replicates of each condition were included, and three replicates were measured.

High-throughput (HTS) FTIR measurements were performed using the High Throughput Screening eXTension (HTS-XT) unit coupled to Vertex 70 FTIR spectrometer (both Bruker Optik, Germany) in absorbance mode. The macrocolonies were mixed with 0,1% (w/v) NaCl. For the samples with the biggest biomass (aerobic macrocolonies of wild-type and *ΔubiE* strains), 100 μl of 0,1% (w/v) NaCl was added. Only 50 μl of the NaCl solution was added to samples with lower biomass (*ΔaroC*, and strains grown under anaerobic conditions). The ECM extract samples were prepared as described before in the quantification of ECM section (**Section 3.13.3**), but the samples were not normalized before analysis as the FTIR-HTS instrument has incorporated algorithms that normalizes the samples.

From each suspension or supernatant, 10 μl were transferred to an IR-light-transparent silicon 384-well microplate (Bruker Optic, Germany) in three technical replicates. Samples were dried at room temperature for approximately 2 hours to form films that were suitable for FTIR analysis. ECM extracts were spotted onto plates in 5 rounds due to low concentrations. The spectra were recorded in the region between 4000 and 400 cm<sup>-1</sup> with a spectral resolution of 6 cm<sup>-1</sup>. For each spectrum 64 scans were averaged. Each spectrum was recorded as the ratio of the sample spectrum to the spectrum of the empty microplate. Chemical similarities were estimated from spectra by using principal component analysis (PCA). All data analysis and interpretations were performed by Dr. Volha Shapaval.

### **3.13.5 Robustness of macrocolonies**

The macrocolonies resistance to mechanical pressure was tested and judged to investigate differences in macrocolony robustness between wild-type and the mutant strains *ΔubiE* and *ΔaroC*. Both macrocolonies grown in aerobic and anaerobic conditions were included. The protocol used for this assay was described by (Wermser & Lopez, 2018). This test was performed by touching the centre of 5-day grown macrocolonies with a pipette tip and moving the tip slowly vertically until the colony were visibly fragmented or disrupted. Pictures were taken before and after the mechanical pressure was applied.

## 4 Results

### 4.1 *ubiE* and *aroC* are important for macrocolony structuring

Macrocolonies are considered a model that can be used to study biofilm formation in different bacteria, including *S. aureus* (Wermser & Lopez, 2018). CRISPRi knockdown of gene expression targeting a diverse collection of genes from the Newman strain of *S. aureus* have earlier been used to identify genes involved in macrocolony formation (Mårli, 2020). During this earlier work, the gene, *ubiE*, was identified to be involved in biofilm formation due to observed changes in the macrocolony morphology. *ubiE* is the last enzyme in the menaquinone biosynthesis pathway in *S. aureus* (**Figure 1.3**). In this work it was further investigated how *ubiE* and menaquinone biosynthesis affects the macrocolony and biofilm formation in *S. aureus*. In addition to *ubiE*, another gene, *aroC*, was included in the study as it is involved in the same biosynthetic pathway as *ubiE*.

Initially in this work, new macrocolony assays were performed with knockout strains of the genes *ubiE* and *aroC* in *S. aureus* to verify the phenotype. The two deletion strains, where the genes had been replaced with a spectinomycin cassette, was generated in previous work in the lab. Overnight cultures of the mutant derivatives and the wild-type strain (Newman) were spotted onto agar plates with TSB and MgCl<sub>2</sub>, which has been reported to induce macrocolony formation, and grown in a 5-day period at 37 °C (Mårli, 2020; Wermser & Lopez, 2018).

The wild-type bacteria form large macrocolonies with a light beige colour during aerobic growth (**Figure 4.1**). The phenotype is also characterised by lots of wrinkles and folds, and the colony has an uneven shape. This corresponds to what has been observed earlier for this strain (Mårli, 2020). *ubiE* and *aroC* deletion mutants show a total loss of this characteristic phenotype. Macrocolonies of both mutants do not present structural wrinkles as the wild-type, and instead show a smooth and flat surface area. The size of the macrocolonies of the mutants are also smaller in size compared to the wild-type strain. The colonies of  $\Delta ubiE$  and  $\Delta aroC$  are approximately 36% and 66% smaller than the wild-type with a diameter of 8,85 mm and 4,65 mm respectively. The wild-type colony is around 13,77 mm in diameter (**Figure 4.1**). Furthermore, the *ubiE* knockout has changed its colour to a bright yellow shade.

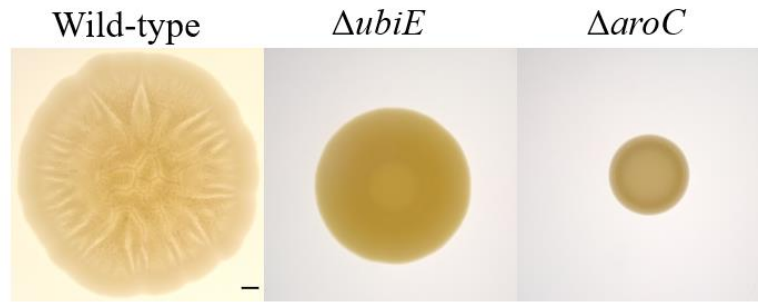


**Figure 4.1** Macrocolony phenotype of wild-type and  $\Delta ubiE$  and  $\Delta aroC$  mutants. Overnight cultures of the bacterial strains were spotted on TSB agar plates with 100  $\mu\text{M}$  of  $\text{MgCl}_2$  and grown under aerobic conditions at 37  $^\circ\text{C}$  for 5 days. Scale bar is 1000  $\mu\text{m}$ .

## 4.2 Growth analysis and complementation of *ubiE* and *aroC* deletion mutants

The results from the macrocolony assay in **Section 4.1** showed an altered phenotype of the knockout strains of *S. aureus*. Furthermore, we observed that the mutant colonies were smaller when grown in aerobic conditions. In order to further analyse the growth of these mutants, growth assays in liquid culture were performed. Strains were grown in BHI medium for approximately 13 hours and the cell density were measured ( $\text{OD}_{600}$ ) at 10-minute intervals. In **Figure 4.2** the growth of the mutants is compared to the wild-type. The results reveal that both mutants ( $\Delta ubiE$  and  $\Delta aroC$ ) grown at a slower rate than the wild-type, and that they do not reach the same cell density when grown in BHI media.

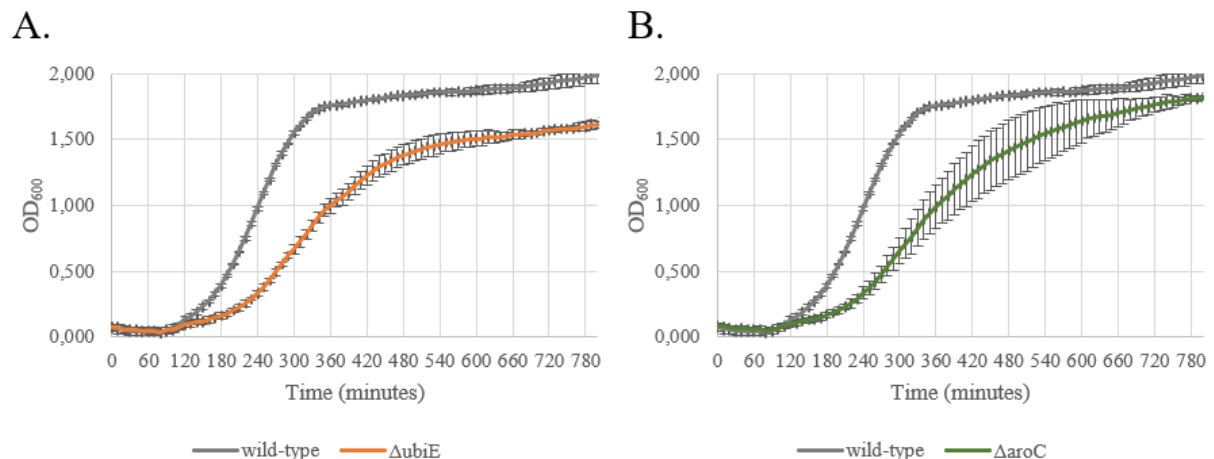


**Figure 4.2** Growth of *ubiE* (A) and *aroC* (B) knockdown strains compared with wild-type (Newman). Strains were grown in BHI medium, with proper antibiotics when necessary. Growth was measured spectrophotometrically ( $\text{OD}_{600}$ ) at 10-minute intervals for ~13 hours

Since both *ubiE* and *aroC* are involved in the biosynthesis of menaquinone, we wanted to see if the deletion mutants could be complemented by external addition of MK-4 (a short chain menaquinone) to the media. The bacterial strains were grown with different concentrations of MK-4 to substitute for the impaired synthesis of MK. Growth was monitored for approximately 13 hours, and the result is presented in **Figure 4.3**.

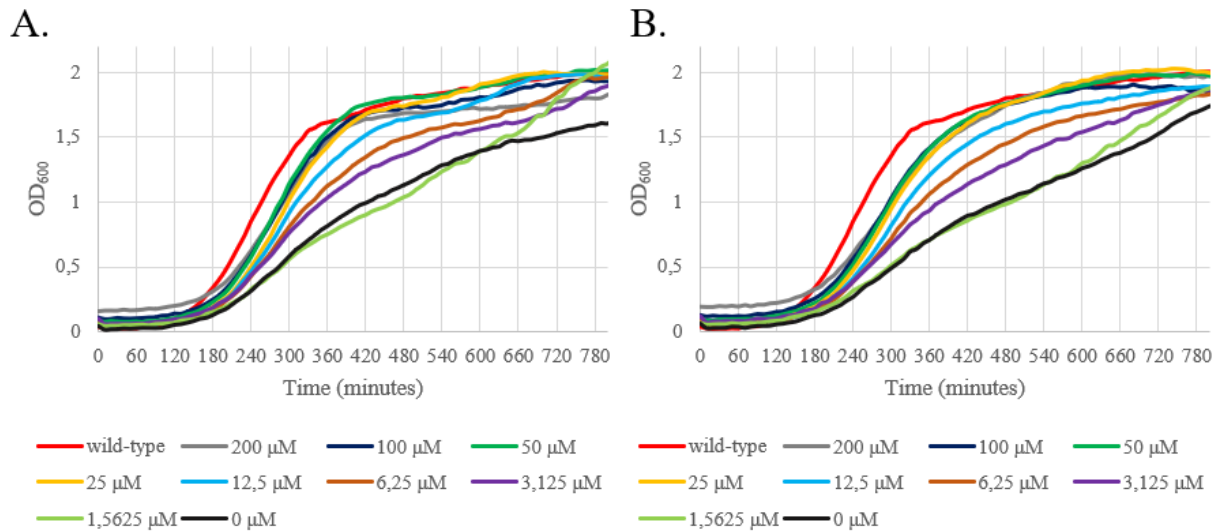


**Figure 4.3** Growth fitness of  $\Delta ubiE$  (A) and  $\Delta aroC$  (B) knockdown strains, when BHI medium were supplemented with MK-4 concentrations ranging from 200  $\mu\text{M}$  – 1,5625  $\mu\text{M}$ . Growth was measured at 10-minute intervals for ~13 hours.

The growth curves show that MK-4 improves the growth of the mutants, and the growth rate improves proportionally with increased concentrations. When the medium is supplemented with 25  $\mu\text{M}$  MK-4, mutants show close to normal growth when compared to the wild-type. Higher concentrations do not improve growth to a considerable extent. The results also imply that the bacterial growth of the mutants reach the same cell density as the wild-type due to the supplementation of MK-4 to the growth media. However, the growth rate of the mutants is lower than wild-type even with the highest MK-4 concentration used.

The results from the chemical complementation show that supplementation of MK-4 to the growth media improve the growth fitness of the mutants. We also wanted to see if we could genetically complement the mutant  $\Delta ubiE$ . The *ubiE* gene is located in an operon upstream of *hepT*, another gene in the MK biosynthesis pathway (**Figure 1.3**). The operon structure of *ubiE*-operon was confirmed by RT-PCR assay (**Figure A1**). Deletion of *ubiE*, could therefore potentially influence the transcription of the downstream *hepT*-gene as well. *ubiE* and *ubiE\_hepT* were therefore cloned into the plasmid pLOW behind the IPTG inducible promoter,

$P_{\text{spac}}$ , in order to construct two plasmids used for the genetic complementation. These were then transformed into the  $\Delta ubiE$  mutant of the Newman strain to make the strains HO18 ( $\Delta ubiE::\text{spc}$ ,  $P_{\text{spac}}-ubiE$ ) and HO19 ( $\Delta ubiE::\text{spc}$ ,  $P_{\text{spac}}-ubiE_{\text{hepT}}$ ) respectively. A control plasmid was also included in the growth assay.

Potentially, the optimal concentration for the inducer IPTG can be found by doing a growth assay with different concentrations of the inducer, followed by a western blot to decide which concentrations that give the amount of protein product closest to the wild-type strain. Because we do not have antibodies that bind our protein of interest, it is not possible to do this. Instead, the growth assay was performed with different concentrations of the inducer IPTG in order to reveal the optimal concentration of the induction of gene expression and complementation of the growth defect. The results are presented in **Figure 4.4**.

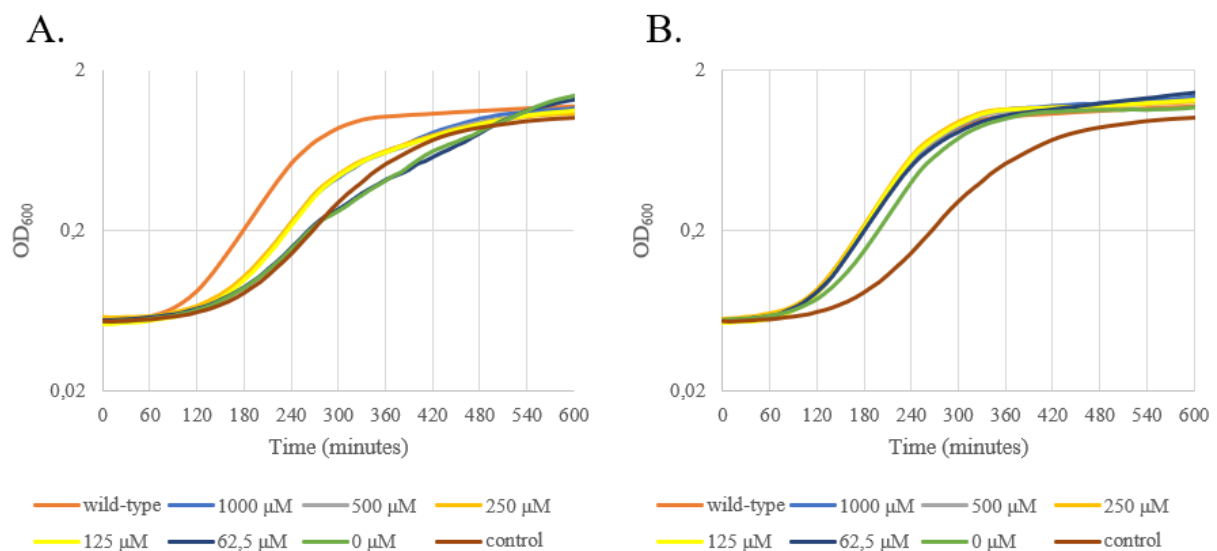


**Figure 4.4** Growth assay investigating required concentration of IPTG for complementation of the growth defects in **A**: HO18 ( $\Delta ubiE::\text{spc}$ ,  $P_{\text{spac}}-ubiE$ ) and **B**: HO19 ( $\Delta ubiE::\text{spc}$ ,  $P_{\text{spac}}-ubiE_{\text{hepT}}$ ). HO21 containing an empty plasmid was included as a control. Bacterial strains were grown in BHI medium supplemented with appropriate antibiotics and various concentrations of IPTG. The optical density (OD<sub>600</sub>) were measured at 10-minute intervals for approximately 10 hours. Curves are presented as logarithmic scale.

The strain complemented with expression of only *ubiE* does not clearly improve growth with increasing concentrations of IPTG, and the growth defect of the deletion mutant is not complemented well with even the highest concentration of IPTG (1000 μM). This strain has in general a poor growth fitness. In contrast, the strain complemented for both *ubiE* and the downstream gene *hepT* has in general an improved growth rate compared to the control strain (HO21), even without induction of gene expression. A likely reason is that the  $P_{\text{spac}}$ -promoter

of this plasmid is known to be leaky (Liew et al., 2011). Expression of *ubiE\_hepT* thus complements the growth defect of the mutant.

### 4.3 Macrocolony structuring are restored upon genetic complementation, but not by chemical complementation

As shown above, the deletion of either *ubiE* or *aroC* lead to an altered macrocolony phenotype. In order to show that the macrocolony phenotype was due to lack of *ubiE*, we performed experiments to complement for the disrupted biosynthesis of menaquinone. Macrocolony assays with both chemical and genetic complementation were performed.

The chemical complementation was performed by growing macrocolonies of the deletion strains of *ubiE* and *aroC* on TSB with 100  $\mu\text{M}$   $\text{MgCl}_2$  plates with and without addition of MK-4. In the chemical complementation assay, macrocolonies of the *ubiE* and *aroC* mutant strains do not present a visible change of phenotype in the presence of MK-4 (**Figure 4.5**). This result was unexpected because in the liquid growth assay, the addition of MK-4 somewhat complemented the mutants. In contrast, in these macrocolonies, MK-4 seems to not affect the growth or phenotypic traits of either of the colonies.

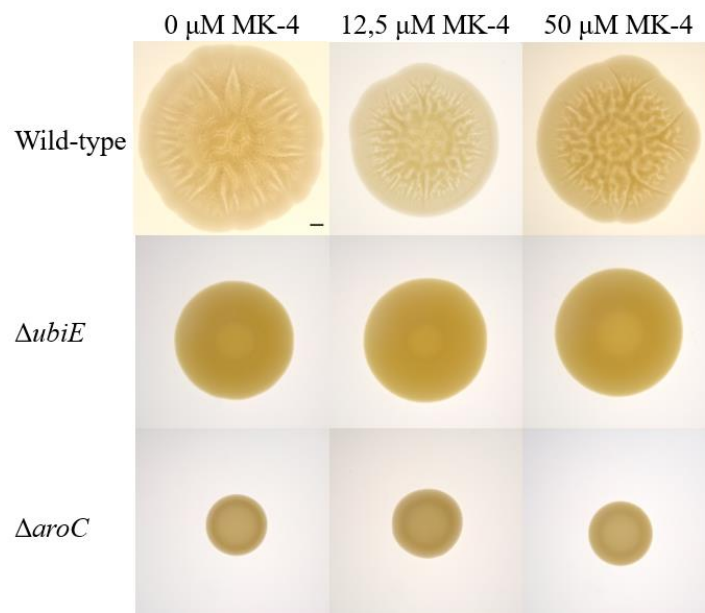


**Figure 4.5** Macrocolony phenotype of wild-type and *ubiE* and *aroC* deletion mutants with chemical complementation. Macrocolonies were aerobically grown on TSB plates with 100  $\mu\text{M}$   $\text{MgCl}_2$ , with and without MK-4 supplementation, at 37  $^{\circ}\text{C}$  for five days before they were imaged using a stereomicroscope (AxioZoom V16, Zeiss). Scale bar is 1000  $\mu\text{m}$ .

The genetic complementation was performed with genetic complementation mutants of the *ubiE* knockout strain grown on TSB with 100  $\mu$ M MgCl<sub>2</sub> plates with and without 50  $\mu$ M inducer IPTG. Similar to the growth experiment above, the complementation strains included strains ectopically expressing *ubiE* (HO18), and both *ubiE* and *hepT* (HO19) through IPTG induction.

When the *ubiE* deletion of *S. aureus* was complemented genetically with only the *ubiE* gene expressed ectopically, there was no visible alteration in the phenotype of the macrocolony grown in aerobic conditions (**Figure 4.6B**). It still had the flat and smooth surface that had been observed as the characteristic phenotype of both the deletion mutants in other macrocolony assays (**Figure 4.1**). In contrast, when the expression of both *ubiE* and *hepT* were induced with 50  $\mu$ M IPTG, there were a clear change in phenotype. The macrocolony had regained more structural traits that resembled that of the wild-type strain (**Figure 4.6A**). It should be noted however that, the complemented mutant was different from the wild-type. As mentioned above, the wild-type formed an irregular shape of the macrocolony, but the genetic complementation form a much more regular round shape.

It should be noted that in the non-induced macrocolony of  $\Delta ubiE::spc$ ,  $P_{spac-ubiE\_hepT}$  (HO19), growth is restored compared to  $\Delta ubiE::spc$ ,  $P_{spac-ubiE}$  (HO18) (same as observed in liquid medium, see **Figure 4.4**), but the structuring of the macrocolony is not evident, although some spots or circular shapes in the middle of the colony were observed (poorly visible in the image). This was not observed for any of the other strains earlier in this work. Together, this suggest that the leaky expression of *ubiE\_hepT* is sufficient to complement growth, but higher expression is necessary to induce the formation of a structured macrocolonies.

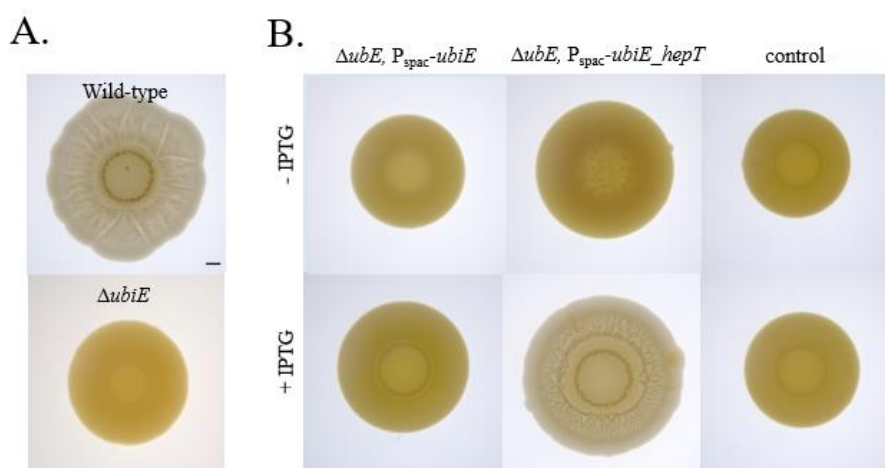


**Figure 4.6** Effect of genetic complementation on  $\Delta ubiE::spc, P_{spac-ubiE}$  (HO18) and  $\Delta ubiE::spc, P_{spac-ubiE\_hepT}$  (HO19) mutants. **A:** Macrocolonies of wild-type and  $\Delta ubiE$ . **B:** Macrocolonies of  $\Delta ubiE::spc, P_{spac-ubiE}$  and  $\Delta ubiE::spc, P_{spac-ubiE\_hepT}$  with and without induction of gene expression with 50  $\mu M$  IPTG. Macrocolonies were grown in oxic conditions for five days at 37  $^{\circ}C$  on TSB with 100  $\mu M$   $MgCl_2$  plates, with antibiotics when appropriate. Imaging were done with a stereomicroscope (AxioZoom. V16, Zeiss). Scale bar is 1000  $\mu m$ .

#### 4.4 *S. aureus* does not form structured macrocolonies under anaerobic conditions

The results so far shows that the expression of *ubiE* and *hepT* are critical for the formation of structured macrocolonies in *S. aureus*. *ubiE* and *hepT* are involved in the synthesis of menaquinone (**Figure 1.1**), and electron carrier required for electron transport during aerobic and anaerobic respiration. While *S. aureus* wild-type performs aerobic respiration, the mutant strain has most likely changed to a fermentative metabolism, where electron carrier menaquinone is no longer needed. This was also shown by measuring the fermentation products by HPLC in the wild-type and mutant strains; the mutant, but not the wild-type produced lactic acid when grown under standard aerobic conditions in liquid culture (Mårli, 2020).

We therefore hypothesized that the lack of structured macrocolony formation was due to lack of respiration. In order to study how the macrocolonies developed under anaerobic conditions, colonies were incubated in anaerobic jars. Strikingly, the wild-type strain does not form the structured macrocolonies under these conditions (**Figure 4.7A**). The illustrations of the anaerobically grown macrocolonies shows that macrocolonies of the mutant strains,  $\Delta ubiE$  and  $\Delta aroC$ , are quite similar to that of the anaerobic wild-type macrocolonies, which is not surprising since menaquinone biosynthesis is not required for fermentation. All colonies have a very round shape with a light beige/off-white colour. These macrocolonies are also characterized by lack of any structural traits (e.g. wrinkles), and instead present a flat smooth surface. The colony sizes are much more similar between the anaerobic samples than what has

been observed in the aerobic samples in **Section 4.1**. The diameter of  $\Delta ubiE$  and  $\Delta aroC$  macrocolonies are approximately 4,04 mm and 3,65 mm, respectively. This corresponds to around 2% and 12% lower than the diameter of the wild-type macrocolony, respectively, which is 4,14 mm. The experiments with chemical and genetic complementation were also performed under anaerobic conditions, but unsurprisingly, no structuring of the macrocolonies was visible in any of the strains (**Figure 4.7B** and **C**, respectively).

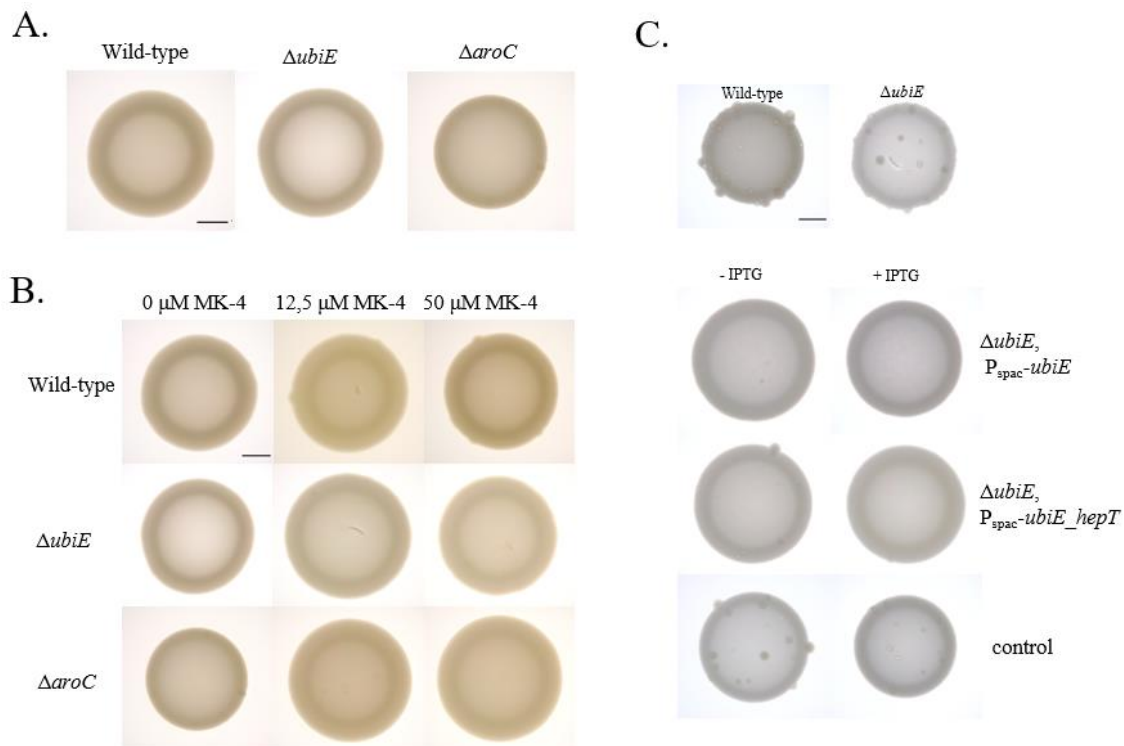


**Figure 4.7** Macrocolony phenotype of anaerobically grown *S. aureus*. **A:** Morphology of wild-type and knockout mutants ( $\Delta ubiE$  and  $\Delta aroC$ ). **B:** Chemical complementation of mutant strains  $\Delta ubiE$  and  $\Delta aroC$  grown with supplementation of MK-4. **C:** Genetical complementation with  $\Delta ubiE::spc$ ,  $P_{spac-ubiE}$  (HO18) and  $\Delta ubiE::spc$ ,  $P_{spac-ubiE\_hepT}$  (HO19) mutants using IPTG for induction of gene expression. Macrocolonies were grown on TSB with 100  $\mu$ M  $MgCl_2$  agar plates, with antibiotics when appropriate, at 37 °C for five days before they were imaged using a stereomicroscope (AxioZoom. V16, Zeiss). Scale bars are 1000  $\mu$ m.

Images of the anaerobic macrocolonies reveal that a few characteristic lumps had formed within the colonies, e.g. in **Figure 4.7C** this can be observed for wild-type,  $\Delta ubiE$  and the control. In order to exclude the possibility that this is caused by contamination in the bacterial frozen stocks, a purification was performed. This was done by streaking bacteria from existing frozen stock on TSB agar plates supplemented with antibiotics when necessary. After an incubation time over night at 37 °C, single colonies were picked and grown in liquid cultures.

After an overnight incubation at 37 °C with shaking, the liquid cultures were mixed with glycerol (3:1) in order to make new freeze stocks that were used in later assays. To investigate if the lumps would still form, macrocolonies were grown from bacterial strains both before and after the cultures had been purified, and the morphology of the colonies were compared. Results are not shown in this work, but revealed that the lumps were still present. These observations exclude the possibility that these phenotypic characteristics are caused by contamination but does not reveal any explanation of what might cause these distinct lumps. This phenotype was not further investigated in this work.

#### **4.5 Knockdown of other *men*-genes in the menaquinone biosynthesis pathway results in altered macrocolony formation**

We have observed that the deletion of *ubiE* and *aroC* have led to altered macrocolony biofilm formation in *S. aureus* (see **Section 4.1**). To further investigate if this also applies to other genes that participates in the biosynthesis of menaquinone, growth and macrocolony formation upon depletion of *menA*, *menF*, and *menE* (three genes that catalyses various steps in the synthesis of menaquinone, see **Figure 1.3**) were investigated. The depletion of these genes was performed using CRISPR interference with 300 µM IPTG. Because we do not know if any of these are essential for the growth of *S. aureus*, a growth assay in liquid TSB media was performed, and the results are presented in **Figure 4.8**. The measured data implies that the decreased expression of either of the three mentioned *men*-genes leads to a decreased growth fitness in Newman. No obvious differences between the growth with and without induction with 300 µM IPTG are observed. Variations between the control and the three depletion strains does not show substantial differences either.

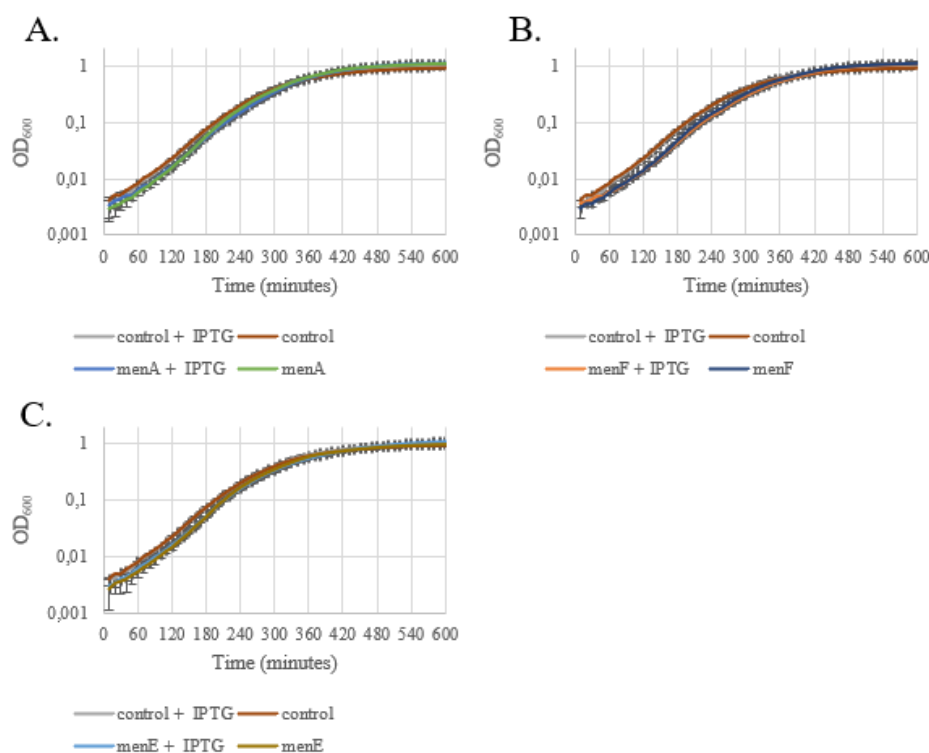


**Figure 4.8** Growth fitness of CRISPRi depletion of genes participating in the biosynthesis of menaquinone: *menA* (A), *menF* (B) and *menE* (C). CRISPR interference were performed with 300  $\mu$ M IPTG. A control carrying a non-targeting sgRNA was included for comparison. Bacterial strains were grown in TSB (with appropriate antibiotics) at 37 °C for ~10 hours, growth was measured spectrophotometrically (OD<sub>600</sub>) at 10-minute intervals.

An assay to further investigate if reduced expression of *menA*, *menF* or *menE* affects the macrocolony biofilm formation in *S. aureus* was performed. The bacterial strains of the CRISPRi depletions were grown as macrocolonies on TSB with 100  $\mu$ M MgCl<sub>2</sub>, with appropriate antibiotics, for five days at 37 °C. Depletion strains were grown in the presence and absence of 300  $\mu$ M of IPTG. Both anaerobic and anaerobic macrocolonies were included. The aerobic macrocolony phenotypes are presented in **Figure 4.9** and is compared with a control strain (Newman with non-targeting sgRNA). The results reveal that the *menA* depletion without IPTG induction forms a relatively large macrocolony with round shape and is characterized by wrinkling. This phenotype resembles what has been observed for the control strain with a non-targeting sgRNA. However, when the *menA* depletion strain is grown on plates supplemented with 300  $\mu$ M IPTG, the phenotype changes. The reduction of *menA* expression leads to a macrocolonies with smaller size and loss of a round shape. The size is substantially smaller and is very different form the non-induced colony if the same strain (measuring the size of the colony is hard due to the irregular shape). In addition, the wrinkling is not as evident as for the non-induced depletion of this strain or the control.

Comparing the phenotypic traits of the macrocolony of the *menF* with and without reduced gene expression reveal very small differences. The only observation is a slight change in the core structure of the macrocolony. Nor does the *menE* depletion show very distinct changes in phenotype as what has been observed for the *menA*. Observations imply that there are small changes in the core structure and reduced number of wrinkles compared to the macrocolony without reduced gene expression. The macrocolony with depleted *menE* also shows a slightly smaller colony morphology than the non-induced macrocolony, with 13,3% smaller diameter. However, it is difficult to confirm that the reduced gene expression of *menF* or *menE* leads to changes in the macrocolony morphology. The differences that we observe for these macrocolonies are not much more evident than the differences that are observed for the control. It might be that the genes are expressed in different rates in *S. aureus*, and that a higher induction concentration of IPTG is required for full depletion in order to see more clear phenotypic changes. Together this implies that *menA* is important for the macrocolony biofilm formation of *S. aureus* in aerobic environments, but it is hard to draw conclusions from this result regarding the effect *menF* or *menE* has on this process.

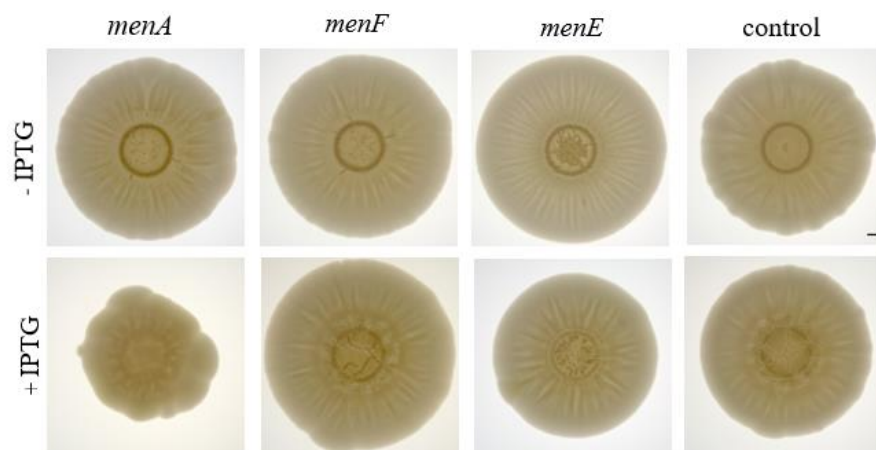


**Figure 4.9** Macrocolony phenotype of CRISPRi knockdown strains (*menA*, *menF* and *menE*) grown in aerobic conditions. The figure visualizes macrocolonies with and without induction of gene expression through supplementation of 300  $\mu$ M IPTG to the agar media. A control strain with a non-targeting sgRNA is included for measures. The bacterial strains were grown on TSB with 100  $\mu$ M  $MgCl_2$  agar plates at 37  $^{\circ}$ C in both anoxic and oxic conditions. After a five-day incubation time, the macrocolonies were imaged using a stereomicroscope (AxioZoom. V16, Zeiss). Scale bar is 1000  $\mu$ m.

The phenotypic traits for macrocolonies with reduced expression of *menA*, *menF* and *menE* were also investigated for colonies grown in absence of oxygen. Because earlier observations in **Section 4.4** revealed no phenotypic changes of anaerobic wild-type macrocolonies or macrocolonies of the deletion strains  $\Delta ubiE$  and  $\Delta aroC$ , we did not expect to

see any changes in the morphology of anaerobically grown macrocolonies of depleted genes in this assay. Results confirms our hypothesis and does not show any changes. All macrocolonies are characterised with relatively small colonies with complete lack of wrinkles or evident structures.

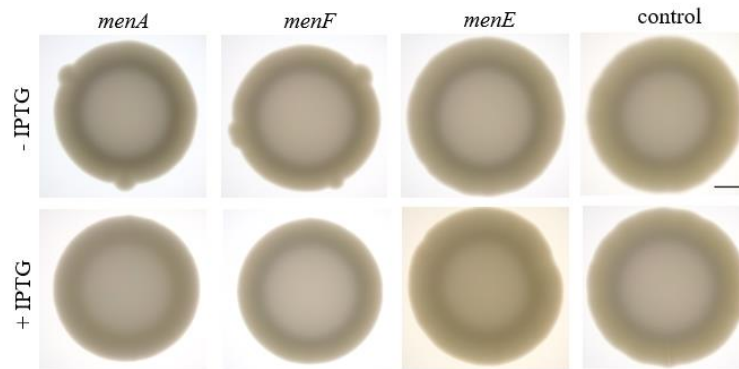


**Figure 4.10** Phenotypic traits observed for CRISPRi depletions of *menA*, *menF* and *menE* grown in anaerobic conditions. Macrocolonies were grown on for five days at 37 °C on TSB with 100  $\mu$ M  $MgCl_2$  agar plates (with appropriate antibiotics) in anaerobic jars. Macrocolony phenotype is presented with and without induction of gene expression with 300  $\mu$ M IPTG. Scale bar is 1000  $\mu$ m.

#### 4.6 The chemical composition of the extracellular matrix (ECM)

We now know, based on the macrocolony assays that oxygen availability and impaired menaquinone biosynthesis heavily influence macrocolony and biofilm formation in *S. aureus*. As mentioned in **Section 1.2**, biofilm formation depends on the composition of the ECM. Therefore, it was interesting to further investigate which differences in the ECM that caused the phenotypic differences observed in the mutant strains,  $\Delta ubiE$  and  $\Delta aroC$ . FTIR spectroscopy as well as direct quantification of nucleic acids, polysaccharides and proteins from the ECM were used to determine differences in the chemical composition of the extracellular matrix of macrocolonies.

##### 4.6.1 FTIR spectroscopy analyses reveal differences in the chemical composition of macrocolonies between aerobic and anaerobic macrocolonies

A FTIR-spectroscopy analysis was performed on macrocolonies of wild-type and deletion mutants ( $\Delta ubiE$  and  $\Delta aroC$ ) grown at aerobic and anaerobic conditions. An attempt to analyse the ECM extracts of macrocolonies was also performed. However, the high concentration of NaCl used as dissolvent of the extracts were not compatible with FTIR spectroscopy, and the signals were low.

FTIR-spectroscopy has shown to be an excellent analysis method to obtain fingerprint spectra of the chemical composition of bacterial isolates, which can be used to characterise microbial strains. This method has also been used to investigate microorganisms in biofilm (Schmitt & Flemming, 1998). In this work, this method was used to get a better understanding of chemical differences in the macrocolony composition between the wild-type and the mutant strains.

The FTIR spectra presents a very complex set of data, and it requires application of multivariate data analysis to interpret the results directly. Therefore, we applied principal component analysis (PCA) and for the analysis we used separate spectral regions. The PCA results are visualized by the score and loading plots. These plots can help to reveal patterns such as clusters, trends and outliers in the results (Rajalahti & Kvalheim, 2011). The PCA gives a more simplified view of the results and still express as much as possible of the total variation in the data (Destefanis et al., 2000).

In the PCA analysis, technical and biological replicates are represented and were not averaged. The PCA results of the whole spectral region covering all chemical components are represented in PCA score plots in **Figure 4.11A** and **B**. There we can observe the main variations pattern and explore how the samples related to each other and investigate if the growth conditions or strain identity alters the chemical composition of the macrocolony. A score plot highlighting the differences between the replicates and between strains with different identity is presented in **Figure 4.11A**, whereas differences in the macrocolonies depending on the growth conditions (aerobic and anaerobic) are shown in **Figure 4.11B**. In both plots, each point represents a technical replicate. In the FTIR analysis that was performed we included two biological replicates for each strain and growth conditions, with three technical replicates for each biological replicate.

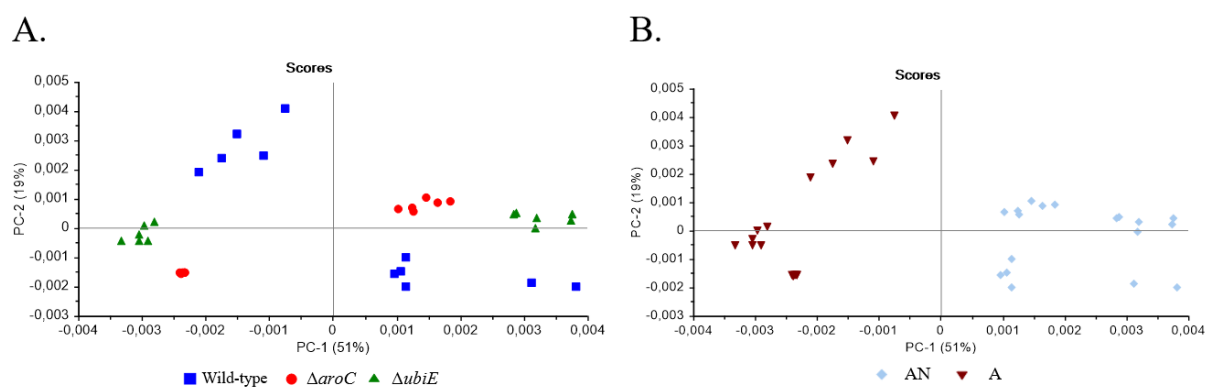


**Figure 4.11 A:** Score plot to highlight the relation between samples based on the chemical differences caused by strain differences. **B:** Score plot with respect to the growth conditions of the samples (AN: anaerobic, A: aerobic).

**Figure 4.11A** shows that the PCA scores for the strains gather in completely distinct groups apart from each other, and we can, therefore, assume that there is a significant difference in the chemical compositions between the three strains. In the same plot it can be observed from the colour codes (blue, red and green) that most of the strains are grouped in two groups clearly separated from each other. The explanation of such differentiation is shown in **Figure 4.11B** where we can see that the same groups are highlighted depending on the growth conditions and there are two groups representing the difference according to the growth conditions. Anaerobic (AN) and aerobic (A) samples are separated more in the PC1 axis. PC1 and PC2 explained 51% and 19% of the variance, respectively. This score plot indicates that there is also a significant difference in the chemical composition of the ECM between aerobically and anaerobically grown macrocolonies.

Because of the differences observed in the total cellular chemical composition between the macrocolonies grown in different conditions, it was of interest to further investigate actual differences in chemical composition between the samples in **Figure 4.11**. Therefore, a PCA of the FTIR spectra at different spectral regions was performed to investigate further differences in the lipid, protein, and polysaccharide profile for wild-type macrocolonies grown with and without oxygen. The results are presented in **Figure 4.12**, **Figure 4.13** and **Figure 4.14**, respectively. Green triangles indicates that the macrocolonies were grown in the presence of oxygen and red dots represents samples grown in absence of oxygen.

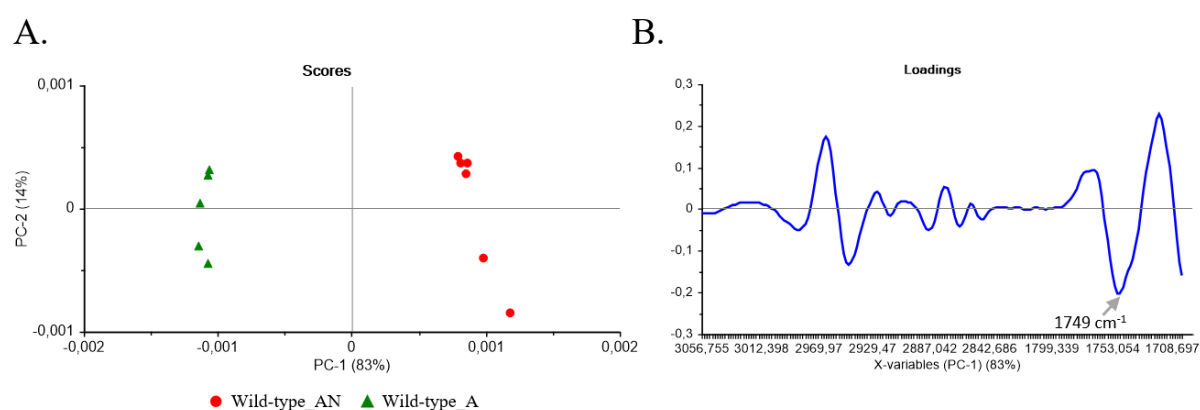


**Figure 4.12** Score (A) and loading plot (B) from PCA of the lipid spectra of wild-type macrocolonies grown in oxic and anoxic conditions.

As we can see in the score plot for the lipid spectral region in **Figure 4.12A**, there is a significant difference between wild-type macrocolonies grown in aerobic and anaerobic conditions in regard to the lipid spectral region due to the distinct groups that are formed. PC1

and PC2 explained 83% and 14% of the variance in the score plot, respectively. The loading plot in **Figure 4.12B** reveals the most significant peaks responsible for the results that are observed in the score plot. This plot indicates that the difference between the samples is due to an ester bond (C=O) peak at  $1749\text{ cm}^{-1}$  indicating that the total lipid content and mainly triacylglycerides and esters in the cells shows to be significantly different in oxic and anoxic samples of the wild-type strain. We can conclude that the aerobic samples are lower in total lipid content than the anaerobic samples.

The differences in the protein spectral region for the wild-type macrocolonies grown with and without oxygen was also investigated by performing PCA. The score plot and loading plot from this PCA analysis is presented in **Figure 4.13A** and **B**, respectively.

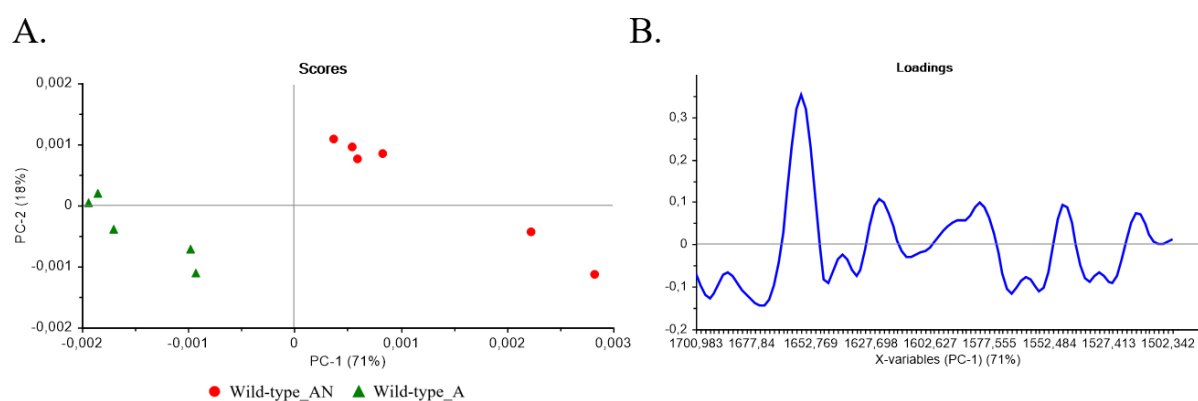


**Figure 4.13** Score (A) and loading plot (B) from a PCA of the protein spectral region for wild-type macrocolonies grown in aerobic and anaerobic conditions.

From the score plot in **Figure 4.13A** it can be observed that there is a significant difference in protein profile between wild-type macrocolonies grown in aerobic and anaerobic conditions. PC1 and PC2 explains 71% and 18% of the variance in the score plot, respectively. The loading plot in **Figure 4.13B** reveals the main peaks that are significant for score plot results. Loading plot identifies several protein related peaks, but it is difficult to draw any conclusions as these are not purified proteins. One thing is clear, that protein content differs depending on the growth conditions.

The polysaccharide spectral region was used to study polysaccharide profile of the wild-type macrocolonies by performing a PCA. A score plot and loading plot of this analysis is presented in **Figure 4.14**.

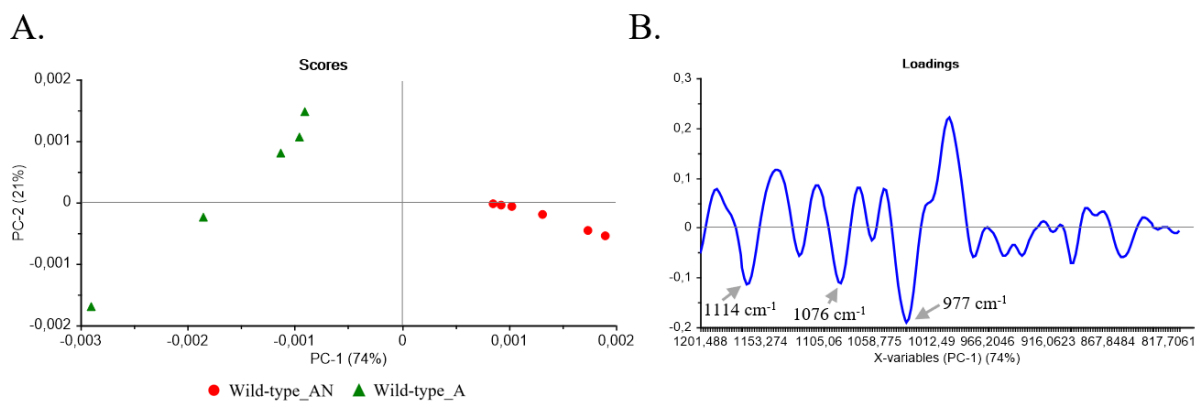


**Figure 4.14** Score (A) and loading plot (B) for the polysaccharide spectral region of wild-type macrocolonies grown in aerobic and anaerobic conditions.

**Figure 4.14A** shows that there is a significant difference in the polysaccharide spectral region between samples grown with and without oxygen. PC1 and PC2 explains 74% and 21% percent of the variance between the samples, respectively. The loading plot in **Figure 4.14B** reveals the most significant peaks responsible for the results observed in the score plot. The loadings indicate that important wavenumbers are 1114 cm<sup>-1</sup>, 1076 cm<sup>-1</sup> and 977 cm<sup>-1</sup>, which indicates that the differences we observe for the samples are caused by several polysaccharide peaks. Some of the relevant peaks are probably related to wall teichoic acids.

Taken together, the FTIR analysis suggest that the extracellular matrix of the aerobic and anaerobic matrix differs both in protein and polysaccharide content. The lipid content also differs but are more likely related to the cell membrane.

#### 4.6.2 FTIR-spectroscopy analyses show variation in chemical composition of macrocolonies between wild-type and menaquinone biosynthesis mutants.

PCA analyses were also performed on the FTIR spectra from the wild-type and the two mutant strains ( $\Delta ubiE$  and  $\Delta aroC$ ) grown in aerobic conditions. The purpose was to investigate if the differences that were observed in **Figure 4.11A** were due to differences in lipid, protein or polysaccharide profiles for the macrocolonies chemical compositions.

**Figure 4.15** presents a score plot and a loading plot based on the PC analysis performed for the lipid spectral region with the different strains (wild-type,  $\Delta ubiE$  and  $\Delta aroC$ ) grown in aerobic conditions.

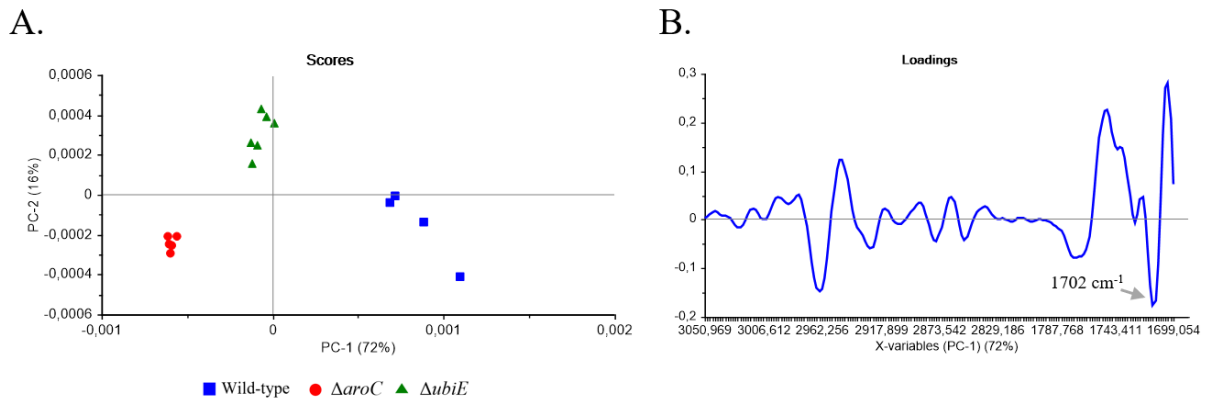


**Figure 4.15** Score (A) and loading plot (B) for the PCA analysis of the lipid spectral region of macrocolonies of different strains grown in aerobic conditions.

The score plot in **Figure 4.15A** shows that there is a difference in lipid profile between the strains, where PC1 and PC2 explains 72% and 16% of the variations observed for the lipid spectral region of the PCA analysis. The loading plot in **Figure 4.15B** reveals the most significant wavenumbers that are important for the score plot results. From the loading plot we observe that these strains have differences in the content and profile of free fatty acids, as the peak at 1702  $\text{cm}^{-1}$ , which represents acid carbonyl groups in fatty acids, shows to be most significant.

A PCA analysis were also performed and illustrated for the protein spectral region of strains grown in aerobic environments. The results from the PCA are presented in **Figure 4.16**.

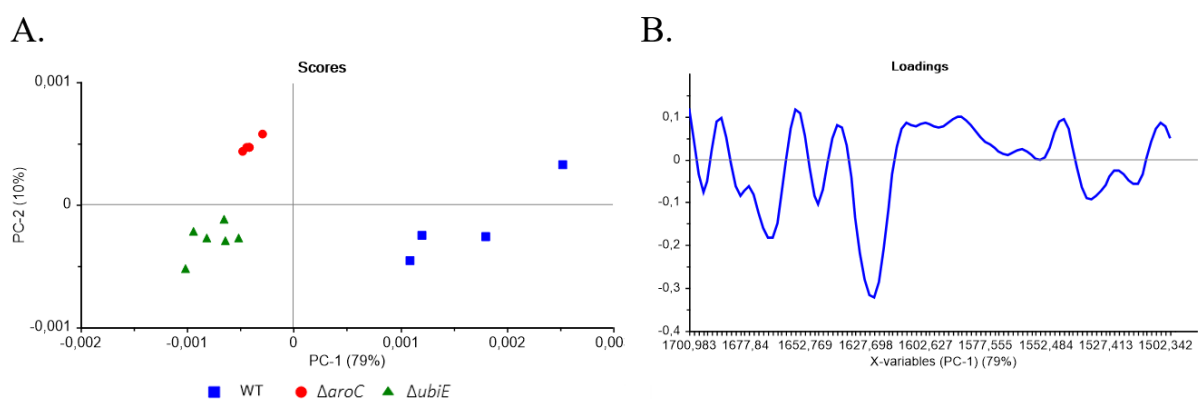


**Figure 4.16** Score (A) and loading plot (B) from a PCA of the protein spectral region of samples from different strains grown in aerobic conditions.

The strain identity clearly has an impact on the protein profile of measured macrocolonies as we can observe from the separations in the score plot (**Figure 4.16A**). However, it is difficult to make conclusions as to which proteins that cause these differences between the mutants and the wild-type because we are not looking at pure proteins.

A PCA of the polysaccharide spectral region for the different strains grown in aerobic conditions were also performed. The results are presented in **Figure 4.17A** and **B** as a score plot and loading plot, respectively.

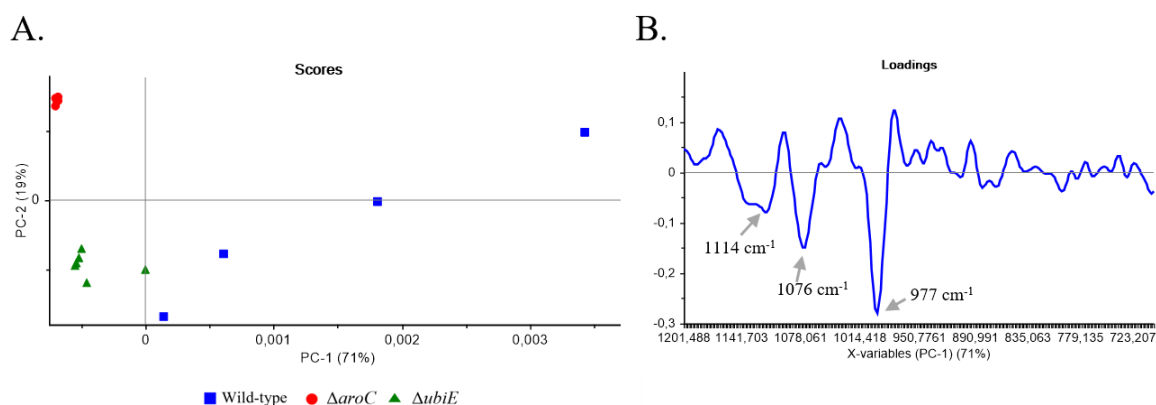


**Figure 4.17** Score (A) and loading plot (B) from a PCA of the polysaccharide spectral region for macrocolonies of different strains including WT,  $\Delta ubiE$  and  $\Delta aroC$  grown in aerobic conditions.

What we can see is that there is a difference in the polysaccharide profile between the different strains as shown in the score plot in **Figure 4.17A**. However, it should be noted that the replicates of the wild-type are very different from each other, and we do not observe a clear grouping of this strain as we can observe for the other two strains,  $\Delta ubiE$  and  $\Delta aroC$ . From this it is therefore difficult to conclude clearly how large the differences are between the wild-type and the mutants. From the PCA of the data, PC1 and PC2 explains 71% and 19% of the variations that are observed for the samples in the score plot. The loading plot in **Figure 4.17B** shows the wavelengths of relevance for the PC1 variations. Main peaks, at 1114  $\text{cm}^{-1}$ , 1076  $\text{cm}^{-1}$  and 977  $\text{cm}^{-1}$ , indicates that differences are potentially related to the wall teichoic acids in the samples, however interpretation of these results should be made with caution due to the observed variability between the replicates.

Again, taken together, the FTIR analysis suggests that the ECMs of the wild-type and mutants differ with regard to protein and probably also polysaccharide composition. As stated above, lipid differences are probably related to the cell membrane, and not the extracellular matrix.

#### 4.6.3 Direct quantification of proteins, extracellular DNA and polysaccharides in ECM

The FTIR analyses, suggested major differences both in content and composition of polysaccharides and proteins. We wanted to confirm this by an alternative method and, at the same time, find out if there were any differences in the content of extracellular DNA in the ECM, since the latter is not easily identified by FTIR. The ECM was extracted from macrocolonies by dissolving the colonies in 1,5 M NaCl, which will disrupt the attractive forces and interactions that holds the macrocolony together and lead to detachment of ECMs from the cells (Chiba et al., 2015). Proteins and extracellular DNA were quantified spectrophotometrically using a Nanodrop 2000 spectrophotometer (Thermo-Fisher Scientific). Further procedures and treatment with 5 % phenol and sulphuric acid is required in order to determine the amount of polysaccharides in the extracellular matrix. Quantification of polysaccharides was performed by measuring absorption at 492 nm in a plate reader (Synergy H1 Hybrid Reader, BioTek®). Glucose was used to make a calibration curve. These assays were performed on macrocolonies grown in both aerobic and anaerobic conditions during a 5-day growth period at 37 °C. The results from the quantification of the aerobic samples are presented in **Figure 4.18**.

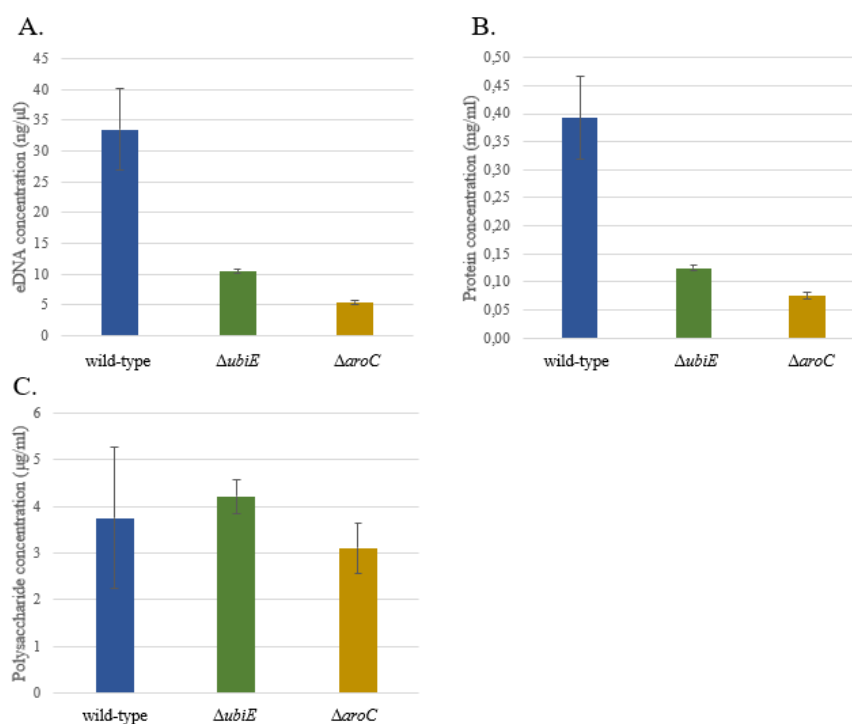


**Figure 4.18** Quantified concentrations of eDNA (A), proteins (B) and polysaccharides (C) from extracellular matrix of wild-type and mutant macrocolonies grown in aerobic conditions in 5-day period at 37 °C.

The measured concentration of eDNA from aerobic samples shown in **Figure 4.18A** indicates that wild-type macrocolonies have significantly higher concentrations than both  $\Delta ubiE$  and  $\Delta aroC$ . The same conclusion can also be said for the extracellular protein concentration in the wild-type compared to the mutants during aerobic growth. It cannot be confirmed from the results in **Figure 4.18C** that mutants and wild-type have different amounts of polysaccharides in the macrocolonies as the standard deviations are too large, however the quantities seem to be quite similar.

The quantified amounts of eDNA, protein and polysaccharides in **Figure 4.19A-C**, respectively, for 5-day-old macrocolonies grown without oxygen does not present as clear differences between the bacterial strains. Due to the considerably lower biomass for the anaerobically grown macrocolonies, the final OD when normalising the samples resulted in lower concentrations of all ECM components. Therefore, we might observe much higher variations between the samples.

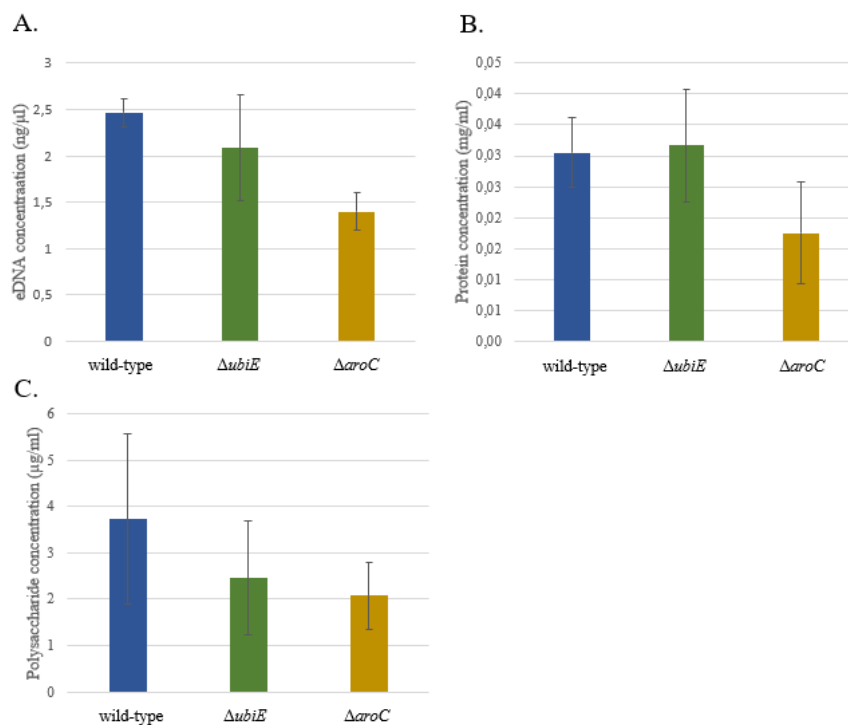


**Figure 4.19** Quantified concentrations of eDNA (A), proteins (B) and polysaccharide (C) from extracellular matrix of wild-type and mutant macrocolonies grown in anaerobic conditions in 5-day period at 37 °C.

#### 4.6.4 Robustness of macrocolonies

The different composition and structures of the macrocolonies imply that they may have different robustness (Wermser & Lopez, 2018). The robustness of wild-type,  $\Delta ubiE$  and  $\Delta aroC$  macrocolonies were compared by testing their resistance to mechanical dispersal. Both aerobic and anaerobic macrocolonies were included. The test was performed by moving a pipette tip in the centre of 5-day grown macrocolonies until colonies were visible disrupted. Results are presented with images before and after mechanical dispersal in **Figure 4.20**.

Notably, wild-type macrocolonies grown with oxygen seems to be very robust compared to the mutant strains. The reason is that the surface of this colony seemed much harder when mechanical pressure was applied (**Figure 4.20A**). The way it broke indicated that the colony were more structured and almost drier compared to the macrocolonies from the mutant strains. The  $\Delta ubiE$  mutant on the other hand broke almost immediately when the pipette tip touched the surface, and the colony had a much softer texture and did not give much resistance to the pressure that was applied. The  $\Delta aroC$  mutant macrocolony was even more soft in texture, and this might imply that the extracellular matrix composition is dominated by a higher volume of liquid than in the wild-type. As seen from the image before and after, when pressure was applied to the colony for the  $\Delta aroC$ , it almost closed again afterwards. In contrast, the rupture of the wild-type macrocolony resulted in a visible puncture or hole in the colony, and it still retained its original shape, despite the missing piece in the centre.

The anaerobic samples showed less variations between the strains (**Figure 4.20B**). All colonies were semi-soft and did not give much resistance to the pipette tip upon touching and vertical movement. These macrocolonies also lack the hard surface as observed for the aerobic wild-type macrocolony.

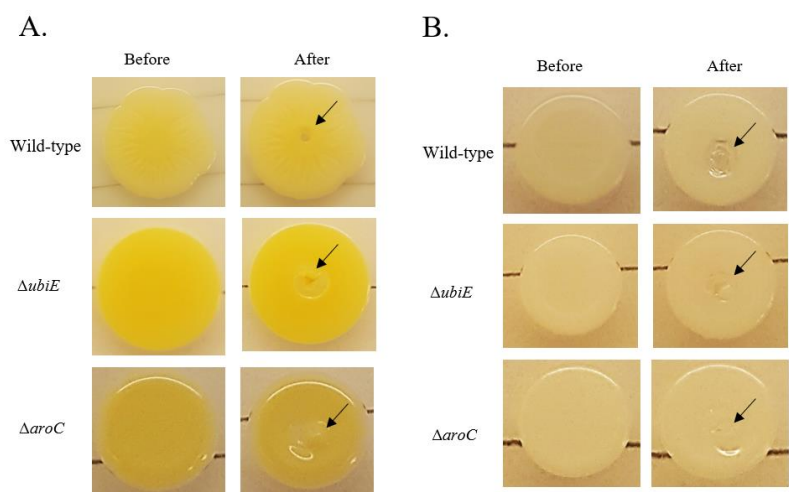


**Figure 4.20** Illustration of aerobic (A) and anaerobic (B) macrocolonies before and after the centre of the colonies were exposed to mechanical pressure. Arrows indicate where the colonies were ruptured.

#### 4.7 Crystal violet assay reveal that the deletion of *ubiE*, but not *aroC*, lead to reduced biofilm formation on the solid liquid interface

We have observed significant differences in the chemical composition of the extracellular matrix in mutant strains of *S. aureus*. We wanted to further determine if the deletion mutants had an effect on the production of total biofilm mass in liquid during biofilm formation. Microtiter plate assays has been widely used to investigate the ability of bacterial strains to attach and form biofilm on abiotic surfaces. This method was therefore applied on deletion mutants ( $\Delta ubiE$  and  $\Delta aroC$ ) and complemented strains (HO18, HO19) in order to determine if there are any differences in the amount of formed biofilm compared to wild-type or a control (HO21). The bacterial strains were initially grown overnight in TSB medium. Overnight cultures were diluted 1/10 in 96-well microtiter plates in TSB supplemented with 1 % (w/v) NaCl + 1 % (w/v) glucose and incubated at 37 °C. Media was supplemented with 50  $\mu$ M IPTG for induction of gene expression, and antibiotics were included when necessary. After 24 hours of incubation, the total biofilm mass was quantified spectrophotometrically (OD<sub>600</sub>) using crystal violet staining. Results are presented in **Figure 4.21A** and **B**.

The results in **Figure 4.21A** show that the ability of  $\Delta ubiE$  to attach to and to form biofilm in the abiotic microtiter plate is less when compared to the measured total biomass of the wild-type.  $\Delta ubiE$  produces approximately 1/3 of the biomass of the wild-type, which gives us the reason to think that the lack of *ubiE* highly affect the ability of this bacteria to form biofilm. The deletion of *aroC*, on the other hand, show higher amount of total biofilm mass compared to the wild-type in this assay. However, a repetition of the assay revealed a more

similar result for *aroC* and wild-type, with overlapping error bars. Therefore, from these results, it cannot be confirmed that the deletion of *aroC* had any effect on the ability of *S. aureus* to form biofilm.

The genetic complementation strains of  $\Delta ubiE$  were also included in this crystal violet quantification assay in order to determine if the complementation of either *ubiE*, or *ubiE\_hepT* restore reduced biofilm formation that was observed for  $\Delta ubiE$  in **Figure 4.21A**. The results of the complemented strains are presented in **Figure 4.21B**. HO18 ( $\Delta ubiE::spc$ ,  $P_{spac-ubiE}$ ) and the control, with an empty plasmid, show similar amounts of total biomass. Because the error bars overlap, we cannot conclude that there are evident differences between the strains in regard to ability to form biofilm on abiotic surfaces. This is not very surprising given that complementation of *ubiE* alone have not made significant differences in earlier assays in this work. In contrast, based on previous observations in this work, we would expect HO19 ( $\Delta ubiE::spc$ ,  $P_{spac-ubiE\_hepT}$ ) to restore the biofilm formation of the  $\Delta ubiE::spc$  to wild-type levels. The results in **Figure 4.21B** confirms that the strain with *ubiE\_hepT* has a higher ability to attach and form biofilm on abiotic surfaces in a microtiter plate when expression is induced with 50  $\mu$ M IPTG. Thus, the amount of total biofilm mass is higher for this strain compared to the control, although it should be noted that the biofilm formation does not reach the same levels as wild-type.

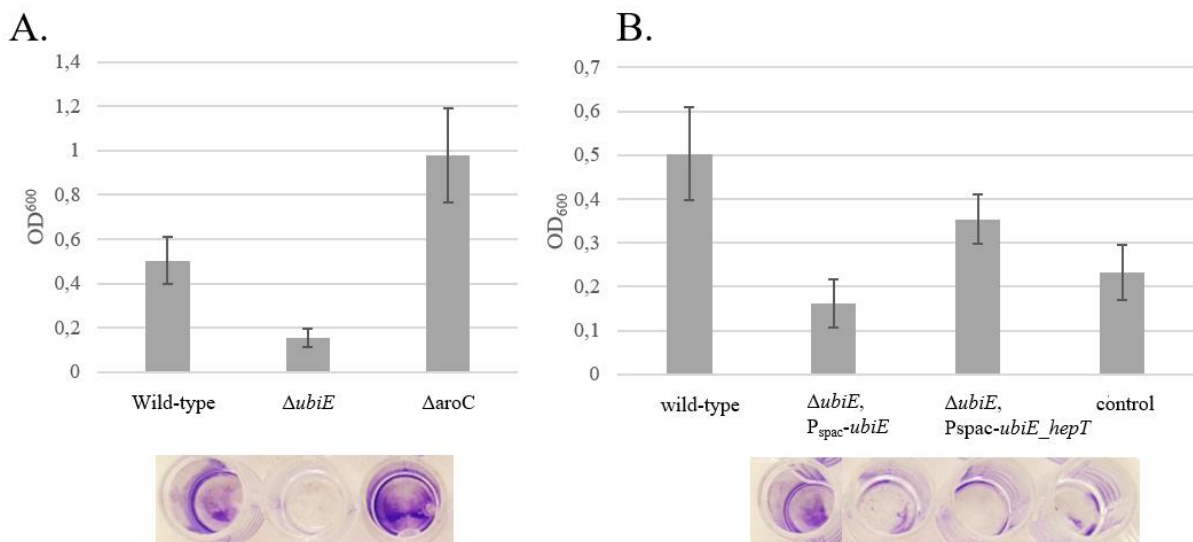


**Figure 4.21** Quantification of total biofilm mass of bacterial strains grown for 24 hours at 37 °C in 96-well microtiter plates with TSB containing 1 % (w/v) NaCl and 1 % (w/v) glucose. Biofilm were grown in aerobic conditions. **A:** Quantified biomass of deletion mutants,  $\Delta ubiE$  and  $\Delta aroC$ , compared with wild-type. **B:** Quantified biomass of  $\Delta ubiE$  complemented strains, HO18 ( $\Delta ubiE::spc$ ,  $P_{spac-ubiE}$ ) and HO19 ( $\Delta ubiE::spc$ ,  $P_{spac-ubiE\_hepT}$ ), and control containing an empty plasmid. Gene expression was induced with 50  $\mu$ M IPTG.

#### 4.8 *S. aureus* form small colony variants when either *ubiE* or *aroC* is deleted

Some clinical isolates of *S. aureus* has been shown to form so-called small colony variants (SCVs). These are bacterial strain that have a slower metabolism, and possess a higher resistance to certain antibiotics, and therefore can lead to persistent infections (Wakeman et al., 2012). The SCV phenotype often form in bacteria that are impaired in respiration due to mutations in genes required for the biosynthesis of menaquinone or heme (two components important for the generation of ATP during respiration) (Hammer et al., 2013; Proctor, 2019). The phenotype of small colony variants are characterized by non-pigmented colonies that are 10-fold smaller than those of its parental strain (Harris & Richards, 2006; Proctor, 2019). An assay testing if  $\Delta ubiE$  and  $\Delta aroC$  would develop such SCVs were therefore performed. The deletion mutants were streaked on TSB agar plates, with appropriate antibiotics and grown for 48 hours at 37 °C in aerobic or anaerobic conditions. In addition, different concentrations of MK-4 were added to agar plates to test if the addition of menaquinone would reverse the SCV phenotype.

Results presented in **Figure 4.22A** show that colonies of the  $\Delta ubiE$  mutant form substantially smaller colonies than the wild-type strain, which in contrast form large colonies that has grown together in a thick coat on the agar plates. SCV, however, are also characterized by non-pigmented colonies, which is not the case of  $\Delta ubiE$ . The reduced size of  $\Delta ubiE$  is also not as evident as for the  $\Delta aroC$ . This mutant is clearly affected by a slower growth due to the reduced metabolism. The  $\Delta aroC$  mutant also develops colonies with the characteristic non-pigmented colonies that normally are observed for SCVs. The chemical complementation with MK-4, does not show any effect on the mutant colonies. The results are, however, not surprising, as the chemical supplementation of MK-4 has failed to complement the deletion mutants in any of the earlier assays performed on solid media.

Anaerobic tests in **Figure 4.22B** suggest that all three strains form SCVs under these conditions, including the wild-type. The addition of 12,5 or 50  $\mu\text{M}$  of MK-4 does not improve the growth rate or colony size of any of the strains. In the case of anaerobic growth, we do not expect any complementation with the supplementations of MK-4, because the bacteria are most likely having a fermentative metabolism. Fermenting bacteria do not require of menaquinone because they do not utilize the electron transport chain for generation of energy.

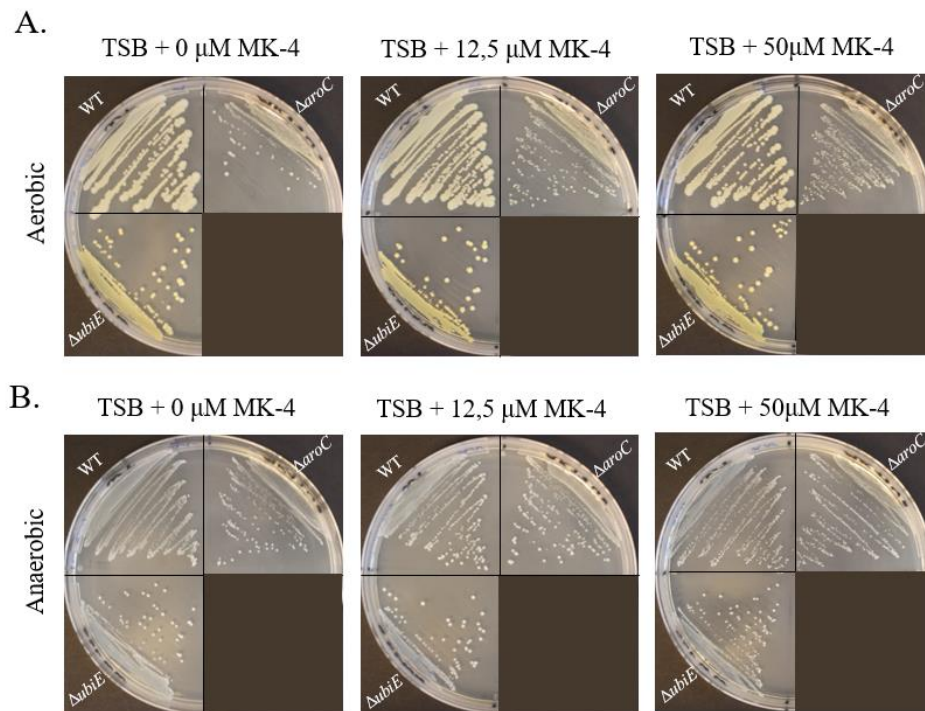


**Figure 4.22** Results from small colony assay showing if  $\Delta ubiE$  and  $\Delta aroC$  form SCV phenotype. The results are presented for bacteria grown in aerobic (A) and anaerobic (B) conditions. Wild-type and mutant strain were streaked on TSA plates, TSA plates with 12,5  $\mu\text{M}$  MK-4 and TSA plates with 50  $\mu\text{M}$  of MK-4 and grown at 37  $^{\circ}\text{C}$ . Pictures were taken after 48 hours of growth.

#### 4.9 Deletion of *ubiE* results in increased resistance to Congo Red

It has been reported by Suzuki et al. (2012) that wall teichoic acids (WTA) protect *S. aureus* from lysis by Congo red and other azo dyes. The lack of these WTAs lead to increased susceptibility to the bactericidal effect of Congo red. The FTIR analysis suggested that there were differences in WTA levels between the wild-type and the mutants. A Congo red assay was therefore conducted to investigate if deletion of *ubiE* or *aroC* led to increased susceptibility, and therefore might further imply that there is a difference in the amount of WTA in the peptidoglycan layer of the cells. In this assay, ten-fold dilutions of overnight cultures of wild-type,  $\Delta ubiE$  and  $\Delta aroC$  were spotted onto plates with pure TSB, TSB with 0,06 % (w/w) Congo red and on TSB plates supplemented with 0,1 % (w/w) of Congo red. The bacteria were incubated in aerobic and anaerobic conditions. The aerobically grown bacteria were incubated for 24 hours, and the bacteria grown in anoxic conditions were incubated for 48 hours.

The results from **Figure 4.23** reveal that both mutant strains have a reduced growth compared to wild-type under aerobic conditions on TSB agar plates. This is in agreement with the observations during growth analysis of the mutants in liquid media (**Figure 4.2**). In contrast

to this, the growth on plates with both concentrations of Congo red (0,06% and 0,1%) show that  $\Delta ubiE$  is less susceptible to the effects of Congo red than the wild-type and  $\Delta aroC$ . Growth of this strain in oxic conditions can be observed for dilutions down to  $10^{-3}$  of the original bacterial culture. Wild-type show very poor growth at the same dilution on aerobically incubated plates. On anaerobic plates, the growth of  $\Delta ubiE$  and wild-type is quite similar.

**Figure 4.23** also indicates that  $\Delta aroC$  is affected by Congo red and shows very poor growth compared to growth on plates without this dye. All dilutions of the *aroC* knockout strain grow on plates without Congo red, but on plates supplemented with 0,06% or 0,1% Congo red, only  $10^0$  and  $10^{-1}$  dilutions show visual growth in aerobic conditions. The growth is even more reduced in anaerobic conditions.

Together this suggest that  $\Delta ubiE$  is less susceptible to Congo red in aerobic conditions, which suggests that the cells might contain higher amounts of WTA. The  $\Delta aroC$ , however, is more susceptible compared to the wild-type, which suggests that this mutant contains lower amounts of WTA.

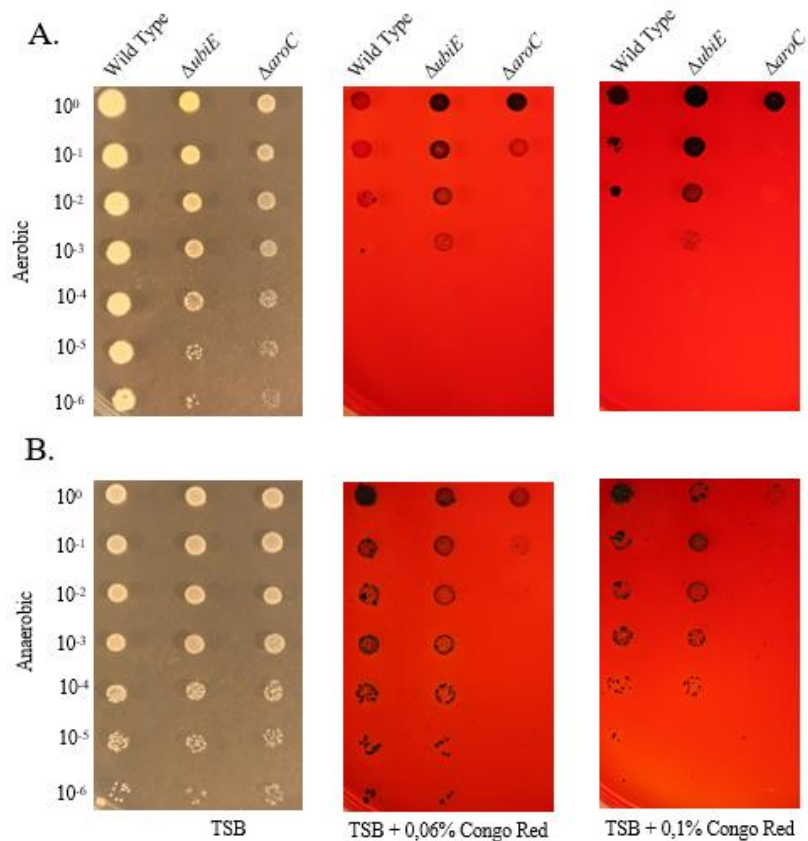


**Figure 4.23** Congo red susceptibility of aerobic (A) and anaerobic (B) mutant derivatives  $\Delta ubiE$  and  $\Delta aroC$ . Ten-fold dilutions of the wild-type strain and *ubiE* and *aroC* mutant derivatives were spotted onto agar plates with pure TSB plates, TSB plates with 0,06% and 0,1% of Congo red. Aerobic samples were grown overnight at 37 °C, and anaerobic samples were grown at 37 °C for two nights before imaging.

## 5 Discussion

Biofilm formation of *S. aureus* leads to more problematic and chronic infections, partly because this mode of growth increases the ability of bacteria to withstand host immune defences and antibiotic agents (Wermser & Lopez, 2018). In order to develop new treatment possibilities for such infections, which are causing many nosocomial infections today, it is important to get a better understanding of which factor that influence biofilm formation and has an impact on the final composition of the biofilm. A model by Wermser and Lopez (2018) using structured macrocolonies to study morphological changes resulting from genetic alterations have been applied in this work to investigate how modifications of the respiratory pathway alter the phenotype of *S. aureus* biofilms and production of ECM. One of the main goals of this work was to investigate how deficient biosynthesis of menaquinone and impaired respiration altered the biofilm formation process. In order to investigate this, we performed assays to visualize and quantify biofilms under aerobic and anaerobic conditions and we analysed *S. aureus* Newman strains harbouring deletions or depletion of genes in the menaquinone biosynthetic pathway (see **Figure 1.3**).

### 5.1 Deletion of *ubiE* results in reduced growth and altered biofilm formation

In a previous work in the lab, it was found that the deletion of *ubiE* in *S. aureus* Newman resulted in the formation of macrocolonies without the structure that are observed for the wild-type (Mårli, 2020). The *S. aureus* Newman *ubiE::spc* deletion strain was further studied in this work and the altered macrocolony structuring was confirmed. In contrast to the wild-type, the deletion strain produced smooth colonies without folds and wrinkles. The macrocolony assays which were performed here also suggested that the mutants had a reduced growth, and this was further verified by growth analysis in liquid medium. Furthermore, a reduction in the ability of this mutant to form biofilms an abiotic surface was also demonstrated by crystal violet assay. Thus, the removal of *ubiE* clearly affect the fitness and biofilm-formation in this strain.

*ubiE* encodes the enzyme catalysing the final step of the MK biosynthesis pathway (Wakeman et al., 2012). Macrocolony and growth analysis was also performed with mutants of other genes catalysing earlier steps in the pathway, including *aroC*, *menA*, *menF* and *menE*. The *aroC* deletion displayed severe growth defect and unstructured macrocolonies similar to *ubiE*-deletion. It should be noted that *aroC* catalyses the formation of chorismate which is not only a precursor of MK, but also for the synthesis of amino acids (Herrmann & Weaver, 1999;

Kanehisa & Goto, 2000). This deletion mutant is therefore likely to have pleiotropic effects and the phenotypes observed for this mutant are not solely due to the lack of MK. By CRISPRi-depletion of *menA*, *menF* and *menE*, a clear effect on macrocolonies was observed for *menA*, while only minor differences were observed for *menF* and *menE*. It would have been expected that the *menF* and *menE* mutants produced similar changes as observed for the *menA*. Possibly, the protein levels in these cells were not sufficiently depleted for the experiment and still harboured enough proteins to be able to synthesise menaquinone and perform respiration.

## 5.2 Complementation of the *ubiE::spc* deletion

To confirm that the observed phenotypes were caused by the *ubiE*-deletion, and not because of other changes occurring in the strain, we complemented the strain with plasmid encoding either *ubiE* alone or the combination of *ubiE\_hepT*.

When we only complemented the knockout of *ubiE*, we did not see large growth improvement during growth assays in liquid media. Macrocolony imaging also showed no change when gene expression of *ubiE* was induced. However, when both *ubiE* and *hepT* was complemented through IPTG induction during liquid growth assays and macrocolony assays, a clear change was observed. Growth improved substantially in its planktonic state, and macrocolonies showed development of structured phenotype with wrinkling characteristics. Likewise, the same trend was observed during the crystal violet assays where only the *ubiE\_hepT* complementation could partially produce biofilms with similar amounts of total biofilm mass as observed for the wild-type.

To understand this, an RT-PCR analysis of the *ubiE* operon was performed and it was shown that *ubiE* is in an operon together with NMWN\_1381, *hepT* and *ndk* (**Figure A1**), where the *ubiE* gene is located between NWMN\_1381 and *hepT*. Because these genes are co-transcribed, the deletion of *ubiE* would most likely affect the gene expression of the downstream genes. *hepT* is a downstream gene of *ubiE* which also participates in the biosynthesis of menaquinone (**Figure 1.3**), on the contrary *ndk* participates in completely different synthesis process, namely adenine, guanine and pyrimidine ribonucleic biosynthesis (Kanehisa & Goto, 2000). Thus, the *ubiE::spc* deletion affect the expression of the downstream *hepT* gene and ectopic expression of both genes are required to restore phenotypes.

Although the combined *ubiE\_hepT* complementation to some extent restored phenotypes there were still some differences compared to the control and wild-type with regard

to biofilm-formation. The structuring of the macrocolonies were somewhat different and the biomass of the biofilms did not reach the levels of the wild-type in crystal violet assay. How can this be explained? It is widely known that bacterial biofilms are heterogenous at many different levels. The individual bacteria that live in the biofilm are greatly affected by environmental factors such as nutrient availability and temperature (Steven S. Branda et al., 2005; López et al., 2010). Therefore, it is likely that the bacterial cells at different locations in a specific biofilm perform metabolism at different rates. For *S. aureus* it is known that the biofilm can divide in different layers depending on the nutrient availability. The top layer will perform respirational processes as long as oxygen or an alternative terminal electron acceptor is available. In the bottom of the biofilm, oxygen levels might not be as high, and the bacteria is forced to perform alternative energy producing processes, such as fermentation. In one layer there may also be cells that is metabolically inactive (Rani et al., 2007). Similarly, it is likely that the gene expression levels of the menaquinone biosynthesis genes vary and are tuned at different locations within a biofilm. In contrast to this, when we induce the expression of genes *ubiE\_hepT* using a specific concentration of the inducer compound (IPTG), such tuning and variation of gene expression is not possible to control. Such artificial induction will in theory affect the bacteria at a similar degree and lead to similar amount of gene expression throughout the biofilm, which we might not find in natural biofilms. Furthermore, it is also possible that the inducer does not distribute equally across the growing biofilm. This is a potential reason for observed differences in biofilms between wild-type and the complemented mutant.

While it was possible to complement the growth of the *ubiE*-mutant in liquid medium by supplementation of MK-4, the macrocolony biofilm structuring could not be complemented at all with this approach. The reason for this is not known, but it is possible that MK-4 added to the agar plates can not enter the staphylococcal cells to support respiration, for instance because they are too sufficiently soluble or distributed in the agar.

### **5.3 The altered macrocolony biofilm formation is a result of altered metabolism in the *ubiE* deletion strain**

*ubiE* codes for the last enzyme in the biosynthetic pathway of menaquinone, which is a quinone electron carrier that is critical for the ability of *S. aureus* to respire. The lack of menaquinone has been shown to stop the transport of electrons in the electron transport chain, evidently stopping the generation of a proton motive force utilised by the protein complex, F<sub>0</sub>F<sub>1</sub>ATPase, to synthesise ATP from ADP (McNamara & Proctor, 2000). Bacteria with impaired respiration

has earlier been shown to lead to development of SCVs (Hammer et al., 2013). We therefore performed an assay in order to investigate if the *ubiE* mutant formed such phenotypes. SCV are known to form non-pigmented colonies due to the lack of carotenoid production which contribute to pigment formation. Carotenoid biosynthesis require electron transport in order to function (Joyce & White, 1971). In our study the *ubiE* deletion strain showed a reduced colony size but formed pigmented colonies. Another study performed by Wakeman et al. (2012) also investigated if a *ubiE* deletion mutant of *S. aureus* would develop a small colony phenotype, but their conclusions were that it still maintained normal colony morphology. They hypothesized that dimethylmenaquinone (DMK), the immediate precursor of MK could function within the electron transport chain of *S. aureus*. DMK has a redox potential and has been shown to function as an electron carrier in other bacteria (Wakeman et al., 2012). It is however likely that DMK is not formed in our deletion strain due to the effect of *hepT* in the *ubiE::spc* strain (see discussion above). Thus, DMK cannot be formed in our deletion strain since the biosynthetic pathway will most likely result in accumulation of 1,4-dihydroxy-2-naphthoate (**Figure 1.3**) and thus no electron carrier that can replace MK. It is also possible that accumulation of this intermediate is a reason for the yellow pigmentation observed in the colonies, however this remain to be verified. SCV cannot respire and produce energy via fermentation which result in accumulation of L- and D-lactate (Proctor, 2019). Production of lactate has indeed been confirmed for our deletion strain (data not part of this thesis). It can thus be concluded that the *ubiE::spc* deletion strain used in this work do not have a functional respiration, but instead produce energy by fermentation even under aerobic conditions.

We hypothesized that the lack of respiration was the reason for the loss of structured macrocolonies. Indeed, by performing macrocolony assays under anaerobic conditions where *S. aureus* cannot respire, non-structured, smoot macrocolonies similar to those observed in the *ubiE*-deletion were formed. These macrocolonies were also colourless, suggesting that the entire respiratory metabolism was shut down.

#### **5.4 Physical biochemical properties of the macrocolonies. Why are structured macrocolonies only formed in the cells growing with a respiratory metabolism?**

Observations of the morphology of macrocolonies revealed that the wild-type formed structured macrocolonies, while genetic mutants with impaired respiration showed lack of wrinkles. It is largely known that the structural property of biofilm is highly depending on the chemical composition of the extracellular matrix in which cells are embedded. Non-covalent bonds

between proteins, polysaccharides and sometimes eDNA contribute to a three-dimensional structure (Flemming & Wingender, 2010). FTIR-assays in this work showed an altered spectral profile of several of the components. It was however difficult to determine if these differences were due to quantities of the mentioned structures, or if it was differences in the chemical structuring that lead to the differentiation. Quantifications of the extracellular matrix component on the other hand could reveal that both of the deletion mutants had significantly lower concentrations of both proteins and eDNA compared to the wild-type. However, differences in regard to polysaccharides were less evident and could not be confirmed from these assays. Nevertheless, this substantiates the theory that wrinkles are caused by EPS, because higher amounts of EPS components lead to more structured phenotypes in forms of wrinkles. Other assays performed in this work involved a more direct approach to test the structuring and robustness of bacterial macrocolonies. This test revealed that wild-type had a much harder surface area, which was less affected by mechanical disruption than the deletion mutants. The aerobic macrocolonies also seemed to be drier compared to the mutant and the anaerobically grown macrocolonies. Water makes up large quantities of the extracellular matrix, but with more structuring due to ECM components, it would probably be experienced as less moist. This work thus suggests that high levels of ECM components is the reason for the structuring of the macrocolonies in aerobically grown wild-type cells, but more work is needed to fully understand which molecules that are the key players. The macrocolony biofilm model has just recently been established in *S. aureus* (Wermser & Lopez, 2018) and is therefore not fully characterized. On the other hand, it is more widely used for other species, such as members of *Bacillus*. A study exploring wrinkling in *B. subtilis* found that cell death and wrinkle structures correlate (Asally et al., 2012), and whether the same is true for *S. aureus* remains to be determined. The findings by Asally et al., suggested that wrinkle formation results in the death of cells or that cell death occurs first and perhaps facilitate wrinkle formation. However, whether it is a passive or active process that drives the cell death remains to be determined.

During macrocolony imaging, we observed very distinct phenotypic traits in the deletion mutants (*ubiE* and *aroC*) compared to the wild-type; structuring was completely lost in the mutants in the same way as for the anaerobically grown macrocolonies. Because we have established that the two mutants and the anaerobically grown cells are fermenting, and the wild-type is respiring aerobically, this might be a possible cause of the difference we observe between the strains. Why is it more important to form a structured macrocolony for a bacterium with respiratory metabolism compared to fermenting cells? One hypothesis is that the

structuring is important for transport of gases (oxygen) and solutes to cells within the biofilm. Oxygen is needed for respiration but not for fermentation (Hammer et al., 2013). Wilking et al. (2013) used a rheological approach to examine the wrinkly colony phenotype exhibited by *B. subtilis*. By injecting dyes into the wrinkles, Wilking et al. could report the presence of a remarkable network of channels that facilitated transport of solutes underneath the wrinkles within the colony, and they suggest that similar structures offer simple systems for rapid liquid transport within biofilms. Evaporation from the surface is hypothesized to drive this rapid fluid movement.

### **5.5 The two-components systems SaeRS and SrrAB may be important for regulation of ECM products in wild-type and $\Delta ubiE$**

During quantification of biofilm formation of the *ubiE* deletion strain, we observed a decreased ability to attach and form biofilm on abiotic surfaces by crystal violet assays. The ability of *S. aureus* to cause device-associated infections is intimately connected to its ability to form biofilms (Mashruwala et al., 2017a). Quantification of EPSs from the biofilm matrix also revealed that the mutant had less of the measured components, eDNA and protein compared to the wild-type. Respiration has in other studies been suggested to influence biofilm formation through the two regulatory systems SrrAB and SaeRS. SrrAB and SaeRS are the dominant regulatory systems influencing fermentative biofilm formation (see **Section 1.3.3**). SrrAB, is stimulated by the accumulation of reduced MK in the electron transport chain, while SaeRS is stimulated by yet unknown signal molecules (Mashruwala et al., 2017a). Because the deletion of *ubiE* stops the synthesis of menaquinone, the SrrAB- and SaeRS-dependent biofilm formation is probably affecting this mutant. A study by Mashruwala et al. (2017a) has reported that a menaquinone auxotroph forms SaeRS-dependent biofilms. SaeRS TCSs governs fermentative biofilm formation by positively influencing Atl hydrolase activity and increase gene expression of the fibronectin binding protein A (FnBPA), both of which leads to increased programmed cell lysis. Earlier assays performed by Marita Thorissen Mårli (NMBU) showed increased Atl transcription production in the *ubiE* deletion mutant, but still in this work we observe lower biofilm formation compared to wild-type. This apparent inconsistent result might be explained by the results from the Congo red assay which showed that *ubiE* mutant had decreased susceptibility to Congo red compared to wild-type. Congo red susceptibility has been shown to correlate to amount of WTA in the cell wall. WTA is a cell wall glycopolymer shown to negatively influence Atl activity (Suzuki et al., 2012). The amount of WTA is known to be

regulated by SrrAB and therefore it is possible that increased Atl transcription does not lead to increased biofilm production because the bacteria is protected by increased levels of WTA. Thus probably, the effects on Atl and WTA in our *ubiE* mutant is a result of a complex regulatory interplay between SrrAB and SaeRS systems, possibly in addition to other factors, that needs to be further investigated.

### **5.6 Interpretation of the Congo Red experiment. Interesting results but unexpected**

In this work it was shown that the *ubiE* deletion mutant was more resistant to Congo Red compared to the wild-type, thus suggesting that the *ubiE* deletion strain has more WTA than the wild-type. The *aroC* mutant were more susceptible compared to wild-type. This is unexpected results given that the two genes participate in the same biosynthesis. On the other hand, *aroC* comes in at a much earlier stage than *ubiE* in the biosynthetic pathway of menaquinone, and it has been shown to affect several other synthesis pathways including synthesis of amino acids. The *aroC* mutant is thus likely to give pleiotropic effects on the cells (see discussion in **Section 5.1**). Without knowing what this could lead to, we can speculate that *aroC* might affect the amount of WTA in a different way than the deletion of *ubiE* does. With that said, the FTIR spectroscopy did also reveal differences regarding the carbohydrate profile of the deletion mutants compared to the wild-type. From the score plot in **Figure 4.17**, it can be hypothesised that the amount of carbohydrates is higher in the carbohydrate composition compared to both deletion mutants. It should however be noted that the score plot does not specifically show WTA composition, but rather show the difference in regard to the entire carbohydrate profile even though it is likely that most of the differences between the strains are correlated to WTA.

### **5.7 *ubiE* and menaquinone as a drug-target**

Antimicrobial agents are most commonly used today to treat biofilm-associated infections. Due to the protective properties of the extracellular matrix, higher doses of the antimicrobial is needed. With increased amounts and long-lasting treatments, the chance for selection of antimicrobial resistant and tolerant strains are higher (Kranjec et al., 2021). Antimicrobials also have a poor efficiency against various biofilms due to complex physical and biological characteristics. Many researchers have therefore switched their focus on using anti-biofilm strategies, that targets biofilm molecules and pathways involved in the formation of biofilms

instead of inhibiting the growth and division of the embedded cells (Chiba et al., 2015; Donlan & Costerton, 2002; Kranjec et al., 2021; Wermser & Lopez, 2018).

New treatment methods might target the attachment of cells in the initial phase of biofilm formation, or it might target and degrade the extracellular matrix components. Another possibility is to target metabolic pathways. This has been shown to be tightly linked to the EPS production and biofilm structuring in *S. aureus* (Fitzpatrick et al., 2005; Jiang, Geng, & Bai, 2020). Menaquinone biosynthesis can be a potential target due to its importance in the respiratory process in *S. aureus*. All enzymes of this pathway are possible targets for inhibition as they are extremely conserved in all Gram-positive bacteria, but not present in human cells (Boersch et al., 2018).

Because the extracellular matrix hugely contributes with the protective properties of biofilm against most antimicrobials, targets that lead to decreased amounts of the EPSs might lead to a more easily treated biofilm-associated infection. In our assay, we confirmed that the deletion of both *ubiE* and *aroC* lead to decreased amounts of several of the key components of the ECM, and macrocolony assays showed lack of structuring. The crystal violet assay did also show decreased production of total biofilm mass for the *ubiE* deletion, but not for the *aroC* deletion. This might suggest that *ubiE* could be a more potential target than *aroC*. With that said, further investigations need to be made before we can say for certain that these are possible targets.

It is interesting to note that several molecules inhibiting the menaquinone biosynthesis has already been discovered (Paudel, Hamamoto, Panthee, & Sekimizu, 2016), and it would be interesting to test these in combination with antibiotics to target staphylococcal biofilms.

## **5.8 Advantages and limitations of FTIR spectroscopy for analysis of staphylococcal macrocolony biofilms**

One of the aims of this work was to set up FTIR spectroscopy to analyse staphylococcal macrocolony biofilms. With the use of FTIR spectroscopy we could identify several chemical structures that varied in amounts or chemical structuring in mutant strains of Newman in regard to carbohydrates and proteins. However, this method could not help to determine specific proteins or give information about the eDNA composition in the different samples. FTIR spectroscopy can be used for high-throughput and rapid analysis of various microbiological samples, including microbial biofilms. The method allows identification of various organisms down to species and even strain level for some organisms. In addition, it can be used for

characterisation of the chemical composition using spectral profiles from vibrational characteristics of bonds and functional groups of molecules in that given sample (Chirman & Pleshko, 2021; Naumann, 2000; Ngo-Thi, Kirschner, & Naumann, 2003). Nevertheless, the methods also have its limitations. Even though the general sample preparation protocol is relatively simple; the obtained data is highly complex. Differences in the spectral profiles of different samples are difficult to determine with the naked eye, and often require use of multivariate analysis. However, in order to extract relevant data from multivariate analysis, knowledge and understanding of chemometrics is required (Gieroba et al., 2020; Naumann, 2000; Rajalahti & Kvalheim, 2011).

In addition, spectral regions of various components overlap, which may lead to misinterpretation (Burgula et al., 2007). In our work, we could only confirm that samples varied in regard to protein profile, but it was not possible to further identify or speculate which proteins this applied to. Normally when proteins are studied using FTIR, pure proteins are used. In addition, the method we used was not suitable for characterisation of the extracellular DNAs due to that the signals for these molecules are overlapping with the signatures of other components which are present at much higher quantities.

## 6 Concluding remarks and future perspectives

In this work we have shown that impaired respiration due to the lack of menaquinone affects both structural properties of biofilm macrocolonies and biofilms formed on abiotic surfaces in liquid. The lack of menaquinone and the switch from aerobic respiration to fermentation result in dramatic changes in chemical composition of the extracellular matrix as determined by FTIR spectroscopy and direct quantitative assays to determine the chemical composition of macrocolonies.

These findings imply that the lack of menaquinone affect the biofilm formation process in *S. aureus* and has consequences for the final composition of the extracellular matrix. How this happens at the molecular level is still not fully elucidated, but it has been suggested that the biofilm formation is regulated by respiration through two-component systems. The SaeRS regulatory system increase programmed cell death by yet unknown signal molecules, and lead to increased biofilm formation. However, as we observed a decreased production of total biofilm formation in  $\Delta ubiE$  and possibly an increased level of wall-teichoic acids, it is possible to believe that menaquinone also affect biofilm formation through yet unknown mechanisms.

To further study the molecular mechanisms that control the biofilm formation in *S. aureus* it could be interesting to perform assays on SaeRS and SrrAB mutants. Further, in order to explore the possibility of menaquinone as a potential drug target, it would be interesting to test menaquinone inhibitors together with antibiotics on *S. aureus* biofilms. This could reveal if the lack of menaquinone and impaired respiration leads to formation of biofilms which are more sensitive to antibiotics. For future studies, confocal microscopy could also be performed on mutant strains targeting genes in the menaquinone pathway in order to study the biofilm structure in more detail.

## References

- Allen, M. S., Welch, K. T., Prebyl, B. S., Baker, D. C., Meyers, A. J., & Sayler, G. S. (2004). Analysis and glycosyl composition of the exopolysaccharide isolated from the flocc-forming wastewater bacterium *Thauera* sp. MZ1T. *Environmental Microbiology*, 6(8), 780-790.
- Ann M. Stock, Victoria L. Robinson, a., & Goudreau, P. N. (2000). Two-Component Signal Transduction. *Annual Review of Biochemistry*, 69(1), 183-215.  
doi:10.1146/annurev.biochem.69.1.183
- Asally, M., Kittisopikul, M., Rué, P., Du, Y., Hu, Z., Çağatay, T., . . . Süel, G. M. (2012). Localized cell death focuses mechanical forces during 3D patterning in a biofilm. *Proceedings of the National Academy of Sciences*, 109(46), 18891-18896.
- Balasubramanian, D., Harper, L., Shopsis, B., & Torres, V. J. (2017). *Staphylococcus aureus* pathogenesis in diverse host environments. *Pathogens and disease*, 75(1), ftx005.
- Balibar, C. J., Shen, X., & Tao, J. (2009). The Mevalonate Pathway of *Staphylococcus aureus*. *Journal of Bacteriology*, 191(3), 851. doi:10.1128/JB.01357-08
- Bentley, R., & Meganathan, R. (1983). Vitamin K biosynthesis in bacteria--precursors, intermediates, enzymes, and genes. *Journal of natural products*, 46(1), 44-59.
- Boersch, M., Rudrawar, S., Grant, G., & Zunk, M. (2018). Menaquinone biosynthesis inhibition: a review of advancements toward a new antibiotic mechanism. *RSC advances*, 8(10), 5099-5105.
- Branda, S. S., González-Pastor, J. E., Ben-Yehuda, S., Losick, R., & Kolter, R. (2001). Fruiting body formation by *Bacillus subtilis*. *Proceedings of the National Academy of Sciences of the United States of America*, 98(20), 11621-11626.  
doi:10.1073/pnas.191384198
- Branda, S. S., Vik, Å., Friedman, L., & Kolter, R. (2005). Biofilms: the matrix revisited. *Trends in Microbiology*, 13(1), 20-26. doi:https://doi.org/10.1016/j.tim.2004.11.006
- Burgula, Y., Khali, D., Kim, S., Krishnan, S. S., Cousin, M. A., Gore, J. P., . . . Mauer, L. J. (2007). Review of Mid-infrared fourier transform-infrared spectroscopy applications for bacterial detection. *Journal of Rapid Methods & Automation in Microbiology*, 15(2), 146-175. doi:https://doi.org/10.1111/j.1745-4581.2007.00078.x
- Chambers, H. F., & DeLeo, F. R. (2009). Waves of resistance: *Staphylococcus aureus* in the antibiotic era. *Nature Reviews Microbiology*, 7(9), 629-641. doi:10.1038/nrmicro2200
- Chang, A. Y., Chau, V., Landas, J. A., & Pang, Y. (2017). Preparation of calcium competent *Escherichia coli* and heat-shock transformation. *JEMI methods*, 1, 22-25.
- Chiba, A., Sugimoto, S., Sato, F., Hori, S., & Mizunoe, Y. (2015). A refined technique for extraction of extracellular matrices from bacterial biofilms and its applicability. *Microbial biotechnology*, 8(3), 392-403.
- Chirman, D., & Pleshko, N. (2021). Characterization of bacterial biofilm infections with Fourier transform infrared spectroscopy: a review. *Applied Spectroscopy Reviews*, 1-29.
- Christensen, G. D., Simpson, W. A., Younger, J., Baddour, L., Barrett, F., Melton, D., & Beachey, E. (1985). Adherence of coagulase-negative staphylococci to plastic tissue culture plates: a quantitative model for the adherence of staphylococci to medical devices. *Journal of clinical microbiology*, 22(6), 996-1006.
- Clements, M. O., & Foster, S. J. (1999). Stress resistance in *Staphylococcus aureus*. *Trends in Microbiology*, 7(11), 458-462. doi:https://doi.org/10.1016/S0966-842X(99)01607-8
- Cucarella, C., Solano, C., Valle, J., Amorena, B., Lasa, Í., & Penadés, J. R. (2001). Bap, a *Staphylococcus aureus* surface protein involved in biofilm formation. *Journal of Bacteriology*, 183(9), 2888-2896.

- Davies, D. G., Chakrabarty, A. M., & Geesey, G. G. (1993). Exopolysaccharide production in biofilms: substratum activation of alginate gene expression by *Pseudomonas aeruginosa*. *Applied and Environmental Microbiology*, *59*(4), 1181. Retrieved from <http://aem.asm.org/content/59/4/1181.abstract>
- Dawson, A., Fyfe, P. K., Gillet, F., & Hunter, W. N. (2011). Exploiting the high-resolution crystal structure of *Staphylococcus aureus* MenH to gain insight into enzyme activity. *BMC Structural Biology*, *11*(1), 19. doi:10.1186/1472-6807-11-19
- DeFrancesco, A. S., Masloboeva, N., Syed, A. K., DeLoughery, A., Bradshaw, N., Li, G.-W., . . . Losick, R. (2017). Genome-wide screen for genes involved in eDNA release during biofilm formation by *Staphylococcus aureus*. *Proceedings of the National Academy of Sciences*, *114*(29), E5969-E5978.
- Destefanis, G., Barge, M. T., Brugiapaglia, A., & Tassone, S. (2000). The use of principal component analysis (PCA) to characterize beef. *Meat Science*, *56*(3), 255-259. doi:[https://doi.org/10.1016/S0309-1740\(00\)00050-4](https://doi.org/10.1016/S0309-1740(00)00050-4)
- Deurenberg, R. H., & Stobberingh, E. E. (2008). The evolution of *Staphylococcus aureus*. *Infection, Genetics and Evolution*, *8*(6), 747-763. doi:<https://doi.org/10.1016/j.meegid.2008.07.007>
- Di Martino, P. (2018). Extracellular polymeric substances, a key element in understanding biofilm phenotype. *AIMS microbiology*, *4*(2), 274-288. doi:10.3934/microbiol.2018.2.274
- Donlan, R. M., & Costerton, J. W. (2002). Biofilms: survival mechanisms of clinically relevant microorganisms. *Clinical microbiology reviews*, *15*(2), 167-193.
- Duthie, E., & Lorenz, L. L. (1952). Staphylococcal coagulase: mode of action and antigenicity. *Microbiology*, *6*(1-2), 95-107.
- Dzurendova, S., Zimmermann, B., Kohler, A., Tafintseva, V., Slany, O., Certik, M., & Shapaval, V. (2020). Microcultivation and FTIR spectroscopy-based screening revealed a nutrient-induced co-production of high-value metabolites in oleaginous Mucoromycota fungi. *PLoS one*, *15*(6), e0234870.
- Fitzpatrick, F., Humphreys, H., & O'Gara, J. P. (2005). The genetics of staphylococcal biofilm formation—will a greater understanding of pathogenesis lead to better management of device-related infection? *Clinical Microbiology and Infection*, *11*(12), 967-973. doi:<https://doi.org/10.1111/j.1469-0691.2005.01274.x>
- Flemming, H.-C., & Wingender, J. (2010). The biofilm matrix. *Nature Reviews Microbiology*, *8*(9), 623-633. doi:10.1038/nrmicro2415
- Foster, T. J., Geoghegan, J. A., Ganesh, V. K., & Höök, M. (2014). Adhesion, invasion and evasion: the many functions of the surface proteins of *Staphylococcus aureus*. *Nature Reviews Microbiology*, *12*(1), 49-62. doi:10.1038/nrmicro3161
- Foster, T. J., & Höök, M. (1998). Surface protein adhesins of *Staphylococcus aureus*. *Trends in Microbiology*, *6*(12), 484-488. doi:[https://doi.org/10.1016/S0966-842X\(98\)01400-0](https://doi.org/10.1016/S0966-842X(98)01400-0)
- Fuchs, S., Pané-Farré, J., Kohler, C., Hecker, M., & Engelmann, S. (2007). Anaerobic gene expression in *Staphylococcus aureus*. *Journal of Bacteriology*, *189*(11), 4275-4289.
- García-Betancur, J.-C., Goñi-Moreno, A., Horger, T., Schott, M., Sharan, M., Eikmeier, J., . . . Kuttler, C. (2017). Cell differentiation defines acute and chronic infection cell types in *Staphylococcus aureus*. *eLife*, *6*, e28023.
- Garibyan, L. A., N. (2013). Polymerase chain reaction. *Journal of Investigative Dermatology*, *133*.
- Gieroba, B., Krysa, M., Wojtowicz, K., Wiater, A., Pleszczyńska, M., Tomczyk, M., & Sroka-Bartnicka, A. (2020). The FT-IR and Raman Spectroscopies as Tools for Biofilm Characterization Created by Cariogenic Streptococci. *International journal of molecular sciences*, *21*(11), 3811. doi:10.3390/ijms21113811

- Gross, M., Cramton, S. E., Götz, F., & Peschel, A. (2001). Key Role of Teichoic Acid Net Charge *Staphylococcus aureus* Colonization of Artificial Surfaces. *Infection and Immunity*, 69(5), 3423. doi:10.1128/IAI.69.5.3423-3426.2001
- Götz, F., & Mayer, S. (2013). Both terminal oxidases contribute to fitness and virulence during organ-specific *Staphylococcus aureus* colonization. *MBio*, 4(6).
- Hammer, N. D., Reniere, M. L., Cassat, J. E., Zhang, Y., Hirsch, A. O., Hood, M. I., & Skaar, E. P. (2013). Two heme-dependent terminal oxidases power *Staphylococcus aureus* organ-specific colonization of the vertebrate host. *MBio*, 4(4).
- Harris, L. G., & Richards, R. G. (2006). Staphylococci and implant surfaces: a review. *Injury*, 37(2, Supplement), S3-S14. doi:https://doi.org/10.1016/j.injury.2006.04.003
- Herrmann, K. M., & Weaver, L. M. (1999). The Shikimate Pathway. *Annual Review of Plant Physiology and Plant Molecular Biology*, 50(1), 473-503. doi:10.1146/annurev.arplant.50.1.473
- Jain, V. M., Karibasappa, G. N., Dodamani, A. S., & Mali, G. V. (2017). Estimating the carbohydrate content of various forms of tobacco by phenol-sulfuric acid method. *Journal of education and health promotion*, 6, 90-90. doi:10.4103/jehp.jehp\_41\_17
- Jiang, Y., Geng, M., & Bai, L. (2020). Targeting Biofilms Therapy: Current Research Strategies and Development Hurdles. *Microorganisms*, 8(8). doi:10.3390/microorganisms8081222
- Joyce, G. H., & White, D. C. (1971). Effect of Benzo(a)pyrene and Piperonyl Butoxide on Formation of Respiratory System, Phospholipids, and Carotenoids of *Staphylococcus aureus*. *Journal of Bacteriology*, 106(2), 403. Retrieved from <http://jb.asm.org/content/106/2/403.abstract>
- Kanehisa, M., & Goto, S. (2000). KEGG: kyoto encyclopedia of genes and genomes. *Nucleic Acids Res*, 28(1), 27-30. doi:10.1093/nar/28.1.27
- Karadenizli, A., Kolayli, F., & Ergen, K. (2007). A novel application of Fourier-transformed infrared spectroscopy: classification of slime from staphylococci. *Biofouling*, 23(1), 63-71. doi:10.1080/08927010601143524
- Koch, G., Yepes, A., Förstner, K. U., Wermser, C., Stengel, S. T., Modamio, J., . . . Lopez, D. (2014). Evolution of resistance to a last-resort antibiotic in *Staphylococcus aureus* via bacterial competition. *Cell*, 158(5), 1060-1071.
- Kraemer, G. R., & Iandolo, J. J. (1990). High-frequency transformation of *Staphylococcus aureus* by electroporation. *Current Microbiology*, 21(6), 373-376.
- Kranjec, C., Morales Angeles, D., Torrissen Mårli, M., Fernández, L., García, P., Kjos, M., & Diep, D. B. (2021). Staphylococcal Biofilms: Challenges and Novel Therapeutic Perspectives. *Antibiotics*, 10(2), 131. Retrieved from <https://www.mdpi.com/2079-6382/10/2/131>
- Kurosu, M., & Begari, E. (2010). Vitamin K2 in Electron Transport System: Are Enzymes Involved in Vitamin K2 Biosynthesis Promising Drug Targets? *Molecules*, 15(3), 1531-1553. Retrieved from <https://www.mdpi.com/1420-3049/15/3/1531>
- Le, K. Y., Dastgheyb, S., Ho, T. V., & Otto, M. (2014). Molecular determinants of staphylococcal biofilm dispersal and structuring. *Frontiers in cellular and infection microbiology*, 4, 167.
- Lee, P. Y., Costumbrado, J., Hsu, C.-Y., & Kim, Y. H. (2012). Agarose gel electrophoresis for the separation of DNA fragments. *JoVE (Journal of Visualized Experiments)*(62), e3923.
- Li, X., Yan, Z., & Xu, J. (2003). Quantitative variation of biofilms among strains in natural populations of *Candida albicans*. *Microbiology*, 149(2), 353-362. doi:https://doi.org/10.1099/mic.0.25932-0

- Liew, A. T. F., Theis, T., Jensen, S. O., Garcia-Lara, J., Foster, S. J., Firth, N., . . . Harry, E. J. (2011). A simple plasmid-based system that allows rapid generation of tightly controlled gene expression in *Staphylococcus aureus*. *Microbiology*, *157*(3), 666-676. doi:<https://doi.org/10.1099/mic.0.045146-0>
- Lindsay, J. A. (2014). *Staphylococcus aureus* genomics and the impact of horizontal gene transfer. *International Journal of Medical Microbiology*, *304*(2), 103-109. doi:<https://doi.org/10.1016/j.ijmm.2013.11.010>
- Liu, G. Y. (2009). Molecular Pathogenesis of *Staphylococcus aureus* Infection. *Pediatric Research*, *65*(7), 71-77. doi:10.1203/PDR.0b013e31819dc44d
- Livermore, D. M. (2000). Antibiotic resistance in staphylococci. *International Journal of Antimicrobial Agents*, *16*, 3-10. doi:[https://doi.org/10.1016/S0924-8579\(00\)00299-5](https://doi.org/10.1016/S0924-8579(00)00299-5)
- Lo, Y. D., & Chan, K. A. (2006). Introduction to the polymerase chain reaction. *Clinical Applications of PCR*, 1-10.
- López, D., Vlamakis, H., & Kolter, R. (2010). Biofilms. *Cold Spring Harbor perspectives in biology*, *2*(7), a000398.
- Lowy, F. D. (1998). *Staphylococcus aureus* infections. *New England journal of medicine*, *339*(8), 520-532.
- Lowy, F. D. (2003). Antimicrobial resistance: the example of *Staphylococcus aureus*. *The Journal of clinical investigation*, *111*(9), 1265-1273.
- Lu, X., Al-Qadiri, H. M., Lin, M., & Rasco, B. A. (2011). Application of mid-infrared and Raman spectroscopy to the study of bacteria. *Food and Bioprocess Technology*, *4*(6), 919-935.
- Mashruwala, A. A., Gries, C. M., Scherr, T. D., Kielian, T., & Boyd, J. M. (2017a). SaeRS Is Responsive to Cellular Respiratory Status and Regulates Fermentative Biofilm Formation in *Staphylococcus aureus*. *Infection and Immunity*, *85*(8), e00157-00117. doi:10.1128/IAI.00157-17
- Mashruwala, A. A., Guchte, A. v. d., & Boyd, J. M. (2017b). Impaired respiration elicits SrrAB-dependent programmed cell lysis and biofilm formation in *Staphylococcus aureus*. *eLife*, *6*, e23845. doi:10.7554/eLife.23845
- Masuko, T., Minami, A., Iwasaki, N., Majima, T., Nishimura, S.-I., & Lee, Y. C. (2005). Carbohydrate analysis by a phenol-sulfuric acid method in microplate format. *Analytical Biochemistry*, *339*(1), 69-72. doi:<https://doi.org/10.1016/j.ab.2004.12.001>
- McNamara, P. J., & Proctor, R. A. (2000). *Staphylococcus aureus* small colony variants, electron transport and persistent infections. *International Journal of Antimicrobial Agents*, *14*(2), 117-122. doi:[https://doi.org/10.1016/S0924-8579\(99\)00170-3](https://doi.org/10.1016/S0924-8579(99)00170-3)
- Monk, I. R., Tree, J. J., Howden, B. P., Stinear, T. P., & Foster, T. J. (2015). Complete bypass of restriction systems for major *Staphylococcus aureus* lineages. *MBio*, *6*(3).
- Moormeier, D. E., & Bayles, K. W. (2017). *Staphylococcus aureus* biofilm: a complex developmental organism. *Molecular Microbiology*, *104*(3), 365-376.
- Mårli, M. T. (2020). *Using CRISPR interference to study novel biofilm-associated genes in Staphylococcus aureus*. (Master). Norwegian University of Life Science, Unpublished.
- Naumann, D. (2000). Infrared spectroscopy in microbiology. *Encyclopedia of Analytical Chemistry: Applications, Theory and Instrumentation*, pp. 102-131.
- Naumann, D., Helm, D., & Labischinski, H. (1991). Microbiological characterizations by FT-IR spectroscopy. *Nature*, *351*(6321), 81.
- Ngo-Thi, N. A., Kirschner, C., & Naumann, D. (2003). Characterization and identification of microorganisms by FT-IR microspectrometry. *Journal of Molecular Structure*, *661-662*, 371-380. doi:<https://doi.org/10.1016/j.molstruc.2003.08.012>
- Nielsen, S. S. (2017). Total carbohydrate by phenol-sulfuric acid method. In *Food analysis laboratory manual* (pp. 137-141): Springer.

- Novick, R. P. (2003). Autoinduction and signal transduction in the regulation of staphylococcal virulence. *Molecular Microbiology*, 48(6), 1429-1449.
- Panthee, S., Paudel, A., Hamamoto, H., Uhlemann, A.-C., & Sekimizu, K. (2020a). Alteration of menaquinone isoprenoid chain length and antibiotic sensitivity by single amino acid substitution in HepT. *BioRxiv*.
- Panthee, S., Paudel, A., Hamamoto, H., Uhlemann, A.-C., & Sekimizu, K. (2020b). The Role of Amino Acid Substitution in HepT Toward Menaquinone Isoprenoid Chain Length Definition and Lysocin E Sensitivity in *Staphylococcus aureus*. *Frontiers in microbiology*, 11, 2076.
- Paudel, A., Hamamoto, H., Panthee, S., & Sekimizu, K. (2016). Menaquinone as a potential target of antibacterial agents. *Drug discoveries & therapeutics*, 10(3), 123-128.
- Pitts, B., Hamilton, M. A., Zilver, N., & Stewart, P. S. (2003). A microtiter-plate screening method for biofilm disinfection and removal. *Journal of Microbiological Methods*, 54(2), 269-276. doi:https://doi.org/10.1016/S0167-7012(03)00034-4
- Pollitt, E. J., Szkuta, P. T., Burns, N., & Foster, S. J. (2018). *Staphylococcus aureus* infection dynamics. *PLoS pathogens*, 14(6), e1007112.
- Proctor, R. (2019). Respiration and small colony variants of *Staphylococcus aureus*. *Gram-Positive Pathogens*, 549-561.
- Qi, L. S., Larson, M. H., Gilbert, L. A., Doudna, J. A., Weissman, J. S., Arkin, A. P., & Lim, W. A. (2013). Repurposing CRISPR as an RNA-guided platform for sequence-specific control of gene expression. *Cell*, 152(5), 1173-1183.
- Rajalahti, T., & Kvalheim, O. M. (2011). Multivariate data analysis in pharmaceuticals: A tutorial review. *International Journal of Pharmaceutics*, 417(1), 280-290. doi:https://doi.org/10.1016/j.ijpharm.2011.02.019
- Rani, S. A., Pitts, B., Beyenal, H., Veluchamy, R. A., Lewandowski, Z., Davison, W. M., . . . Stewart, P. S. (2007). Spatial Patterns of DNA Replication, Protein Synthesis, and Oxygen Concentration within Bacterial Biofilms Reveal Diverse Physiological States. *Journal of Bacteriology*, 189(11), 4223. doi:10.1128/JB.00107-07
- Richardson, D. J. (2000). Bacterial respiration: a flexible process for a changing environment 1999 Fleming Lecture (Delivered at the 144th meeting of the Society for General Microbiology, 8 September 1999). *Microbiology*, 146(3), 551-571.
- Ringnér, M. (2008). What is principal component analysis? *Nature biotechnology*, 26(3), 303-304.
- Santos, C. F. D., Sakai, V. T., Machado, M. A. d. A. M., Schippers, D. N., & Greene, A. S. (2004). Reverse transcription and polymerase chain reaction: principles and applications in dentistry. *J Appl Oral Sci*, 12(1), 1-11. doi:10.1590/S1678-77572004000100002
- Schilcher, K., & Horswill, A. R. (2020). Staphylococcal biofilm development: structure, regulation, and treatment strategies. *Microbiology and Molecular Biology Reviews*, 84(3).
- Schmitt, J., & Flemming, H.-C. (1998). FTIR-spectroscopy in microbial and material analysis. *International Biodeterioration & Biodegradation*, 41(1), 1-11.
- Serra, D. O., & Hengge, R. (2014). Stress responses go three dimensional – the spatial order of physiological differentiation in bacterial macrocolony biofilms. *Environmental Microbiology*, 16(6), 1455-1471. doi:https://doi.org/10.1111/1462-2920.12483
- Serra, D. O., Klauck, G., & Hengge, R. (2015). Vertical stratification of matrix production is essential for physical integrity and architecture of macrocolony biofilms of *Escherichia coli*. *Environmental Microbiology*, 17(12), 5073-5088. doi:https://doi.org/10.1111/1462-2920.12991

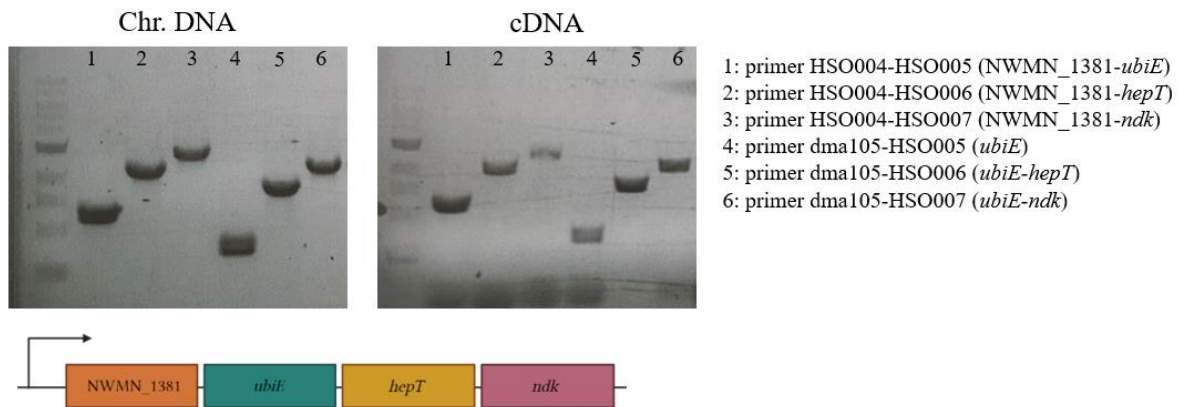
- Simon, J., van Spanning, R. J. M., & Richardson, D. J. (2008). The organisation of proton motive and non-proton motive redox loops in prokaryotic respiratory systems. *Biochimica et Biophysica Acta (BBA) - Bioenergetics*, *1777*(12), 1480-1490. doi:<https://doi.org/10.1016/j.bbabi.2008.09.008>
- Stamsås, G. A., Myrbråten, I. S., Straume, D., Salehian, Z., Veening, J. W., Håvarstein, L. S., & Kjos, M. (2018). CozEa and CozEb play overlapping and essential roles in controlling cell division in *Staphylococcus aureus*. *Molecular Microbiology*, *109*(5), 615-632.
- Stepanović, S., Vuković, D., Dakić, I., Savić, B., & Švabić-Vlahović, M. (2000). A modified microtiter-plate test for quantification of staphylococcal biofilm formation. *Journal of Microbiological Methods*, *40*(2), 175-179. doi:[https://doi.org/10.1016/S0167-7012\(00\)00122-6](https://doi.org/10.1016/S0167-7012(00)00122-6)
- Stephenson, K., & Hoch, J. A. (2002). Two-component and phosphorelay signal-transduction systems as therapeutic targets. *Current Opinion in Pharmacology*, *2*(5), 507-512. doi:[https://doi.org/10.1016/S1471-4892\(02\)00194-7](https://doi.org/10.1016/S1471-4892(02)00194-7)
- Stewart, P. S., & Franklin, M. J. (2008). Physiological heterogeneity in biofilms. *Nature Reviews Microbiology*, *6*(3), 199-210. doi:10.1038/nrmicro1838
- Suzuki, T., Campbell, J., Kim, Y., Swoboda, J. G., Mylonakis, E., Walker, S., & Gilmore, M. S. (2012). Wall teichoic acid protects *Staphylococcus aureus* from inhibition by Congo red and other dyes. *Journal of Antimicrobial Chemotherapy*, *67*(9), 2143-2151. doi:10.1093/jac/dks184
- Swords, W. E. (2003). Chemical transformation of *E. coli*. In *E. coli Plasmid Vectors* (pp. 49-53): Springer.
- Szterk, A., Bus, K., Zmysłowski, A., & Ofiara, K. (2018). Analysis of Menaquinone-7 Content and Impurities in Oil and Non-Oil Dietary Supplements. *Molecules (Basel, Switzerland)*, *23*(5), 1056. doi:10.3390/molecules23051056
- Tiwari, N., López-Redondo, M., Miguel-Romero, L., Kulhankova, K., Cahill, M. P., Tran, P. M., . . . Herfst, C. A. (2020). The SrrAB two-component system regulates *Staphylococcus aureus* pathogenicity through redox sensitive cysteines. *Proceedings of the National Academy of Sciences*, *117*(20), 10989-10999.
- Tong, S. Y., Davis, J. S., Eichenberger, E., Holland, T. L., & Fowler, V. G. (2015). *Staphylococcus aureus* infections: epidemiology, pathophysiology, clinical manifestations, and management. *Clinical microbiology reviews*, *28*(3), 603-661.
- Wakeman, C. A., Hammer, N. D., Stauff, D. L., Attia, A. S., Anzaldi, L. L., Dikalov, S. I., . . . Skaar, E. P. (2012). Menaquinone biosynthesis potentiates haem toxicity in *Staphylococcus aureus*. *Molecular Microbiology*, *86*(6), 1376-1392. doi:10.1111/mmi.12063
- Wermser, C., & Lopez, D. (2018). Identification of *Staphylococcus aureus* genes involved in the formation of structured macrocolonies. *Microbiology*, *164*(5), 801-815. doi:<https://doi.org/10.1099/mic.0.000660>
- Wilking, J. N., Zaboradaev, V., De Volder, M., Losick, R., Brenner, M. P., & Weitz, D. A. (2013). Liquid transport facilitated by channels in *Bacillus subtilis* biofilms. *Proceedings of the National Academy of Sciences*, *110*(3), 848-852.
- Xia, G., Kohler, T., & Peschel, A. (2010). The wall teichoic acid and lipoteichoic acid polymers of *Staphylococcus aureus*. *International Journal of Medical Microbiology*, *300*(2), 148-154. doi:<https://doi.org/10.1016/j.ijmm.2009.10.001>
- Xu, Z., Liang, Y., Lin, S., Chen, D., Li, B., Li, L., & Deng, Y. (2016). Crystal Violet and XTT Assays on *Staphylococcus aureus* Biofilm Quantification. *Current Microbiology*, *73*(4), 474-482. doi:10.1007/s00284-016-1081-1

Yip, E. S., Geszvain, K., DeLoney-Marino, C. R., & Visick, K. L. (2006). The symbiosis regulator rscS controls the syp gene locus, biofilm formation and symbiotic aggregation by *Vibrio fischeri*. *Molecular Microbiology*, 62(6), 1586-1600.  
doi:10.1111/j.1365-2958.2006.05475.x

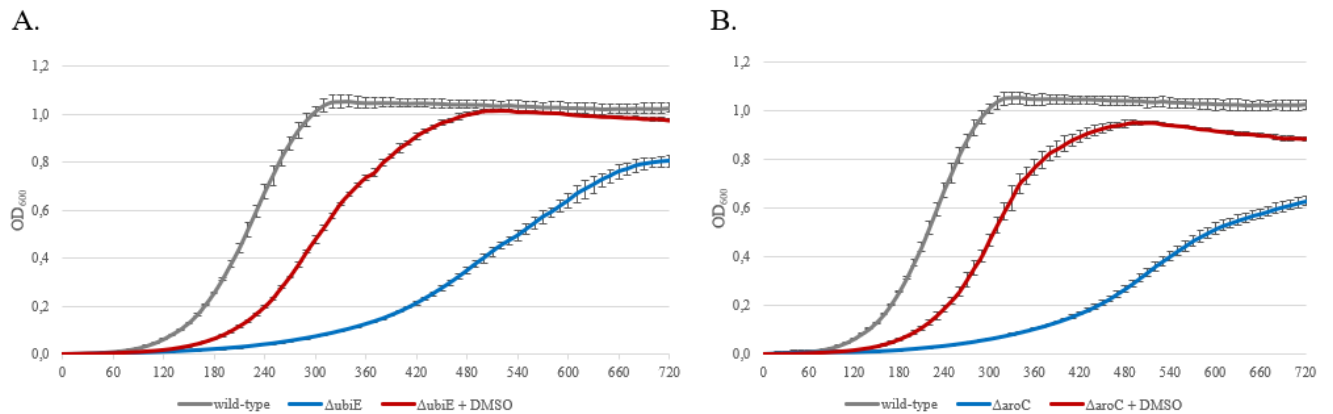
Zecconi, A., & Scali, F. (2013). *Staphylococcus aureus* virulence factors in evasion from innate immune defenses in human and animal diseases. *Immunology letters*, 150(1-2), 12-22.

## Appendix

**A1.** Visualisation of amplicons from RT-PCR through agarose gel electrophoresis show how the four genes that were tested (NWMN:1381, *ubiE*, *hepT* and *ndk*) are in the same operon. Primers were verified on chromosomal DNA, and genes were then confirmed to be in the same operon through RT-PCR with cDNA from *S. aureus*.



**A.2** Growth curves of  $\Delta ubiE$  (A) and  $\Delta aroC$  (B) presenting how 1,6% (v/v) DMSO affects the growth of the deletion mutants. Bacteria were grown in liquid BHI medium for approximately 12 hours. OD<sub>600</sub> were measured in 10-minute intervals.







**Norges miljø- og biovitenskapelige universitet**  
Noregs miljø- og biovitenskapelige universitet  
Norwegian University of Life Sciences

Postboks 5003  
NO-1432 Ås  
Norway